



A model estimate on the effect
of anthropogenic land cover change
on the climate of the last millennium

Julia Pongratz



Hinweis

Die Berichte zur Erdsystemforschung werden vom Max-Planck-Institut für Meteorologie in Hamburg in unregelmäßiger Abfolge herausgegeben.

Sie enthalten wissenschaftliche und technische Beiträge, inklusive Dissertationen.

Die Beiträge geben nicht notwendigerweise die Auffassung des Instituts wieder.

Die "Berichte zur Erdsystemforschung" führen die vorherigen Reihen "Reports" und "Examensarbeiten" weiter.



Notice

The Reports on Earth System Science are published by the Max Planck Institute for Meteorology in Hamburg. They appear in irregular intervals.

They contain scientific and technical contributions, including Ph. D. theses.

The Reports do not necessarily reflect the opinion of the Institute.

The "Reports on Earth System Science" continue the former "Reports" and "Examensarbeiten" of the Max Planck Institute.

Anschrift / Address

Max-Planck-Institut für Meteorologie
Bundesstrasse 53
20146 Hamburg
Deutschland

Tel.: +49-(0)40-4 11 73-0
Fax: +49-(0)40-4 11 73-298
Web: www.mpimet.mpg.de

Layout:

Bettina Diallo, PR & Grafik

Titelfotos:

vorne:

Christian Klepp - Jochem Marotzke - Christian Klepp

hinten:

Clotilde Dubois - Christian Klepp - Katsumasa Tanaka

A model estimate on the effect
of anthropogenic land cover change
on the climate of the last millennium

Dissertation zur Erlangung des Doktorgrades der Naturwissenschaften
im Department Geowissenschaften der Universität Hamburg
vorgelegt von

Julia Pongratz

aus München

Hamburg 2009

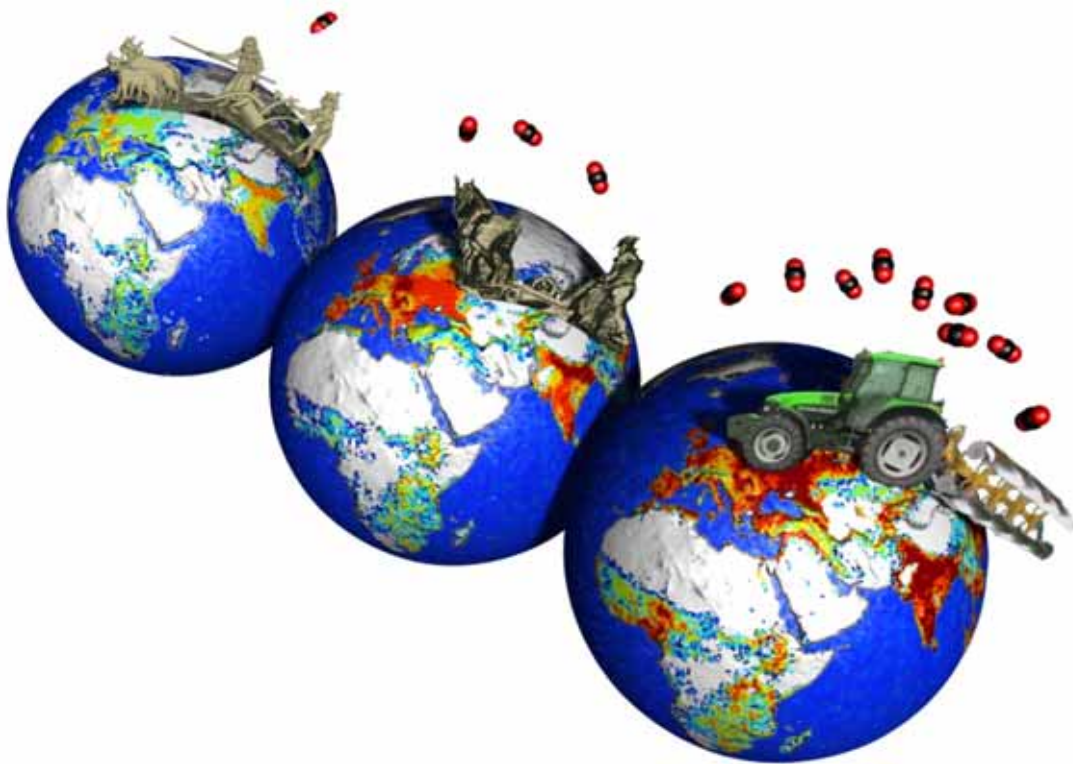
Julia Pongratz
Max-Planck-Institut für Meteorologie
Bundesstrasse 53
20146 Hamburg
Germany

Als Dissertation angenommen
vom Department Geowissenschaften der Universität Hamburg

auf Grund der Gutachten von
Prof. Dr. Martin Claußen
und
Dr. Christian H. Reick

Hamburg, den 29. April 2009
Prof. Dr. Jürgen Oßenbrügge
Leiter des Department Geowissenschaften

A model estimate on the effect
of anthropogenic land cover change
on the climate of the last millennium



Julia Pongratz

Hamburg 2009

Cover picture

The image on the front page illustrates the expansion of agriculture in the last millennium and the associated increasing influence of humankind on climate and the carbon cycle. From back to front: Late-medieval farmers¹ on the cropland map of the year 1500. Farmer of the late preindustrial period² on the cropland map of the year 1850. Modern plough³ on the cropland map of the year 1992. Each molecule of CO₂ stands for approximately 100 Tg C/year primary emissions in the respective year, indicating emissions of 40, 320, and 900 Tg C/year for the three years. Cropland maps and CO₂ estimates are described in Chapters 2 and 4, respectively.

Picture credits:

¹ Modified from Project Gutenberg. Illustration probably from the early 16th century with legend “God Spede ye Plough, and send us Korne enow”.

² modified from a sketch by Vincent van Gogh, 1883.

³ modified from Rasbak, Wikimedia Commons, licensed under “GNU-Lizenz für freie Dokumentation” (Licence text see

http://en.wikipedia.org/wiki/Wikipedia:Text_of_the_GNU_Free_Documentation_License).

Contents

Abstract	1
List of Abbreviations	3
1 Introduction	5
1.1 The importance of anthropogenic land cover change for climate	6
1.2 “Anthropogenic land cover change” - definition and quantification	8
1.3 A brief summary of the history of agriculture	10
1.4 The last millennium	12
1.5 Biosphere-atmosphere interactions and goals of this study	14
2 A Reconstruction of Global Agricultural Areas and Land Cover for the Last Millennium	21
2.1 Introduction	22
2.2 Step 1: Adaptation of agricultural data since AD 1700	23
2.2.1 Cropland	24
2.2.2 Pasture	25
2.3 Step 2: Reconstruction of agricultural areas AD 800 to 1700	25
2.4 Step 3: From agricultural areas to land cover	28
2.5 Assessing uncertainty and validity	30
2.5.1 Inclusiveness of the millennium reconstruction	30
2.5.2 Validation of the base data AD 1700 to 1992	30
2.5.3 Uncertainty of the population data	31
2.5.4 Effects of agrotechnical improvements	32
2.6 Changes in land cover AD 800–1992	34
2.6.1 Europe and Former Soviet Union	38
2.6.2 North Africa/Middle East	40
2.6.3 South Asia and Southeast Asia	40
2.6.4 China	42
2.6.5 Pacific Developed	42
2.6.6 Tropical Africa	43
2.6.7 The Americas	44
2.7 Conclusion	45

3	Radiative Forcing from Anthropogenic Land Cover Change since AD 800	47
3.1	Introduction	47
3.2	Radiative forcing calculations	49
3.3	Results	49
3.4	Discussion	51
3.5	Conclusions	53
4	Effects of Anthropogenic Land Cover Change on the Carbon Cycle of the Last Millennium	55
4.1	Introduction	56
4.2	Methods	58
4.2.1	Model	58
4.2.2	ALCC data	60
4.2.3	Simulation protocol	60
4.3	Primary emissions and carbon cycle feedback	62
4.3.1	Overview	62
4.3.2	Spatial patterns	62
4.3.3	Primary emissions	63
4.3.4	Coupling flux	67
4.4	Anthropogenic influence on the preindustrial carbon cycle and climate	69
4.4.1	Anthropogenic contribution to Holocene CO ₂ increase	69
4.4.2	Effect of ALCC on global mean temperatures	72
4.4.3	Epidemics and warfare	72
4.5	Conclusions	74
5	Biogeophysical Contributions to the Effects of Anthropogenic Land Cover Change	77
5.1	Introduction	78
5.2	Model and data	80
5.3	Climate response to ALCC	81
5.3.1	Biogeophysical mechanisms	82
5.3.2	Biogeochemical mechanisms	86
5.4	Biogeophysically-induced changes in the carbon cycle	86
5.5	Relevance of the radiative forcing concept	87
5.6	Historical ALCC in the context of climate mitigation	91
5.7	Summary and conclusions	95
6	Summary and Conclusion	99
6.1	Summary of methods	99
6.2	Main findings concerning the beginning of the Anthropocene	100
6.3	Main findings beyond the historical aspect	101
6.4	Next steps to be taken	102

Appendices	105
A Auxiliary material to the millennium land cover reconstruction	105
B Supplementary figures for biogeophysical mechanisms	109
C Error estimate for local radiative forcing from emissions	113
List of Figures	115
List of Tables	117
List of Publications	133
Acknowledgements	135

Abstract

Anthropogenic land cover change (ALCC) represents one of the most substantial human impacts on the Earth system, altering land surface properties and carbon fluxes. In this study, the role of ALCC for climate and the carbon cycle are assessed using a complex climate model. A special focus is placed on the preindustrial period, for which only few studies exist.

First, a method is developed to reconstruct spatially explicit changes in global agricultural areas and the resulting ALCC over the last millennium. Published maps for the last 300 years are extended into the past using country-level population data as a proxy for agricultural activity. This reconstruction is applied to calculate radiative forcing (RF) from ALCC-induced surface albedo changes. RF is found to be small throughout the preindustrial period on the global scale (negative with a magnitude less than 0.05 W/m^2) and not strong enough to explain the Northern Hemisphere cooling reconstructed from climate proxies between AD 1000 and 1900. An early anthropogenic impact on the energy balance, however, is found for the regional scale.

In transient coupled climate simulations the effects of ALCC are isolated by applying ALCC as the only climate forcing. The terrestrial biosphere releases 96 Gt C during AD 800–2000 in the simulations, increasing atmospheric CO_2 by 20 ppm. Primary emissions are quantified to 53–61 Gt C and 108 Gt C over the preindustrial and the industrial period, respectively. A high restorage of carbon by the biosphere due to the coupling to climate and atmospheric CO_2 occurs over the preindustrial period (48% of the primary emission). Nevertheless, the atmospheric CO_2 concentration is significantly increased by ALCC by 5–6 ppm prior to the Industrial Revolution. Historic events such as epidemics and warfare are found unlikely to be the cause for drops in ice-core CO_2 . Global mean temperature increase due to ALCC amounts to 0.13–0.15 K in the 20th century, but remains within natural variability in the preindustrial era.

A simulation is performed to quantify the contribution from only the biogeophysical effects of ALCC in addition to the full climate response. Biogeophysical effects are found to contribute a weak cooling (-0.03 K in the 20th century). The rise in CO_2 from ALCC emissions is therefore the driving force of the simulated global warming. A comparison of biogeophysical temperature change and RF from albedo changes indicates that RF is not a comprehensive measure for the climatic importance of ALCC, especially in the tropical regions. Finally, the mitigation potential of reversing past ALCC is assessed: When reversing ALCC of the last millennium, most regions, including the northern mid- to high latitudes, would contribute a cooling effect.

Zusammenfassung

Einen der entscheidenden Prozesse, durch die der Mensch in das Erdsystem eingreift, stellen Änderungen der Landbedeckung dar. Durch diese verändert der Mensch die Eigenschaften der Erdoberfläche und beeinflusst die Kohlenstoffflüsse. In der vorliegenden Studie wird die Rolle von anthropogener Landbedeckungsänderung (“anthropogenic land cover change”, ALCC) auf das Klima und den Kohlenstoffkreislauf mithilfe eines komplexen Klimamodells untersucht. Ein Schwerpunkt liegt dabei auf der vorindustriellen Zeit, für die nur wenige Studien existieren.

Zuerst wird eine Methode entwickelt, um räumlich explizit Änderungen in den globalen landwirtschaftlichen Flächen im letzten Jahrtausend und die sich daraus ergebende ALCC zu rekonstruieren. Länderbasierte Bevölkerungsdaten werden als Proxy für landwirtschaftliche Aktivität genutzt, um bestehende Karten der letzten 300 Jahre in die Vergangenheit zu erweitern. Mithilfe dieser Rekonstruktion wird der Strahlungsantrieb (SA) berechnet, der sich aus den ALCC-bedingten Änderungen der Oberflächenalbedo ergibt. SA wird auf globaler Ebene für die gesamte vorindustrielle Zeit als klein abgeschätzt (negativ mit einem Betrag von weniger als 0.05 W/m^2) und als nicht stark genug, um die Abkühlung der nördlichen Hemisphäre zu erklären, die aus Klimaproxies für die Zeit zwischen dem Jahr 1000 und 1900 rekonstruiert wurde. Auf regionaler Ebene wird jedoch ein früher Einfluss des Menschen auf die Energiebilanz gefunden.

In transienten gekoppelten Klimasimulationen werden die Effekte von ALCC isoliert, indem ALCC als einziger Klimaantrieb im Modell verwendet wird. Die Landbiosphäre verliert in diesen Simulationen etwa 96 Gt Kohlenstoff (C) über den Zeitraum von 800 bis 2000 und erhöht dadurch die CO_2 -Konzentration der Atmosphäre um 20 ppm. Primäremissionen werden auf 53–61 Gt C für die gesamte vorindustrielle Zeit, und auf 108 Gt C für die gesamte industrielle Zeit quantifiziert. Für die vorindustrielle Zeit findet man eine starke Wiederaufnahme von Kohlenstoff in die Biosphäre (48% der Primäremissionen) aufgrund der Kopplung an Klima und atmosphärischem CO_2 . Trotzdem wird bereits vor der Industriellen Revolution die atmosphärische CO_2 -Konzentration durch ALCC signifikant um 5–6 ppm erhöht. Es zeigt sich, dass historische Ereignisse wie Epidemien und Kriege wahrscheinlich nicht der Grund für CO_2 -Abnahmen in Eisbohrkernen sind. Die globale Mitteltemperatur erhöht sich durch ALCC um 0.13–0.15 K im 20. Jahrhundert, bleibt aber in der vorindustriellen Zeit im Rahmen der natürlichen Variabilität.

Eine weitere Simulation wird durchgeführt, die den Beitrag der biogeophysikalischen Effekte von ALCC zusätzlich zur vollen Klimaänderung quantifiziert. Die simulierten biogeophysikalischen Effekte bewirken einen leichten Kühlungseffekt (-0.03 K im 20. Jahrhundert). Der CO_2 -Anstieg aus ALCC-Emissionen ist deshalb die treibende Kraft hinter der simulierten Erwärmung. Ein Vergleich von biogeophysikalischer Temperaturänderung und SA aus Albedoänderungen zeigt, dass SA besonders in den Tropen kein vollständiges Maß für die Bedeutung von ALCC für das Klima ist. Abschließend wird das Potential einer Umkehrung von ALCC zur Verminderung des Klimawandels untersucht: Bei einer Umkehr der ALCC der letzten tausend Jahre würden die meisten Regionen, darunter auch die mittleren und hohen Breiten, eine Abkühlung bewirken.

List of Abbreviations

ALCC	anthropogenic land cover change
AOGCM	atmosphere/ocean general circulation model
BVOC	biogenic volatile organic compounds
C	carbon
DJF	winter season
ECHAM5	atmosphere model applied in this study
EMIC	Earth system model of intermediate complexity
ENSO	El Niño/Southern Oscillation
FAO	Food and Agriculture Organization of the United Nations
FAOSTAT	Statistical database of the Food and Agriculture Organization of the United Nations
FSU	Former Soviet Union
GCM	general circulation model
HAMOCC5	ocean biogeochemistry model applied in this study
HYDE	History Database of the Global Environment
IAM	Integrated Assessment Model
IPCC	Intergovernmental Panel on Climate Change
JJA	summer season
JSBACH	land surface scheme applied in this study
LAI	leaf area index
LUCID	“Land-Use and Climate, IDentification of robust impacts” project
MAM	spring season
MPI-OM	ocean and sea ice model applied in this study
NEP	net ecosystem productivity
NPP	net primary productivity
PFT	plant functional type
RF	radiative forcing
R_h	heterotrophic respiration
SA	Strahlungsantrieb
SAGE	Center for Sustainability and the Global Environment, University of Wisconsin
SON	fall season
UNFCCC	United Nations Framework Convention on Climate Change

Chapter 1

Introduction

If we follow the notion by [Diamond \[1999\]](#), the advent of agriculture was the decisive factor that enabled cultural developments such as writing, technology, and industrial applications that characterize the modern societies of today. Agriculture has evolved over several thousand years: at first, few people inhabited the Earth and agriculture was "invented" in just a few places; later, the majority of a much larger population worked as farmers; today, a relatively small number of farmers supports a population of billions of people. Somewhere along this way, humans started to shape the world in a way that scientists have coined the term "Anthropocene" for it [[Crutzen and Stoermer, 2000](#)]. But, besides being the prerequisite for an industrial society that takes decisive influence on the Earth system, agriculture may well have been in itself a strong contributor to changing the Earth system. Research over the last decades has more and more confirmed this notion as far as agriculture at its present extent is concerned. But the long history of agriculture implies a potentially early impact on the climate, which is much less well known. This thesis follows the last thousand years of agricultural development and investigates its influences on the climate system from different perspectives.

The task of the present chapter is (1) to exemplarily sketch the importance of agriculture for climate; (2) to define the subject matter of this study — agriculture and anthropogenic land cover change; (3) to give a synopsis of the history of agriculture to embed the timespan under investigation in its historical context; (4) explain why exactly the timespan under investigation was chosen for this study; (5) to motivate the interest in the historical aspects of agriculture. In the last section, the different mechanisms through which anthropogenic land cover change influences climate will be explained. The different mechanisms will be studied in the different parts of this thesis, and the objectives of the individual chapters will be explained in their context. The main objectives of this thesis are highlighted by blue lines in the following.

1.1 The importance of anthropogenic land cover change for climate

Anthropogenic climate change, expressed prominently in a global warming over the last decades [Trenberth et al., 2007], is foremost driven by the increase in atmospheric greenhouse gas concentration. Here in turn CO₂ has been identified as the main actor [Forster et al., 2007]. Anthropogenic CO₂ emissions originate primarily from the combustion of fossil fuels and from cement manufacture, estimated to 6.4 Gt carbon (C) per year for the 1990s; but another 1.6 Gt C per year are added by CO₂ emissions from the transformation of natural vegetation to managed areas (“anthropogenic land cover change”, ALCC, see Sec. 1.2)[see Trenberth et al., 2007, for error estimates]. However, vegetation is not only a source of CO₂, but also a sink: Knowing the atmospheric CO₂ increase and the ocean-atmosphere CO₂ flux, we can infer that the land has been a net sink of carbon over the last decades, with an uptake of about 1.0 Gt C per year [Trenberth et al., 2007]. Comparing this against estimates of ALCC emissions of about 1.6 Gt C, 2.6 Gt C per year must thus have been stored on land. This means that almost one third of total anthropogenic CO₂ emissions are taken up each year by the terrestrial biosphere. The reason for a net CO₂ uptake on land despite carbon loss from ALCC is, among others, increased plant productivity initiated from the rise in CO₂. This demonstrates that not only does the biosphere alter climate and CO₂, but climate and CO₂ in turn feed back on biospheric activity. We would like to better understand all these processes and their interactions since understanding is a prerequisite to take appropriate action. On the one hand, we need exact quantifications of the CO₂ emissions in time and space in order to determine where emissions can be reduced — emissions from fossil-fuel combustion are very well known, but the land use carbon source has currently the largest uncertainties in the global carbon budget [Denman et al., 2007], propagating its uncertainties to estimates of the terrestrial sink. On the other hand, we need to understand the processes behind the sink term in order to be able to project its future evolution and to possibly increase its mitigation potential.

The relevance of the biosphere and the influence humans exert on it have initiated political actions on the highest international level. Several articles of the Kyoto Protocol and following agreements make provisions for the inclusion of land use, land-use change, and forestry activities as part of the efforts to implement the Kyoto Protocol and contribute to the mitigation of climate change. The Intergovernmental Panel on Climate Change (IPCC) has noted that reducing and/or preventing deforestation is the mitigation option with the largest and most immediate carbon stock impact in the short term per area and year [Nabuurs et al., 2007]. Therefore, it is being discussed to admit to a Party’s credit the emission reduction from a reduction in deforestation in developing countries [UNFCCC, 2007]. Already agreed on is credit for activities in the own country that lead to higher absorption of carbon from the atmosphere or increased storage. This includes carbon sequestration increases above 1990 levels resulting from reduced deforestation rates or increase in

forest area, but also changes in management of forest, cropland, and grazing land, and general re-vegetation [UNFCCC, 1998]. Several tiers are proposed for quantifying and reporting changes in carbon stock and greenhouse gas emissions, including spatially explicit biosphere modeling [IPCC, 2003] — the approach taken also in the present study.

Biosphere services are also considered to reduce the need of fossil fuels by providing bioenergy. For example, substituting gasoline by first generation biofuels (mostly sugar- or oil-rich food crops) have been expected to reduce greenhouse gases because biofuels remove carbon from the atmosphere through the growth of the feedstock instead of taking carbon from fossil sources [e.g., Commission of the European Communities, 2006]. Recent studies, however, suggest that this may not be the case: The expected emission savings may be outdone by the increased rates of ALCC that may occur when both food and energy demand need to be fulfilled in parallel by agricultural production [Searchinger et al., 2008]. Again, this highlights the need for a process understanding of source and sink terms associated with ALCC, as well as an integrated assessment thereof.

ALCC and the terrestrial biosphere are, however, relevant for climate and climate change beyond the aspect of sources and sinks of greenhouse gases. As will be explained in detail in Sec. 1.5, ALCC alters the physical properties of the land surface, and thus exerts a direct impact e.g. on water and energy fluxes. ALCC until today may have decreased surface temperatures by 1–2 K over midlatitude agricultural regions [Betts, 2001, Bounoua et al., 2002, Feddema et al., 2005]. Future scenarios, anticipating large-scale deforestation in the tropical region, project warming of up to 2 K and drier hydrological conditions in the areas undergoing ALCC [DeFries et al., 2002, Sitch et al., 2005].

From these examples of recent climate research and policy, we can conclude three points relevant to this study: (1) We need to improve our process understanding in order to realistically estimate current and future climatic consequences of ALCC and to assess its potential for climate change mitigation. (2) We need to investigate biosphere-climate interactions with respect to a range of very different mechanisms. These may act in the same or in opposite directions concerning their effects on important climate variables, such as temperature. An integrated assessment of the different mechanisms as well as their two-way interaction with climate is essential. If modeling is chosen as tool to assess these mechanisms, then a coupled setup is essential to allow the full representation of biosphere-atmosphere feedbacks. (3) For the present situation as well as for a range of future scenarios, the significance of ALCC for climate change has been acknowledged. Considering the long history of agriculture, it is logical to ask about the importance of ALCC for past climate and about the starting point of significant human interference.

1.2 “Anthropogenic land cover change” - definition and quantification

“Anthropogenic land cover change” (ALCC) denotes land cover changes due to human land use. It is thus important to define and distinguish the terms land cover and land use. According to [Turner II et al., 1995], “*land cover*” is the “biophysical state of the Earth’s surface and immediate subsurface”. Land cover may change due to natural factors, such as changes in climate to which the natural vegetation distribution adapts. It is possible to simulate climate-related natural changes of the biogeographic distribution of land cover in the modeling framework applied in this study [Brovkin et al., submitted]. However, these natural changes are assumed to be small over the time period considered here and are deemed negligible in comparison to anthropogenic land cover change. “*Anthropogenic land cover change*” denotes those changes in land cover that are caused by human land use. Land use has, under contemporary conditions, been identified as the main driver of land cover change [Turner II et al., 1995]. Such human land use may be cultivation, livestock rearing, forestry, or use of land as settlement. Here, “*land use*” denotes both the intent of usage and the related manipulation of the land properties, e.g., the intent of using an area for livestock herding may imply the manipulation of the land surface properties by introducing new grass species [Turner II et al., 1995]. These manipulations have consequences beyond the intended ones of producing food-stuff, raw materials, timber, fuelwood, and space for settlements. They may, for example, change water and energy cycles and influence climate (see Sec. 1.5). Trade-offs must often be found between the competing intended and unintended consequences [DeFries et al., 2004, Foley et al., 2005]. To understand the human influence on the Earth system, it is important to quantify the change in land cover due to human land use and to describe the associated manipulation of the land surface.

The present study focuses on ALCC as caused by the expansion or abandonment of agricultural area, comprising cropland and pasture. This is the dominant type of ALCC: At present, there exist about 15 million km² of cropland and 34 million km² of pasture [FAO, 2007, data for year 2003]. Both forests and natural grass- and shrublands are affected by the agricultural expansion — the regional distribution for the early 1990s is shown in Fig. 1.1. Compared to the 49 million km² of agriculture, urban areas currently cover only about 4 million km² [Douglas, 1994]. They certainly exhibit a strong local influence on climate [e.g., Jin et al., 2005], but their larger contribution to global climate change must be expected via the food demand of a growing population, increasing the demand for agricultural areas [DeFries et al., 2004]. Forestry, on the other hand, is second-order to agriculture both in terms of area and emissions — wood harvest contributed on the order of 10% to land-use change emissions over the last 150 years [Houghton, 1999]. As long as forest is used in a sustainable way, loss of biomass is largely compensated by regrowth [Houghton, 2003]. Part of the global wood demand is also covered by wood harvest on areas subsequently used for agriculture; such areas contribute to the ALCC taken into

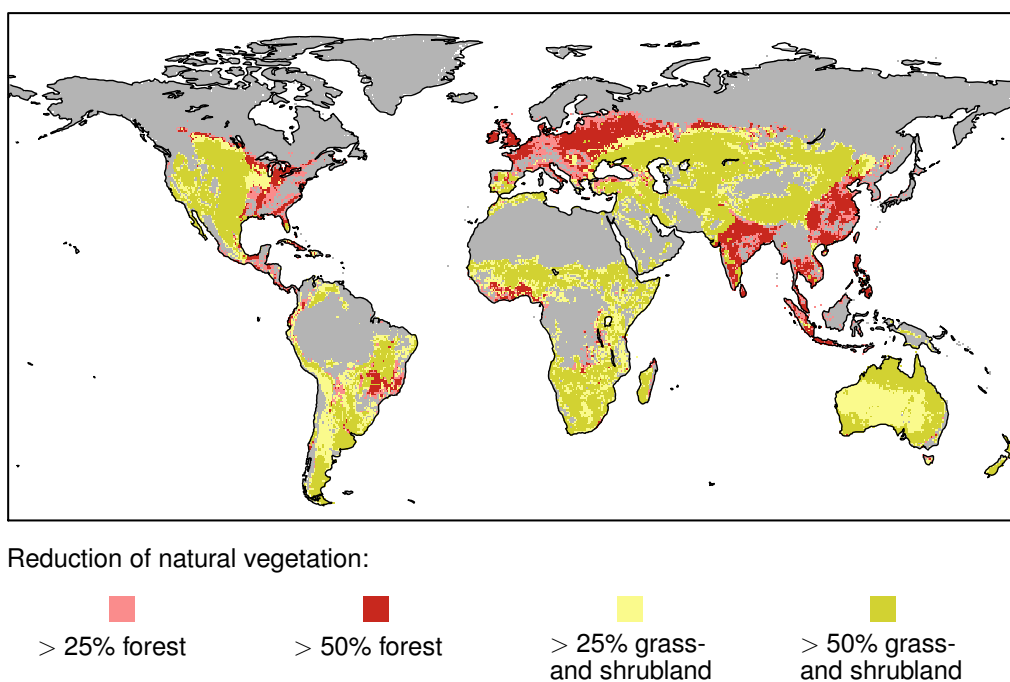


Figure 1.1— Reduction of natural vegetation until 1992. Light and dark red colors depict areas, where more than 25% and 50%, respectively, of the grid cell has undergone a transformation from forest to agricultural use; light and dark yellow colors depict areas, where more than 25% and 50%, respectively, of the grid cell has undergone a transformation from natural grass- and shrubland to agricultural use. Data as described in Chapter 2.

account in this study. Not considered in this study are any effects of degradation, such as soil degradation or changes in vegetation composition e.g. due to fragmentation from small-scale agriculture. These effects, too, are assumed to be negligible compared to land cover change which transforms natural vegetation to agricultural use.

The quantification of agricultural area has been greatly promoted by international organizations such as the Food and Agriculture Organization (FAO). Remote sensing became an indispensable tool for objective estimates of land cover change over the last decades [e.g., [Townshend et al., 1991](#), [Hansen et al., 2008](#)]. For the last few centuries, some historical estimates exist concerning regional conversion rates [[Richards, 1990](#)]. Such datasets have been combined to yield globally consistent, spatially explicit information of the change in agricultural area over the last 300 years [[Ramankutty and Foley, 1999](#), [Klein Goldewijk, 2001](#)]. Modeling has been applied to estimate the future development of agricultural extent under scenario assumptions. Models of land-use change within the framework of Integrated Assessment Models (IAM) represent one such approach. They simulate, in a simplified manner, human behavior and decision making under economic, political, and environmental constraints [[Turner II et al., 1995](#), [Lambin et al., 2001](#)], and use this to project type

and extent of future agriculture. Modeling is also applied to assess the very beginnings of agriculture. For example, there exist models that simulate the emergence of agriculture depending on the geographical conditions of a region, and the subsequent spread of agricultural practices [Wirtz and Lemmen, 2003]. However, the time period after the emergence of agriculture and prior to the last three centuries poses a problem, since neither process-based simulation nor inference from statistical information is possible. Local, and mostly indirect, evidence for agricultural extent for earlier times exists from archeology and historical records, but no globally consistent approach has yet quantified area and distribution of agriculture.

There exists thus a gap in our knowledge of global agricultural expansion, encompassing the last several thousand years. This gap needs to be closed before detailed statements can be made concerning the past effects of ALCC on climate. Filling the gap for the last 1200 years is the topic of Chapter 2.

This chapter has been published in *Global Biogeochemical Cycles* [Pongratz et al., 2008b] (verbatim quote, but with references merged in the thesis bibliography; same for the following Chapters), and in altered form in *Reports on Earth System Science* [Pongratz et al., 2008a].

The historical context, in which the agricultural development of the last millennium must be seen, will be outlined in the following section.

1.3 A brief summary of the history of agriculture

Several theories have been proposed on how and why agriculture has developed. These theories include (1) the fortuitous invention and subsequent spread of the idea of cultivation or livestock farming due to apparent advantages; (2) a forced change to agriculture due to population pressure, reduced availability of wild food, or an environmental change at the Pleistocene-Holocene transition; (3) a coevolution of domesticates, human management, and agricultural society, i.e. an unintended selection of plants and animals in the habitat of man [Vasey, 1992, ch. 2],[Diamond, 1999, ch. 6]. Though little more than protection of suitable plants was enough for cultivation in some cases, [Grigg, 1974, ch. 2] agriculture was most often associated with the process of domestication, i.e. a change in morphology by selection under human management towards favorable features. Such features may be larger edible parts than wild forms, less shattering or dropping of fruits and seeds after maturation, and outcompeting wild forms on managed land [Vasey, 1992, ch. 2]. Domestication greatly increased yields, probably by a factor of 2–3, e.g. for cereals during the first thousand years following the Neolithic Revolution [Gepts, 2004]. In parallel, management methods evolved that intensified the cultivation, leading to an overall increase of the nutritional density of land. As a consequence, an agricultural system could upkeep population densities a factor 10–100 higher than in hunting and

gathering societies [Diamond, 1999, ch. 4]. Surpluses of food could be created and in combination with a sedentary lifestyle facilitated the formation of stratified societies, in which large numbers of people are supported by few farmers. As suggested e.g. by Diamond [1999, ch. 13], agriculture may therefore have been the trigger for many of the features of modern societies, allowing for rapid development of technology. Agriculture proved to be advantageous over the hunting and gathering lifestyle in many regions and was frequently adopted by neighboring hunters and gatherers. Agricultural people with their high population growth and advanced technologies also simply replaced or destroyed non-farming societies — all with the consequence that agriculture became the by far dominating lifestyle over hunting and gathering.

The “invention” of this new lifestyle happened at only few independent locations. The most certain origins of agriculture lie in the Fertile Crescent (around 8500 B.C), North China (by 7500 B.C), southern Mexico (by 3500 B.C.), and coastal Peru (around 3000 B.C.) [Diamond, 1999, ch. 5]. All these places hold evidence of cereal domestication and are thus the founders of “seed agriculture” [Grigg, 1974, ch. 2]. Several other regions are possible candidates for an independent development of agriculture. In particular regions of tropical “vegeculture”, which relies mainly on root crops, may also have taken the step to agriculture independently, e.g. Amazonia and tropical West Africa. From these centers of origin, agriculture spread. The spread may have taken place in the form of the domesticated plant or animal, of the farmers themselves and their knowledge, or of only the idea of agriculture [Grigg, 1974, ch. 2]. The spread of agricultural systems was still continuing during the last millennium, the period covered in this study, including the Bantu expansion on the African continent, the European settlement of Australia, and the exchange of plants between the New and the Old World. On the other hand, Europe and the Mediterranean, Southwest, South and Southeast Asia, and several other regions have been reached by the spread of agricultural systems already millennia earlier. Here, it is not the advent, but the expansion of agricultural area that changes the land cover. All these developments are described in more detail in Chapter 2. A special focus is laid on the links between population and agricultural areas. As stated before, the onset of agriculture as well as the refinement of techniques may have been triggered by population pressure; and they allowed for population growth by increasing the nutritional density of land. Population number and agricultural area are further immediately linked during times where the development of new agrarian methods was slow; then, dietary requirements of a person under a given nutritional density determine the areas of cropland and pasture in a region as a function of its population number. This connection has been employed to reconstruct agricultural extent for the preindustrial period of the last millennium. It would be futile, however, to apply this argument to the recent development of agriculture. Technology developed during industrial times, e.g. artificial fertilizers, mechanization and the broad application of fuel-driven machines, and systemized breeding up to genetically modified plants have again multiplied nutritional density [Vasey, 1992, ch. 10].

1.4 The last millennium

Immanent in the expansion of agriculture was an increasing modification of the Earth's land surface. Especially seed agriculture needs complete clearing of the natural vegetation, and vegeculture was often implemented in a system of shifting cultivation, meaning that forest was burnt down. This modification of the land surface must have been particularly strong during the last millennium: Between AD 800 and the early 18th century the world's population tripled to one billion people, while it had remained at below 220 million for the preceding millennia (Fig. 1.2). The last millennium must therefore have been associated with an agricultural expansion at unprecedented pace. This makes it particularly appropriate for studies on preindustrial human impact — if no significant impact from ALCC can be determined for this period, an anthropogenic signal is unlikely to be detectable for earlier millennia.

The last millennium is particularly suitable for ALCC-climate studies for two further reasons: First, ALCC was the dominating anthropogenic perturbation up until the 20th century — only after the 1930–50s, CO₂ emissions from fossil-fuel combustion grew substantially larger than ALCC emissions [Houghton, 2008, Marland et al., 2008], and prior to the industrialization ALCC was the only anthropogenic disturbance. The preindustrial period allows an analysis of the ALCC impact unaffected of other human activity. Second, the last millennium represents one of the best-documented periods of climate change on a multi-century timescale. Climate proxies such as ice core records and tree rings give detailed insight into the evolution of temperature and CO₂. Once all known natural and anthropogenic forcings have been isolated in their effect on climate, their combined impact can be validated against such climate reconstructions.

With its focus on preindustrial ALCC and climate, parts of this work evaluate with more detailed methods aspects of previous studies. Two challenging hypotheses are the possible early impact of humans on atmospheric CO₂, and the possible contribution of ALCC to the “Little Ice Age”:

A scientific dispute has been started with the “early anthropogenic hypothesis” by Ruddiman [2003, 2007]. Ruddiman concludes that the rise in atmospheric CO₂ reconstructed from ice core data for the last few millennia is anomalous as compared to what should be expected from its natural evolution in analogy to previous glacial and interglacial cycles. The beginning of the anomalous rise in CO₂ coincides with the beginning of agricultural activity about 8000 years ago. This anomaly, summing to 40 ppm by the end of the preindustrial period, can be explained at least in part by ALCC, according to his hypothesis. In addition, temporal variability of global CO₂ may be caused by historic events that cause regional abandonments of agricultural area, e.g. epidemics and warfare associated with a large reduction in population. The hypothesis extends further to a similarly anomalous rise in CH₄, which may also be attributable to human action. Subsequent studies by other groups have investigated aspects of this work and come to different conclusions, ranging from a substantially smaller contribution of human activity to the anomaly than suggested

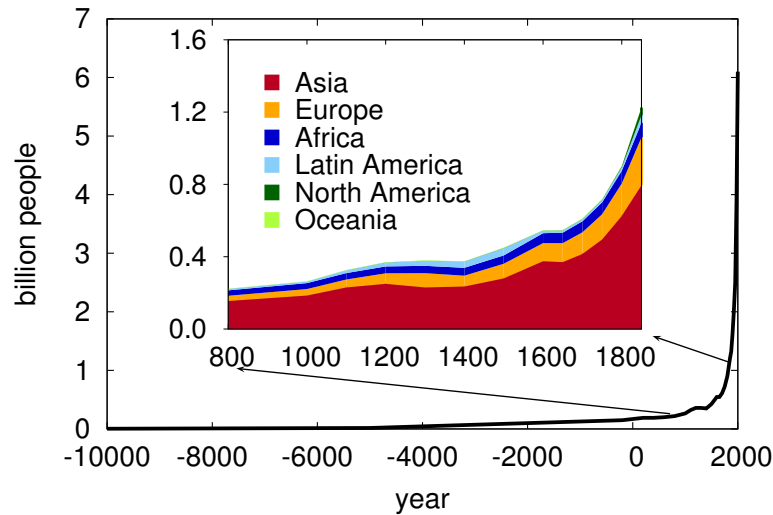


Figure 1.2— The world’s population 10,000 B.C. to AD 2000. Data from [Clark \[1967\]](#), [McEvedy and Jones \[1978\]](#).

[[Olofsson and Hickler, 2008](#)] to negligible human influence [[Joos et al., 2004](#)]. Natural processes have been put forward to explain the evolution of CO_2 over the Holocene and scrutinized the estimate of the natural trend [e.g., [Claussen et al., 2005](#)]. No consensus, however, has been found. Even if it was not several millennia into the past that may have been affected by ALCC-induced emissions, it has been noted that a high CO_2 concentration as far back as the early 1800s precludes large-scale fossil-fuel combustion as the only substantial contribution to changes in atmospheric composition [e.g., [Kammen and Marino, 1993](#)]. The CO_2 aspects of this hypothesis will be reassessed in Chapter 4 of this thesis, with a combination of data and methods that goes beyond any of the mentioned studies and allows a novel level of detail in the analysis.

The beginning of the last millennium is termed the “Medieval Warm Epoch” for at least some regions, like western Europe, which experienced relatively high temperatures during that time [[Lamb, 1965](#)]. Following the 14th century, a long-term cooling set in on the Northern Hemisphere leading to the so-called “Little Ice Age” [[Mann and Bradley, 1999](#)]. Various reconstructions of Northern Hemisphere temperature show a considerable range for timing and strength of the cooling, but all agree in a general downward trend between the medieval times and the 16th–19th century [[Osborn and Briffa, 2006](#), [Jansen et al., 2007](#)]. In the reconstruction by [Mann and Bradley \[1999\]](#), for example, temperatures at the end of the preindustrial period were about 0.2 K lower than at the beginning of the millennium. This cooling has been thought to be possibly related to astronomical forcing which may have induced a long-term downward trend in global temperature since the mid-Holocene at an average rate of -0.01 to -0.04 K/century [see [Berger, 1988](#), [Mann and Bradley,](#)

1999]. Recent modeling studies, however, suggest that the orbital forcing may indeed induce noticeable changes in the monthly response, but has only negligible influence on the annual temperature response in the Northern Hemisphere over the last millennium [Bauer and Claussen, 2006]. Further possible contributions to the cooling may come from century-scale variations in solar irradiance [Mann et al., 1998]. Another hypothesis, however, assumes ALCC as driving force behind the Northern Hemisphere cooling. In a study on Europe, Goosse et al. [2006] simulate a cooling of 0.4–0.5 K during the past millennium until today due to changes in the physical properties of the land surface by ALCC. This notion is supported by other modeling studies that find a Northern Hemisphere cooling of 0.35 K over the past millennium [Bauer et al., 2003], 0.25 K AD 1000–1900 [Govindasamy et al., 2001], and global cooling of 0.13–0.25 K [Brovkin et al., 2006]. All of these studies have applied ad-hoc approximations of preindustrial ALCC. However, assessing regional effects of ALCC for specific time periods needs detailed knowledge concerning the evolution of the climate forcing. Chapters 2, 3, and 5 quantify this forcing and its possible climatic influence.

1.5 Biosphere-atmosphere interactions and goals of this study

Preliminary remark on the methodology. As will become clear in the following Chapters, this thesis relies on modeling to assess the effects of ALCC on climate and the carbon cycle. Climate modeling is a valuable tool in particular for theoretical studies, e.g. to assess the climate response to only a subset of climate forcings as done in this study for ALCC only, or for an estimate of quantities that are not directly observable. In this thesis, the interaction of the biosphere with the other parts of the climate system are simulated using a complex Earth system model: Climate is simulated by a climate model comprising an atmosphere/ocean general circulation model (AOGCM), which consists of an atmosphere model (ECHAM5, Roeckner et al. [2003]) and an ocean and sea ice model (MPI-OM, Marsland et al. [2003]). Coupled to the ocean is an ocean biogeochemistry model (HAMOCC5, Wetzel et al. [2005]). Coupled to the atmosphere is a modular land surface scheme (JSBACH, Raddatz et al. [2007]). The human dimension is integrated into the model by prescribing changing maps of land cover as boundary condition to the atmosphere. The setup of the model is chosen according to the respective question, e.g., either equilibrium or transient studies are chosen, and all or only parts of the four model components may be included. In some cases, the original model code is adapted or extended to answer a particular question. All interactions of the biosphere with the other components of the climate system that are described in detail in the following can be simulated by this Earth system model.

Radiative forcing from albedo changes. The biosphere and atmosphere interact via a multitude of mechanisms, which can all be altered by ALCC. Generally,

two groups of mechanisms are distinguished, biogeophysical and biogeochemical ones [Claussen, 2004]. Biogeophysical mechanisms describe the influence on climate by the modification of the physical properties of the land surface such as albedo, roughness, and evapotranspiration. Both morphological and physiological properties of the vegetation cover are therefore important for the biosphere-atmosphere fluxes of energy, momentum, and substances like water. An immediate impact on the energy balance is induced by albedo changes. Albedo, the “reflectivity” of the land surface, usually increases with ALCC that implies deforestation, due to the higher snow-free albedo of non-forest vegetation and the snow masking effect of forest [Bonan et al., 1992]. The difference is particularly large during the winter and spring season for those areas with snow cover, where albedo may change from 0.2 for forest to 0.8 on an open field [Robinson and Kukla, 1984]. Only in cases with dark underlying soil albedo may decrease, when the vegetation cover is sparser under agricultural use. An increase in albedo decreases the absorption of solar radiation and thereby reduces turbulent heat fluxes [Pitman et al., 2004]. A decrease in the latent heat flux may decrease the water vapor content in the boundary layer, while holding back water in the soil or increasing runoff. A decrease in the sensible heat flux may reduce the heating of the boundary layer. Both may decrease cloud cover (a potential negative feedback on net radiation by decreasing planetary albedo) and convection [Bonan, 2002]. The reduction in absorbed solar radiation and heat fluxes also has consequences on surface temperature. Modeling studies suggest that through these biogeophysical effects ALCC at mid- and high latitudes induces cooling [e.g., Bonan et al., 1992, Claussen et al., 2001, Bounoua et al., 2002].

A common measure to quantify the biogeophysical implications of ALCC is radiative forcing (RF). RF, in W/m^2 , is a convenient first-order measure of the importance of a perturbation in causing climate change. It is defined as the radiative flux change of the tropopause after the stratospheric temperature has come to a radiative equilibrium, but prior to any feedbacks [e.g., Hansen et al., 1997]. It is convenient because the RF, ΔF can be related to the change in global mean surface temperature, ΔT , in a simple linear equation:

$$\Delta T = \lambda \cdot \Delta F . \quad (1.1)$$

The climate sensitivity parameter λ is usually determined for each model from the equilibrium change of global mean surface temperature in a simulation forced by 2-CO_2 . Typical values of λ lie in the range of $0.5\text{--}1.1 \text{ K}/(\text{W}/\text{m}^2)$ [Meehl et al., 2007]. Two advantages of the RF measure are: (1) It is computationally less expensive than the full climate response. For greenhouse gases, for example, it implies only a double-calculation of the radiative transfer scheme in the same climate. (2) RF is less model-dependent than the climate response: Questions like “what are the consequences of a doubling of CO_2 ?” result in very different answers from different models. The reason for this lies in different parameterizations of important feedbacks like changes in water vapor, cloud properties, sea ice and snow extent. Excluding any feedbacks, the RF implies a smaller uncertainty than the climate response. It therefore allows one to more objectively compare perturbations of different nature in

their climatic importance. The RF measure has been successfully applied to classic climate perturbations such as well-mixed greenhouse gases and solar variability. It has also become the standard tool to compare the importance of ALCC to other perturbations, despite known shortcomings in this application (see Sec. 3.1). With respect to ALCC, RF is used as a predictor of the climate response towards all biogeophysical effects of ALCC, although it is determined only for the changes in surface albedo.

In Chapter 3 the RF measure is applied to ALCC for the entire last millennium, with the following objectives:

1. To give a measure of the climatic importance of preindustrial ALCC that can be compared consistently to estimates of the last two to three centuries, for which there exist studies.
2. To compare the importance of preindustrial ALCC to concurrent, natural climate perturbations such as volcanic eruptions and solar variability.

These two first items give a first-order answer to the question of whether ALCC could indeed have significantly altered preindustrial global or hemispheric mean temperature and be responsible for the Northern Hemisphere cooling.

With the help of the high-detail ALCC reconstruction from Chapter 2, new insight is gained in the regional distribution of the anthropogenic climate perturbation and the temporal evolution over the preindustrial period. This allows

3. To indicate “hot spots” of the perturbation of the energy balance a millennium ago and their change through history. As mentioned above, the agricultural centers shifted regionally with time, which prohibits us to infer the history from the present state.
4. To follow the change of forcing pattern over history and to assess the effects of historic events on the energy balance.

This chapter has been published in *Geophysical Research Letters* [Pongratz et al., 2009].

Biogeochemical effects of anthropogenic land cover change. In addition to the biogeophysical mechanisms, the biosphere interacts with atmosphere and ocean via various biogeochemical cycles. Biogeochemical mechanisms of ALCC involve the emissions of methane (CH₄) [e.g., Hein et al., 1997], emission of aerosols from biomass burning and dust [e.g., Andreae and Merlet, 2001], and influence on nutrient cycles such as nitrogen, iron, and phosphorus cycles [e.g., Galloway et al., 1995, Denman et al., 2007]. Plants further interact with the carbon cycle via the emissions

of biogenic volatile organic compounds (BVOCs), reactive carbon compounds that affect aerosol formation and atmospheric chemistry, influencing e.g. ozone concentration [Fehsenfeld et al., 1992, Andreae and Crutzen, 1997].

The most important biogeochemical effect, however, through which the biosphere influences present climate change, is the altered exchange of CO₂ with the atmosphere [Denman et al., 2007]. By altering the atmospheric concentration of the greenhouse gas CO₂, ALCC modifies the Earth's energy balance and thus climate. On the one hand, the CO₂ flux from the biosphere to the atmosphere is increased by ALCC, mostly caused by a loss of terrestrial biomass. About one third of the anthropogenic CO₂ emissions over the last 150 years are the direct result of ALCC [Houghton, 2003]. Counteracting the emissions, on the other hand, is an enhanced uptake of CO₂ during photosynthesis by both natural and agricultural vegetation. The underlying increase in productivity is presumably caused, among other factors, by CO₂ fertilization: Experimental studies of the physiological response of plants to increased ambient CO₂ indicate increased photosynthetic rates and reduced stomatal conductance. This effect is larger for plants with a C3 photosynthetic pathway (trees and the majority of mid- and high-latitudinal herbaceous plants) than for those with a C4 photosynthetic pathway (tropical herbaceous plants) [e.g., Bazzaz, 1990].

The net effect is that the terrestrial biosphere has turned from a source to a sink during the recent decades; quantifications of the individual fluxes have been cited in Sec. 1.1. This quantification is crucial for understanding past and present climate change, and for potentially mitigating future changes, but still involves large uncertainties (see Sec. 4.1). Considering the long lifetime of atmospheric CO₂, it is further important to cover the long history over which the perturbation of carbon fluxes may have accumulated. Last but not least, it is crucial to take into account that the biosphere is just one of three interacting compartments; the coupling of ocean, atmosphere, and biosphere needs to be taken into account to assess the influence of ALCC on the global carbon cycle.

In Chapter 4 the effects of ALCC on the carbon cycle are assessed in detail in coupled model simulations, with the following main goals:

1. To assess the historical effects of ALCC on temperature and the carbon cycle in an isolated form, i.e. isolated from other forcings. This requires an idealized modeling study, in which only ALCC is allowed to change.
2. To quantify both source and sink terms of carbon: An estimate will be given for primary CO₂ emissions from ALCC, which are not known in high temporal resolution prior to AD 1850. In addition to carbon emissions, uptake in the ocean as well as by biospheric restorage will be quantified spatially for different eras. This leads to estimates of how much ALCC mitigated its own carbon signal in different time periods.
3. To determine the beginning of significant human influence on the individual

carbon pools, including atmospheric CO₂. Thus, Ruddiman's hypothesis of the early anthropogenic impact will be assessed. The setup of the simulations allows such an assessment at unprecedented detail.

4. To determine whether historic events could indeed have been responsible for drops in CO₂ as reconstructed from ice core records, and if not, which processes inhibit a detectable signal. The medieval Black Death in Europe, the Mongol invasion, and the fall of the Ming Dynasty in China will be assessed.

This chapter has been submitted to *Global Biogeochemical Cycles* [Pongratz et al., submitted].

Biogeophysical effects of anthropogenic land cover change. The previous part focuses on the carbon cycle, but the simulations performed include the biogeophysical mechanisms in addition to the biogeochemical mechanisms. Temperature and turbulent heat fluxes may be altered by the increase in albedo, as explained above. But further biogeophysical processes are at work in the coupled system: First, ALCC alters roughness length. Surface roughness length is a measure for the drag force that the land surface exerts on the the lowest layer of the atmosphere; the aerodynamic resistance impeding the transfer of momentum and scalar properties such as heat, water vapor, and CO₂ depends inversely on the roughness length. Deforestation usually reduces roughness length, resulting in higher aerodynamic resistances and smaller fluxes for otherwise identical conditions [e.g., Bounoua et al., 2002, Pitman et al., 2004]. Second, fluxes of water are also directly influenced by vegetation as it controls the availability of water for evapotranspiration. ALCC alters the photosynthetic activity on leaf and canopy level, e.g. by a change of the photosynthetic pathway between C3 and C4 or a change in phenology and leaf area index. Coupled to the photosynthetic activity are the stomatal and canopy conductances, which control the transpiration of the plant and canopy. ALCC may therefore alter the amount of water transpired, and influences thereby soil moisture, runoff, and the partitioning of energy into latent and sensible heat fluxes. Via stomatal conductance and photosynthesis, the fluxes of carbon and water through the plants are coupled [e.g., Sellers et al., 1992]. As indicated in Sec. 1.1, via reduced evapotranspiration ALCC may lead to a warming counteracting the cooling effect of albedo changes, which may regionally add to a net warming or cooling effect.

In Chapter 5 the climate change from the biogeophysical mechanisms of ALCC is quantified on regional and global scale for the last millennium. The same methods and data are applied as in Chapter 4; this implies not only an analysis of the biogeophysical effects of historical ALCC at unprecedented detail, but it also allows a consistent comparison of the strength of biogeophysical and biogeochemical effects in their influence on climate and the carbon cycle. This chapter presents

new results for the biogeophysical aspects of historical ALCC, but is also a synopsis of the previous parts of this thesis with the following goals:

1. The strength of the climatic response to biogeophysical mechanisms will be compared to that of biogeochemical mechanisms for past and present, thereby answering the question whether global mean temperatures have been dominated by biogeophysical or biogeochemical effects of ALCC. A spatially explicit analysis identifies strength and sign of regional contributions to the global signal. The biogeophysical response of the model is analyzed and compared to other models.
2. A substantial influence of ALCC on carbon source and sink terms has been found in Chapter 4. Here, the question is answered whether biogeophysical effects of ALCC contribute to the disturbance of carbon pools.
3. Two forcings of ALCC have been quantified: RF from albedo changes in Chapter 3, and CO₂ emissions in Chapter 4. Their counteracting strength is assessed and compared to the temperature responses to biogeophysical and biogeochemical mechanisms. The question is answered whether the forcings are a good indicator for the individual and overall temperature responses.
4. As outlined in Sec. 1.1 ALCC features prominently as tool for climate change mitigation. Considering that different mechanisms are counteracting each other it is not clear whether ALCC in a specific geographical location results in a cooling or warming contribution to global climate change. The net radiative contribution of ALCC to global climate change will be quantified in a geographically explicit form, indicating whether a local reversion of ALCC could mitigate climate change.

Parts of this chapter are in preparation for submission to *Geophysical Research Letters*.

Chapter 2

A Reconstruction of Global Agricultural Areas and Land Cover for the Last Millennium

Abstract

Humans have substantially modified the Earth's land cover, especially by transforming natural ecosystems to agricultural areas. In preindustrial times, the expansion of agriculture was probably the dominant process by which humankind altered the Earth system, but little is known about its extent, timing, and spatial pattern. This study presents an approach to reconstruct spatially explicit changes in global agricultural areas (cropland and pasture) and the resulting changes in land cover over the last millennium. The reconstruction is based on published maps of agricultural areas for the last three centuries. For earlier times, a country-based method is developed that uses population data as a proxy for agricultural activity. With this approach, the extent of cropland and pasture is consistently estimated since AD 800. The resulting reconstruction of agricultural areas is combined with a map of potential vegetation to estimate the resulting historical changes in land cover. Uncertainties associated with this approach, in particular owing to technological progress in agriculture and uncertainties in population estimates, are quantified. About 5 million km² of natural vegetation are found to be transformed to agriculture between AD 800 and 1700, slightly more to cropland (mainly at the expense of forested area) than to pasture (mainly at the expense of natural grasslands). Historical events such as Black Death in Europe lead to considerable dynamics in land cover change on regional scale. The reconstruction can be used with global climate and ecosystem models to assess the impact of human activities on the Earth system in preindustrial times.

2.1 Introduction

One of the most striking impacts of humankind on its environment is the transformation of natural ecosystems to managed areas. At present, 30–50% of the Earth’s land cover have been substantially modified by human land use, primarily by the expansion of agriculture [Vitousek et al., 1997]. By 2003, about 15 million km² of cropland and 34 million km² of pasture have replaced natural land cover [FAO, 2007], providing much of the ecosystem goods and services humanity has become dependent on. Such large-scale modifications of the land surface can have important consequences for the Earth system, most notably through their impact on ecological functioning, and the biogeophysical and biogeochemical interactions with the atmosphere. Significant changes in structure and functioning of ecosystems and a loss of biodiversity have already been attributed to human interference [UNEP, 1995, Haberl et al., 2007]. Energy balance and hydrological cycle are significantly affected by present-day land use activity [Betts, 2001, Davin et al., 2007], and global carbon and nitrogen cycles have been altered severely [Galloway et al., 1995, Denman et al., 2007]. For example, about 35% of anthropogenic CO₂ emissions during the last 150 years resulted directly from land use [Houghton, 2003], making it one of the key agents of anthropogenic climate change. Recognition of land use as a possible way to mitigate climate change and the increasing concern of the scientific community about the availability of natural resources has further brought the consequences of human-induced land cover change to public awareness [Millennium Ecosystem Assessment, 2005, Barker et al., 2007].

Given the growing evidence of the impact anthropogenic land cover change exerts on the Earth system, it is not surprising that today much effort is put into quantifying these changes. In recent years, remote sensing offers a valuable tool for monitoring land cover change [Townshend et al., 1991, Brown de Colstoun et al., 2006]. Historical data of agricultural activity allow rather solid estimates for the last 300 years [Ramankutty and Foley, 1999, Klein Goldewijk, 2001]. By contrast, quantifications of global land cover change prior to AD 1700 are scarce, although it is well known that humans have actively managed and transformed the world’s landscapes already for millennia [Grigg, 1974]. It is also recognized that these preindustrial land cover changes may have significantly contributed to the variability of atmospheric composition observed from ice core records [DeFries et al., 1999, Ruddiman, 2007]. Yet, the strength of human impact is still highly controversial [Joos et al., 2004]. Much of the dispute is centered around the lack of knowledge concerning extent, timing, and spatial pattern of historical land cover change. Those studies that have so far accounted for anthropogenic land cover change in preindustrial times in global and regional Earth system studies used the simplification to either keep land cover fixed prior to the 18th century (e.g. Stendel et al. [2006], Tett et al. [2007]) or to linearly interpolate between potential vegetation in AD 1000 and the state of land cover of AD 1700 (e.g. Brovkin et al. [1999], Goosse et al. [2006]). Both approaches, however, entirely disregard any detail of human history.

In this study, we present the first detailed reconstruction of global agricultural

areas (cropland and pasture) and the resulting changes in land cover over the last millennium. Special emphasis is placed on the preindustrial period, as it has not been subject of consistent analysis before. In the time period between AD 800 and the early 18th century, the world's population tripled [McEvedy and Jones, 1978]. As more people required more food and commodities from agriculture and natural resources, this period must have been associated with agricultural expansion at an unprecedented pace [Grigg, 1974, Richards, 1990]. As reliable data on historical agricultural areas is sparse, we develop a simple method for its reconstruction based on population estimates. Agriculture is inherently linked to population [Vasey, 1992], which allows us to use country-based estimates of historical population as proxy for agricultural areas. With this method, the cropland and pasture maps of Ramankutty and Foley [1999] and Foley et al. [2003] at 0.5 degree resolution for the last 300 years are extended back into the past to give consistent estimates of cropland and pasture since AD 800 on a geographically explicit basis. This “millennium reconstruction” of agricultural areas is combined with a map of potential vegetation to also estimate historical changes in land cover.

The reconstruction of agricultural areas is restricted to cropland and pasture. For cropland, the definition of “arable and permanent crops” from the Food and Agricultural Organization (FAO) is adopted, which includes land under temporary and permanent crops, temporary meadows for mowing or pasture, land under market and kitchen gardens, and land lying temporarily fallow. The abandoned land resulting from shifting cultivation is not included. For pasture, the FAO category “permanent pasture” is used. It includes all land used permanently for herbaceous forage crops, either cultivated or growing wild.

The following sections describe in detail the different steps taken to reconstruct global agricultural areas and land cover for the last millennium. These steps are summarized in Fig. 2.1.

2.2 Step 1: Adaptation of agricultural data since AD 1700

Recent years have seen an increasing interest in developing data sets of agricultural areas covering at least the entire industrial period. Most noteworthy are the achievements of the Center for Sustainability and the Global Environment (SAGE), University of Wisconsin [Ramankutty and Foley, 1999, Foley et al., 2003] and the History Database of the Global Environment (HYDE), Netherlands Environmental Assessment Agency [Klein Goldewijk, 2001]. These are high-resolution maps of cropland and pasture for the last three centuries based on various contemporary and historical statistical inventories on agricultural land. Different spatial allocation algorithms were applied to provide geographically explicit maps, intended in the first place for the use in ecosystem, climate, and integrated models. In the following, we describe how we integrate these maps into a single consistent data set for cropland and pasture for AD 1700 to 1992 (Step 1 of Fig. 2.1). We thereby rely on the

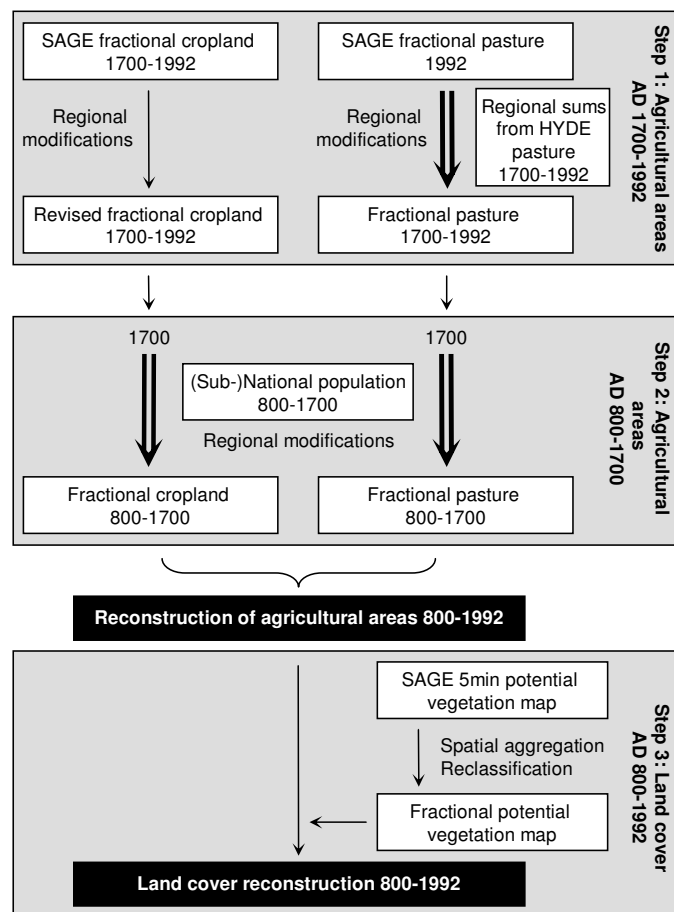


Figure 2.1— Scheme for reconstructing agricultural areas and land cover AD 800 to 1992. Double arrows indicate linear backscaling.

SAGE data where possible as its fractional character supplies additional sub-grid information.

2.2.1 Cropland

Ramankutty and Foley [1999] developed a simple algorithm to link present remote sensing data and historical cropland inventories. Inventory data was compiled on the level of today's political units (subnational data for some of the largest countries) and is based on data published by the Food and Agricultural Organization (FAOSTAT) for 1961-1992 and a variety of sources for earlier times, most notably estimates from Houghton and Hackler [1995] and Richards [1990]. We use their time series AD 1700 to 1992 of global croplands for the millennium reconstruction, but apply some revisions. First, we replace the West Africa region by the improved regional data set of Ramankutty [2004], which we extend to previous years using

population trends [Klein Goldewijk, 2001]. We apply some further corrections of the cropland pattern in the 18th and 19th century for specific regions to better match historical evidence. They were necessary in order to provide suitable maps as starting point for the reconstruction of earlier centuries. In particular, the lack of subnational data in the Former Soviet Union (FSU) led to maintenance of the 1992 crop pattern and to significant crop area in Siberia in historical times. We redistribute total crop area using subnational population data derived from McEvedy and Jones [1978] and United Nations Statistics Division [2006]. In a similar way, the crop pattern of Australia and New Zealand are adjusted to reflect the history of European immigration (for details see Pongratz et al. [2008a]).

2.2.2 Pasture

For global pastures, where SAGE provides only a single map for 1992, we extend this data to a time series AD 1700 to 1992. First, we calculate regional totals of pasture area for each year from the 1992 areas and rates of change from Klein Goldewijk [2001]. Calculations are performed on country level after 1960 and for the 10 regions defined by Houghton et al. [1983] prior to 1960 adapting the same regional breakdown as has been used for the temporal information of HYDE. For each year, the pasture totals are then distributed spatially within each country or region. While the method of Ramankutty and Foley [1999] to extend the 1992 map of cropland back into the past was to generally maintain the 1992 pattern of cropland throughout time (i.e. the grid cells within a country keep their cropland fractions in the same proportion relative to each other, while the total area changes with time), we chose a different method for pasture. The pasture area is thereby distributed around the existing cropland in a way that not the pattern of pasture, but of total agricultural area (cropland plus pasture) is maintained throughout time. The advantage of this method is that it allows to take into account the expansion of crop on pasture area that has been observed in the past [Grigg, 1974]. The modifications applied to the crop time series concerning Australasia are also applied to the pasture time series. The modifications concerning the FSU are unnecessary as the pasture areas here are connected to the extensive areas of traditional nomadic pastoralism of Kazakhstan and Mongolia [Kerven et al., 2006].

2.3 Step 2: Reconstruction of agricultural areas AD 800 to 1700

Statistical databases built by international organizations and, more recently, remote sensing provide us with data and methods to consistently measure agricultural areas and land cover change of the last decades. Great efforts have been undertaken to extend this data back into the past; most notable with respect to its global coverage is the work by Houghton [1999], who compiled a multitude of regional studies related to historical land cover, and the data compilation by Richards [1990], which are basis

also of the SAGE and HYDE studies. However, sources which address more than the local level become scarce when going back in time and rarely go beyond AD 1650. Thus, we search for a proxy for agricultural area for which historical data is more readily available on global scale.

We therefore utilize in this study the fact that agriculture is inherently linked to population. Prior to the 19th century, technology played a minor role in resource extraction, and transportation was a limiting factor in preindustrial times for trading large quantities of agricultural input and output over long distances [Vasey, 1992]. Even if most societies had outgrown individual subsistence farming, autonomy for basic needs still had to be largely realized on a regional level [Allen, 2000]. It is therefore appropriate to assume that agriculture occurred where people had settled, and the amount of land under human use is likely well correlated to the number of people who had to be nourished. For this reason, we use population estimates as proxy for agricultural areas. Information on historical population numbers are much more readily available than on land cover; our main source of population data for AD 800–1700 is the Atlas of World Population History by McEvedy and Jones [1978], with regional modifications for Central and South America based on Clark [1967]. McEvedy and Jones provide totals for most of today’s countries from 400 BC to AD 1975 based on a multitude of publications and support their estimates with short essays stressing among others the role of agriculture. Where only data for larger regions is provided, we break the historical numbers down to country level using the HYDE population density map of AD 1700, assuming that the national proportions within a region remain constant. For some regions, sub-national data was used, especially for the FSU and Central and South America. In the latter region, national numbers are broken down to better represent the spatial heterogeneity between the high cultures, with a significantly higher population density, and other tribes in pre-Columbian times (for details see Pongratz et al. [2008a]).

Population numbers are then translated for each country into estimates of crop and pasture area. In the absence of further information, it seems inappropriate to use anything more than the simplest assumptions. Thus, our basic assumption is that in each country the ratio of area used per capita for crop and pasture did not change prior to AD 1700. This ratio — the inverse of the nutritional density — is calculated for AD 1700 from the earliest agricultural map of the 300-years series described in Sec. 2.2 and our population database. Today’s political borders, with a few subnational divisions where necessary, were chosen in order to be consistent with the scale of Ramankutty and Foley [1999] and to allow for easy comparison with today’s statistical data. Using population as proxy for agricultural areas is not a new approach; it has been suggested e.g. by Ramankutty et al. [2006] and has been applied to more recent times by Houghton [1999]. Possible errors resulting from this method will be discussed in Sec. 2.5.

In order to convert national totals of crop and pasture area to geographically explicit information, we make a second basic assumption: The pattern of agricultural areas that we observe in each country in AD 1700 (Figs. 2.2 and 2.3) is similar to earlier spatial patterns. The persistence of the agricultural pattern in each coun-

try through time is a basic assumption in claiming only that the relative intensity of agricultural use within one country does not change between pixels. In other words, this generally means that suitable areas are cultivated more intensively than less suitable ones within a country, independently of total cultivated area. The supra-national pattern, however, is reconstructed independently each year from the population-based national estimates of agricultural areas. Within the accuracy of the AD 1700 global pattern, the relative importance between countries is thereby correctly represented in earlier times. While human migrations across political borders are implicitly taken into account by using country-based population data, the shift of settlement and cultivation pattern within the countries of the Americas after the European conquest is explicitly corrected for (see below).

The existing time series is scaled back in time, combining the above stated key assumptions with the agricultural areas and population numbers of AD 1700 on national level (step 2 of Fig. 2.1): The total area of agriculture of a country — cropland and pasture are each treated separately — is calculated for each year from the agricultural area per capita and historical population. The pattern of AD 1700 determines the relative fractions of the agricultural area of the pixels within a country. In countries where agricultural area in earlier years exceeds the AD 1700 value it may occur that the agricultural fractions of single pixels becomes larger than 1. For these timesteps the surplus cropland or pasture area is redistributed among the other pixels relative to their fractions such that the total agricultural area of the country is conserved. Since we keep agricultural area per capita constant throughout time, we call the resulting millennium reconstruction the “persistent” estimate in the following.

For some regions it is well known that agricultural pattern or practices changed severely over time. With such knowledge we had already modified the original crop time series by Ramankutty and Foley; the new patterns of agriculture we introduced are also propagated back in time when extending the time series to AD 800. For the Former Soviet Union, we continue to provide population data on subnational level in the same way as in Sec. 2.2. Some more modifications had to be made in regions where not only pattern but also agricultural methods changed prior to AD 1700. This includes the establishment of agricultural tribes in New Zealand, and the colonization of the Americas. In the latter, European conquest was extremely effective in fundamentally replacing traditional cultures with the ones of the invaders. The pattern of agriculture we observe in AD 1700 thus already reflects much of the European influence. We implement these historical changes in agricultural pattern by using subnational population data, which allow to represent the change in population pattern after European conquest. We further abandon the figures for agricultural area per capita derived from the AD 1700 map prior to colonization, acknowledging that the European agricultural behavior is inherently different from the native one, and use independent estimates from literature instead. Details can be found in [Pongratz et al. \[2008a\]](#).

2.4 Step 3: From agricultural areas to land cover

So far, the reconstruction of a time series of agricultural areas was described, indicating area and pattern of global cropland and pasture over the course of the last millennium. For many applications involving human impact on natural ecosystems and the climate, it is essential to know the land surface properties before agriculture emerged or after it ceased. For this purpose, the reconstruction of agricultural areas can be overlaid over maps of natural vegetation. Data source and vegetation types can be freely chosen according to the application, but an allocation scheme of agriculture on natural vegetation has to be developed. One possible method is outlined below and uses 11 natural vegetation types as background to the agricultural classes. These are part of the data set published by the World Data Center for Climate and can be used in addition to the agricultural information.

Step 3 in Fig. 2.1 outlines the transformation of the reconstruction of agricultural areas into a land cover reconstruction. In this study, we use the 5 min resolution potential vegetation classification described by [Ramankutty and Foley \[1999\]](#), which is consistently derived from the same sources as their agricultural maps. We first reclassify the 15 existing classes into 11 natural vegetation types on the basis of the descriptions of the cover types, which in many cases is straightforward. Mixed classes are assigned to several types based on bioclimatic criteria [[Pongratz et al., 2008a](#)]. The reclassified data set is then aggregated from 5 min to 0.5 degree resolution. In a next step, agriculture is introduced into the potential vegetation map. Different methods are used for crop and pasture to determine how much each vegetation type in each 0.5 degree grid cell is affected by agriculture. For crop, we compare 5 min resolution crop cover maps (N. Ramankutty, personal communication) for each year with the reclassified 5 min potential vegetation. This comparison indicates what fraction of each vegetation type in a half degree pixel is lost to crop. Prior to AD 1700, the proportions of area lost to crop between the natural types are kept constant as far as possible. Only in cases where the crop area assigned to a certain vegetation type exceeds its area, the surplus crop area is proportionally distributed on the other types. For pasture, where no sub-grid information is available, we assume a certain land cover priority. Pasture is first allocated on grass as far as possible, then on the area of the woody vegetation types. This procedure reflects human behavior of minimizing effort: Clearing of forest is generally not performed if sufficient natural grassland is available for grazing [[Houghton, 1999](#), [Ramankutty et al., 2006](#)]. The resulting changes in land cover over the course of the last millennium can be found in Tab. 2.1, where the natural vegetation types are aggregated to 5 more general classes.

Abandoned agricultural area is attributed to the type of natural vegetation indicated by the potential vegetation data set. The different structure of this secondary vegetation compared to primary one, specifically the gradual regrowth of vegetation, needs to be adequately represented when the proposed land cover reconstruction is used to derive land surface properties. Many biosphere models allow for these gradual transitions. In such cases errors are limited to abandoned agricultural area

Table 2.1— Estimated global extent of land cover types (in 10⁶ km²). Values in brackets are estimates disregarding pastures.

	Potential					
	vegetation	800	1100	1400	1700	1992
Tropical forest	22.44	22.03 (22.07)	21.87 (21.93)	21.70 (21.78)	21.22 (21.36)	16.30 (18.24)
Temperate broadleaf forest	10.48	10.15 (10.19)	9.92 (10.00)	9.87 (9.97)	9.26 (9.47)	5.95 (6.71)
Temperate needleleaf forest	15.75	15.61 (15.63)	15.51 (15.55)	15.47 (15.52)	15.17 (15.27)	12.36 (12.98)
Total forest	48.68	47.78 (47.89)	47.31 (47.47)	47.05 (47.26)	45.65 (46.09)	34.60 (37.93)
Grass and shrubs	46.79	44.90 (46.23)	44.22 (46.04)	43.84 (45.89)	42.14 (45.39)	13.63 (38.89)
Tundra	4.08	4.07 (4.07)	4.06 (4.07)	4.06 (4.06)	4.05 (4.06)	2.94 (3.98)
Total natural vegetation	99.55	96.75 (98.19)	95.60 (97.58)	94.95 (97.22)	91.84 (95.54)	51.16 (80.80)
Crop	—	1.36 (1.36)	1.97 (1.97)	2.33 (2.33)	4.01 (4.01)	18.76 (18.76)
Pasture	—	1.44 (0.00)	1.98 (0.00)	2.27 (0.00)	3.70 (0.00)	29.63 (0.00)
Total agriculture	—	2.80 (1.36)	3.95 (1.97)	4.60 (2.33)	7.71 (4.01)	48.39 (18.76)

that does not return to potential vegetation, e.g. where forest re-establishment is inhibited through degraded soil conditions.

2.5 Assessing uncertainty and validity

The method developed in this study relies on only few, basic assumptions when historical sources and modern estimates fail to provide the necessary information. The aim is to keep methods, results, and uncertainties at any time straightforward and comprehensible. In the following, we discuss sources of possible errors and assess uncertainties associated with data and method.

2.5.1 Inclusiveness of the millennium reconstruction

This study focuses on anthropogenic land cover change that permanently changes the type of vegetation, taking into account the permanent expansion and abandonment of cropland and pasture. Two important land use types, however, are not included: (1) Wood harvesting is not considered in this study. Our reconstruction can be combined with wood harvest data once such statistics become available for preindustrial times, but it should be kept in mind that the clearing of forest for timber or fuelwood is not an entirely independent land use alongside agriculture. A part of the area cleared for wood harvest is subsequently used for agriculture, and another part is quickly regrown in a system of managed forest and does therefore not represent a permanent change of the type of vegetation. (2) The long-term fallow area that results from shifting cultivation is not covered by this study. A sensitivity analysis [Hurt et al., 2006] showed that the omission of shifting cultivation may lead to a significant underestimation of secondary land area created by agriculture, but the very high resolution data needed to resolve such small-scale processes is usually not available for large regions. However, shifting cultivation only increases the area undergoing gross transition, while net transition, as represented by our data set, is unaffected. Similarly, the representation of wood harvest would only alter the area of undisturbed vegetation, but not the area estimates of cropland and pasture derived in this study. Therefore, our results for cropland and pasture remain valid within the accuracies discussed in the following, as long as no subnational and sub-grid information is derived.

2.5.2 Validation of the base data AD 1700 to 1992

Ramankutty and Foley [1998] compared their remote-sensing-based cropland map of 1992 to three other estimates and conclude that their data set provides a “reasonably accurate and quantitative depiction of croplands across the globe”. The SAGE maps have also been compared to the HYDE data for cropland in both present and historical times (for details, see Klein Goldewijk and Ramankutty [2004] and Ramankutty et al. [2006]). They are found to be generally consistent with HYDE in representing cropland over the last 300 years. A strong caveat of this comparison

is the fact that the two data sets are not entirely independent and partially rely on the same input data. The SAGE time series has further been proven to represent common knowledge about the evolution of cropland in different parts of the world [Ramankutty and Foley, 1999].

Few independent data sets exist that could be used to validate the pattern of pasture. It is often impossible to distinguish between pristine grasslands and such used for grazing (pasture) in observation data, and classification strongly depends on subtleties in definition. When compared to the HYDE data (revised version 3.0, K. Klein Goldewijk, personal communication), the present-day pasture extent of Foley et al. [2003] agrees well in Europe, America and Africa, though in the latter the HYDE data concentrates pasture more strongly in the Maghreb coast and the Sahel. Some differences exist in the Middle East. Especially the semi-desert and desert of the Arabian peninsula show much higher intensities of pasture in the HYDE data, while the SAGE map is more closely coupled to the maximum possible vegetation cover. We believe that this is the more appropriate pattern for historical times, where population pressure was low and less suitable areas did not have to be included into agricultural activity. The interior of the Australia continent is less intensely used for pasture in the SAGE data, but this discrepancy is unimportant for historical times as Aboriginal agricultural activity was very low. The most extensive pasture lands in Mongolia and Tibet are identified in both SAGE and HYDE 3.0, but with a higher intensity in the SAGE data. In our reconstruction, this high intensity reflects back to historical times.

We conclude that the overall pattern of cropland and pasture of Ramankutty and Foley [1998, 1999] and Foley et al. [2003] are in good agreement with other studies. This is an important point, as historical patterns are derived from present day data in both the SAGE approach and our method and errors would propagate to earlier times. Concerning total agricultural areas, some uncertainty exists not only for past, but also present times. In absolute numbers, the 1992 Ramankutty and Foley map used in this study (including the modifications described in Sec. 2.2) shows a cropland area of $18.8 \cdot 10^6$ km², while estimates by Richards [1990] for the year 1980 are $15.0 \cdot 10^6$ km², by Houghton [1999] for the year 1990 are $13.6 \cdot 10^6$ km², and by Klein Goldewijk [2001] for the year 1990 are $14.7 \cdot 10^6$ km² (note that all estimates partially rely on the same input data). The pasture map used in this study shows an area of $29.6 \cdot 10^6$ km² as opposed to the estimate of Klein Goldewijk [2001] for the year 1990 of $34.5 \cdot 10^6$ km². Obviously, notable uncertainties exist despite the growing availability of ground- and satellite-based observations and international statistical databases. We cannot assume that data uncertainties are any smaller between AD 1700 and 1992 than at present. As this time series is also the base data for our reconstruction, this uncertainty is passed on to all earlier time steps.

2.5.3 Uncertainty of the population data

Despite the long tradition of demographic research, no outright consensus exists concerning quantitative estimates of historical population, especially for times earlier

than the 18th century. Global numbers differ by up to a factor of two for the first millennium AD; regional estimates can be even more disputed. The data set predominantly used in this study [McEvedy and Jones, 1978] is largely acknowledged in recent literature and stands out through its consistency and high spatial and temporal resolution. The uncertainties introduced by the choice of this specific population database are estimated in the following.

The population database of this study is compared to six other historical estimates (Clark [1967], Biraben [1979], Maddison [2001], and high, mean, and low estimates by Durand [1977]). For the Americas, we further include the original data from McEvedy and Jones [1978] without our modifications. Data for the years AD 1000, 1500 and 1700 are used in aggregated form for four regions following Maddison [2001] (Tab. A.1). There is good agreement between the studies with respect to Europe and Asia, where estimates differ by less than a factor of 2 even for early years. Not surprisingly, however, large differences exist for Africa and the Americas, where much of the continents was still unexplored by the end of the 17th century. Still in debate, for example, is the number of native Americans prior to European arrival, where estimates range between 14 and 63 million, as well as the rate of population growth before.

The population dynamics of the temporally highly-resolved data used in this study are superimposed on the alternative estimates. Then, for each year and each region the two data sets are chosen that give the highest and lowest changes in population relative to their AD 1700 value. This method thus results in an uncertainty range around the population estimates used for the millennium reconstruction. It is important to note that the extreme ranges do not represent consistent time series of likely alternative scenarios. Rather, they indicate the entire range of possible estimates of agricultural areas for a given year, where the outer bounds can only be reached for a certain time period throughout the millennium, if at all. The maximum uncertainty range we assign to the persistent estimate due to uncertainties in population estimates, based on the described approach, for the year AD 800 is 1.1 to $1.6 \cdot 10^6$ km² around the persistent estimate of $1.4 \cdot 10^6$ km² for crop, and 1.1 to $1.7 \cdot 10^6$ km² around the estimate of $1.4 \cdot 10^6$ km² for pasture. In relative terms, the largest underestimation that could occur in AD 800 due to errors in the population data used in this study is in the Americas. Here, the high estimate of Durand [1977] does acknowledge that there has been significant decrease in population with European conquest, but believes in steadily high population before that. The largest overestimation of our study could occur in Africa. Here, Biraben [1979] suggests much stronger population dynamics prior to AD 1700 than all other data sets.

2.5.4 Effects of agrotechnical improvements

A major assumption of our approach in reconstructing historical agricultural areas is that the ratio of agricultural areas per capita did not change prior to AD 1700. Agricultural areas per person is the inverse of nutritional density and corresponds to land (not labor) productivity — per-area yields — in the absence of major dietary

changes and trade. Dietary changes and trade are considered to be minor drivers of changes in agricultural areas in the time period under investigation. Trade, specifically, was largely limited to high-value products such as silk, wool, and spices, unless water transport became possible, as costs of transport prior to the 19th century were too high to move general foodstuff [Grigg, 1974]. Theory predicts that land productivity increases within a civilization as agrotechnical innovations are continuously triggered through population pressure and shortages [Boserup, 1965, Sieferle, 1997], but published data is not sufficiently available for use in a consistent global analysis and is frequently in contradiction to theory [Slicher van Bath, 1963].

Nevertheless, an estimate of the uncertainties of the persistent estimate of the millennium reconstruction is desirable. For this, we recalculate crop area within a maximum range of possible changes in per-capita values of cropland. In these values, we try to not only include agrotechnical progress, but also regression due to land degradation and socioeconomic disturbances, changes in crop types, and changes in the fraction of population incorporated in an agricultural system for those regions where we know that these factors play a non-negligible role. Based on these factors, we try to give an upper and lower boundary of possible changes in per-capita cropland. Where available, we base our estimates on quantitative data, such as yield ratios from Slicher van Bath [1963] for European countries and nutritional densities cited in Grigg [1974] for East Asian countries. Where quantitative data is missing, we classify regions as one of three cases based on the information of Grigg [1974] and Vasey [1992]: regions with general decrease in per-capita cropland values (range of 0.7 to 1.7 in AD 800 relative to AD 1700 around the persistent estimate), with no change (0.5–1.5), and with general increase (0.3–1.3) (see Tab. A.2; for details see Pongratz et al. [2008a]). With these numbers, the time period under consideration is characterized as a period where the overall pace of technological change in farming has been “remarkably slow” [Grigg, 1974, p. 50] and most of the preindustrial increases in crop and animal production occurred as a result of increases in agricultural areas [Ruttan, 2002].

Changes in the per-capita use of pastures have not been assessed for historical times in literature. Here, we generally use the same ranges for pastures as for cropland. Most factors affecting changes in cropland per person will also affect the use of pasture. Changes in productivity will be less pronounced than for crop, but the general trend may be similar, since many agrotechnical improvements such as manuring can also be applied to forage crops and the number of draught animals per capita is linked to cropland productivity.

The maximum uncertainty range we assign to the persistent estimate due to changes in per-capita agricultural areas, for the year AD 800, is 0.8 to $2.2 \cdot 10^6$ km² around the persistent estimate of $1.4 \cdot 10^6$ km² for crop, and 0.8 to $2.1 \cdot 10^6$ km² around the estimate of $1.4 \cdot 10^6$ km² for pasture. Changes in the agricultural systems of the world thus introduce a significantly higher uncertainty in our approach than the decision for a specific population data set. Except for the Americas, this statement also holds true at regional level. This difference can largely be explained by the fact that population data itself is less uncertain than information on per-

capita agricultural area. The reasons for this include a greater administrative interest in documenting population throughout history in combination with a much better agreement on the definition of “population” than of “agricultural area” or “yields”. Furthermore, the spatial coverage is higher for population estimates, which are usually documented at a regional scale. On the other hand, information on the per-capita demand of agricultural area has to be extrapolated from local measurements and qualitative descriptions, which was done in a conservative way in this study. For the following analysis of historical land cover change, we combine both uncertainty factors, per-capita agricultural areas and population, in a way that results in the maximum possible range at every timestep in every part of the world. Joining highest agrotechnical progress with lowest population growth and vice versa give possible, but unlikely estimates of agricultural areas. This range of uncertainty assigned to the persistent estimate therefore does not indicate a range of equal preference, which would be much smaller. Instead, it is intended to define limits of possible errors in the estimates caused by our approach. We did not assign an uncertainty range to the base data AD 1700 to 1992, but it should be kept in mind that errors in the maps of AD 1700 propagate back in time (Sec. 2.5.2).

2.6 Changes in land cover AD 800–1992

We present our reconstructions in two ways: The full spatial information is depicted in the maps for historical crop and pasture in Figs. 2.2 and 2.3, shown for four time slices. More information about the temporal evolution of cropland and pasture are presented in Figs. 2.4 and 2.5. Here, the total areas of the agricultural types and the natural vegetation types are plotted for 10 world regions. The persistent estimates are surrounded by the range which was determined from the uncertainties in our method associated with population data as well as changes in per-capita agricultural areas (see Sec. 2.5). Additionally shown with the natural vegetation types is the persistent estimate for land cover change due to the expansion of cropland only, disregarding pasture. It is thus possible to separate the impact of changes in cropland on natural vegetation from the impact of changes in pasture.

We can compare the millennium reconstruction against the common knowledge about the history of agriculture in order to test its plausibility and interpret our results. The map for AD 800 (Fig. 2.2) clearly highlights the regions with the longest history of agriculture: High intensities of crop cultivation are found in the Mediterranean, the Fertile Crescent, and India. Large areas of cropland are also deduced for China. In all these regions, the domestication of crops or the spread of crops into the region had taken place thousands of years ago [Vasey, 1992]. On the other hand, many parts of the world show little human impact in the map of AD 800. Agriculture had developed early also in the Americas, but intensity remained low outside the centers of high cultures until Europeans arrived [Grigg, 1974]. Most of central Asia was not settled until the 19th century, and the agricultural tribes in Australasia were few and low in numbers [McEvedy and Jones, 1978]. Much

of Africa must still have been pristine in AD 800, but the continent competes in our reconstruction with India for the strongest and steadiest growth of cropland over all centuries in preindustrial times. At the same time, other regions experience repeated set-backs in their agricultural history, driven by political and economic instability as in China and Europe, by epidemics as in Europe and the Americas, or changes in cultural habit and environmental conditions as in Southwest Asia and the Mediterranean [Grigg, 1974]. By their impact on population, these events are captured by the millennium reconstruction.

The distribution of pasture is quite different from that of cropland in both historical and present times (Fig. 2.3). Some of the most important areas are found in AD 800 in Europe and Southwest Asia. Here, animals had been used early already as draught animals [Grigg, 1974]. Vast areas of pasture are found in the steppe and semi-deserts of Asia and the savannas of Africa. In these regions, animals were rarely incorporated in crop production, and nomadic pastoralism prevailed in preindustrial times, often persisting until today [Grigg, 1974]. As for crop production, general cultural development and historical events imprint their dynamics on the extent of pasture. The many factors that contribute to both pattern and changes of the extent of crop and pasture are highly variable through time and space.

Table 2.1 summarizes the human-induced changes of land cover on a global scale. By AD 800, $2.8 \cdot 10^6$ km² of natural vegetation have already been transformed to agricultural land, which is about 3% of the area potentially covered by vegetation. This transformation was almost equally caused by cropland and pasture, but both types of agriculture affected quite different ecosystems. On the one hand, $0.8 \cdot 10^6$ km² of pristine forest were cleared for the cultivation of crop, large parts of it in the temperate and the tropical broadleaf deciduous forests. On the other hand, $1.3 \cdot 10^6$ km² of pastures are located on areas that were naturally covered by grassland anyway and are thus not associated with major changes in the type of vegetation. By AD 1700, agricultural area has extended to $7.7 \cdot 10^6$ km²: $3.0 \cdot 10^6$ km² of forest have been cleared, 85% of this for cropland, the other 15% for pasture; $4.7 \cdot 10^6$ km² of grassland and shrubland are under human use, but only 30% are used for the cultivation of crop. Grassland, temperate and tropical broadleaf deciduous forest remain the most strongly affected ecosystems. Within the next 300 years, total agricultural area rises to $48.4 \cdot 10^6$ km², especially pasture expands. The ecosystems that lose the largest areas to human use are now natural grasslands, summergreen shrubs, temperate and tropical broadleaf deciduous forest and tropical evergreen forest. Between AD 800 and AD 1700, there were thus $4.9 \cdot 10^6$ km² of natural vegetation brought under agricultural use, compared to $40.7 \cdot 10^6$ km² in the following three centuries. Despite these largely different values we should not consider the land cover change during the early centuries of our reconstruction as irrelevant. First, the expansion of agriculture during these 900 years was likely much greater than during the millennia that had passed since the Neolithic Revolution, considering the strong population growth during this period and the steadily growing dominance of agriculture over hunting and gathering cultures. Secondly, there are significant differences between different parts of the world. Some regions developed amazing rates of agricultural

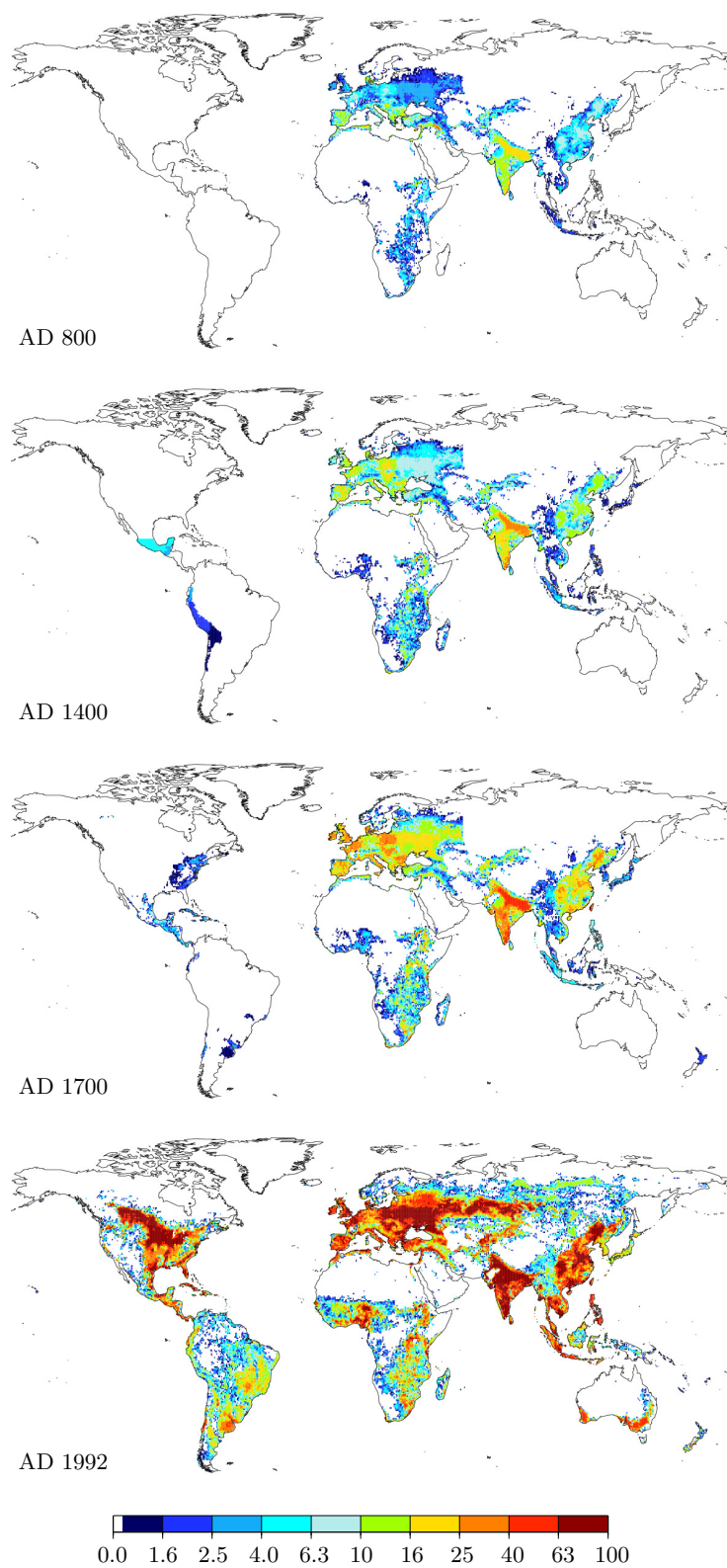


Figure 2.2— Global historical cropland area. Units are percent of grid cell. Values smaller than 1% are colored white. Note the logarithmic scale.

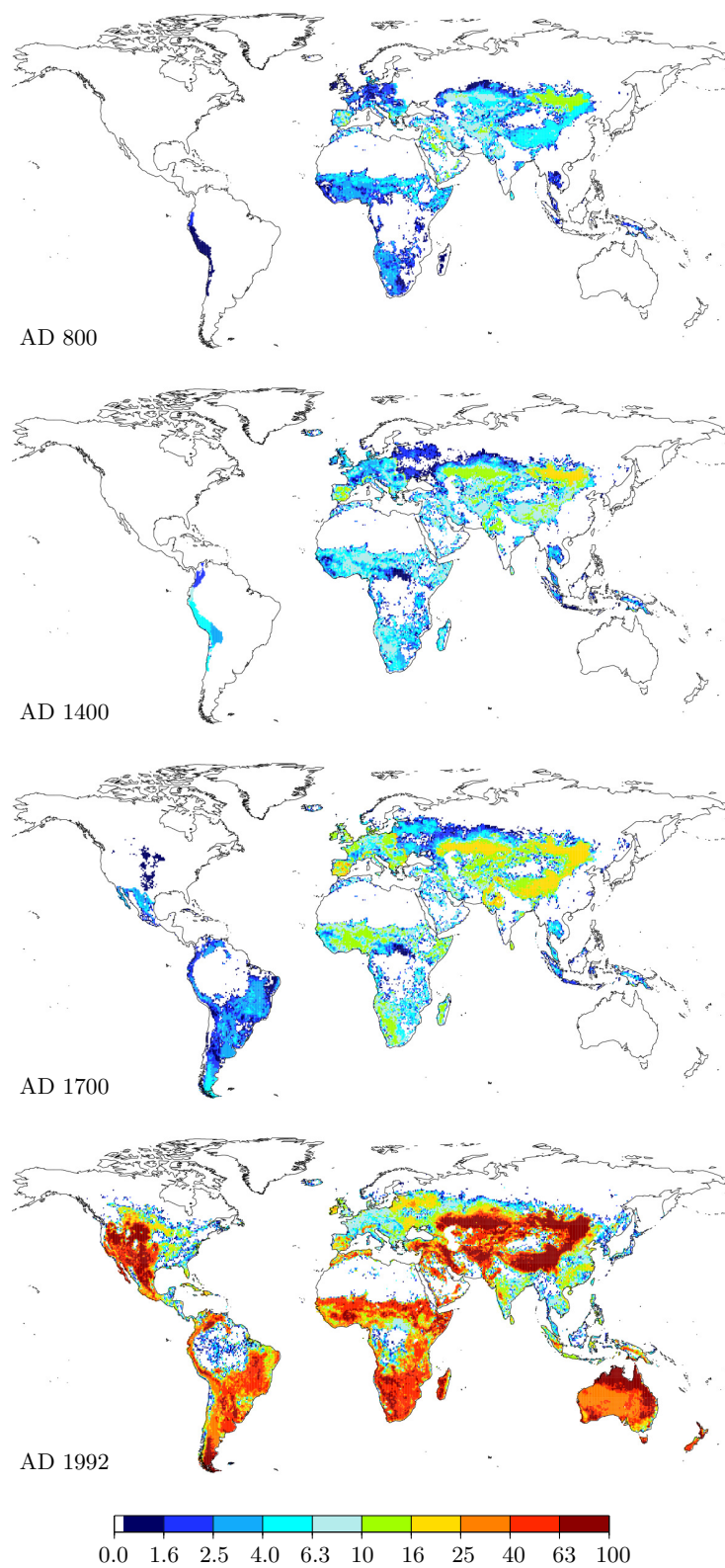


Figure 2.3— Global historical pasture area. Units are percent of grid cell. Values smaller than 1% are colored white. Note the logarithmic scale.

expansion that cannot be discerned on global scale, and regional dynamics, including decline of agriculture, are remarkable. In the following subsections, we present the reconstruction of agricultural areas on the regional level in the context of agricultural history. We will mainly focus on the time period prior to AD 1700; for details on the last 300 years we refer the reader to [Ramankutty and Foley \[1999\]](#).

2.6.1 Europe and Former Soviet Union

Farming and herding were spreading westward from the ancient centers of agriculture in Southwest Asia to Europe and reached the shores of the North and Baltic Seas as well as the Iberian peninsula by 4000 BC [\[Grigg, 1974\]](#). With about $3.2 \cdot 10^5$ km² of cropland and pasture in AD 800, Europe had become one of the agriculturally important regions of the world by early medieval times (Fig. 2.4). European agricultural colonization progressed fast until the 14th century and agrotechnical advances opened up land that was previously considered unsuitable for agricultural use [\[Crombie, 1977\]](#). The steady increase in agricultural area and the corresponding clearing of forest came to a sudden halt with Black Death, the plague epidemics AD 1347–53 that killed a quarter to a third of the population. In the following decades an estimated $2.3 \cdot 10^5$ km² of farmland were abandoned and allowed for some regrowth of forest (Fig. 2.5 a). Fast rates of land cover transformation were returned to in the 15th century, but agricultural expansion stagnated again in the early 17th century in Europe as a whole as a consequence of several regional processes, including the Thirty Years War and economic crises in the Mediterranean countries. A rapid expansion of cropland on forested areas dominated until the middle of the 19th century.

The large uncertainties of agricultural estimates in Europe are a consequence of the uncertain changes in land productivity rather than disagreement in population numbers. Technological progress was fast, especially in the Northwestern countries, but at the same time centuries had to pass before a useful innovation found widespread application, and more marginal land had to be brought under cultivation [\[Vasey, 1992\]](#). Still, we estimate total agricultural areas in the early centuries of the reconstruction more probably at the low than at the high end of the displayed uncertainty range.

While rates of change slowed down in most of Europe in recent decades and even allowed for regrowth of natural vegetation, notable land cover changes occurred in the FSU. In this region agriculture had mainly been restricted to the European part prior to the 19th century, when for the first time significant number of settlers started to colonize Siberia. Only Russian Turkestan looks back on an ancient history of agriculture with a strong predominance of pastoralism [\[Vasey, 1992\]](#). During 1940–1960 rapid land cover conversions took place in the FSU associated with the opening up of the “New Lands” [\[Ramankutty and Foley, 1999\]](#). While agricultural expansion took place mainly at the expense of forested regions in Europe, expansions in the FSU affected both forests and steppe and reduced natural grasslands to a fifth of their potential area.

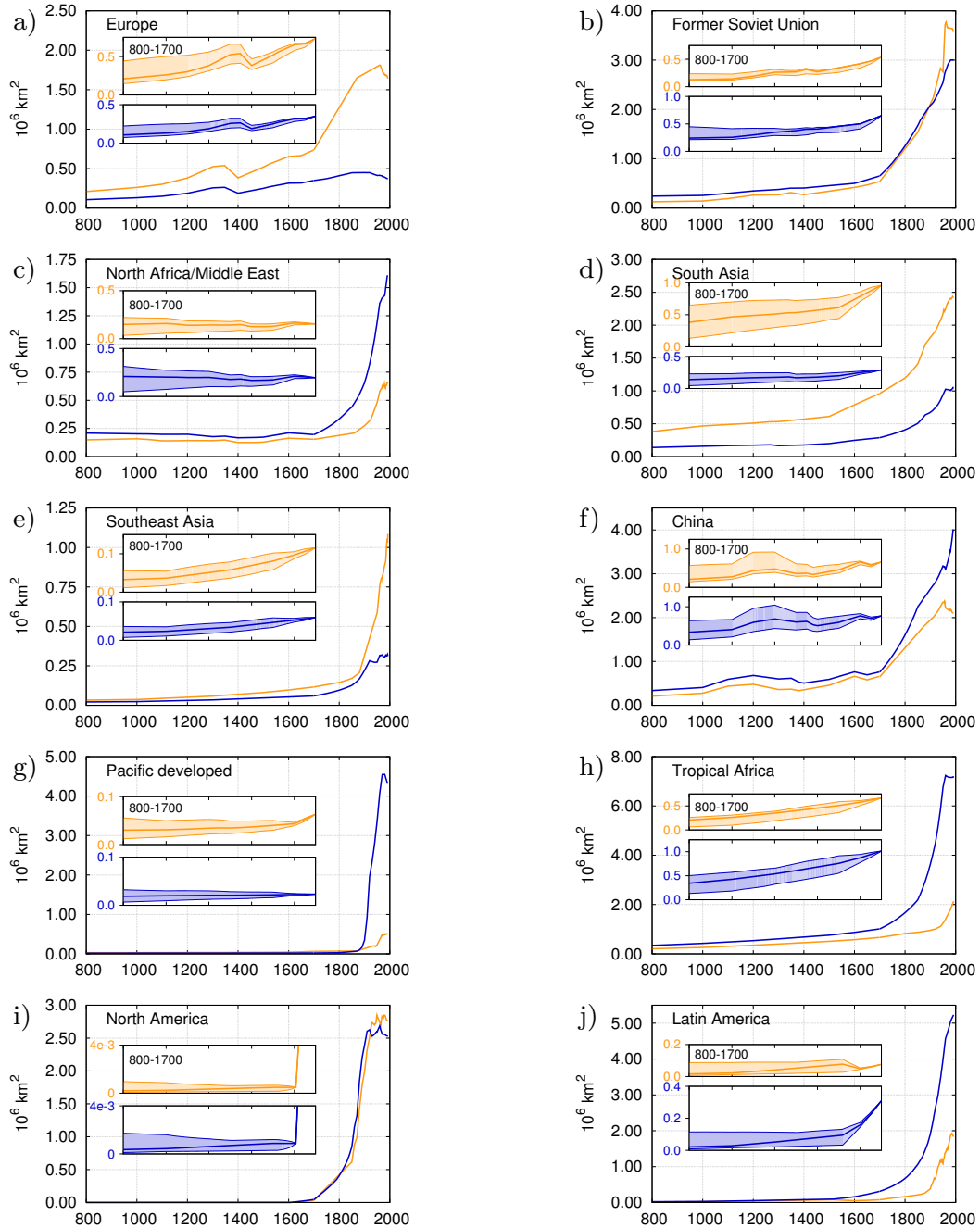


Figure 2.4— Total area of crop (orange) and pasture (blue) for the 10 world regions defined by Houghton et al. [1983] from AD 800 to 1992 (in 10^6 km^2). The insets show the time period AD 800 to 1700 at different scale and with shaded area indicating the uncertainty range (see text for explanation).

2.6.2 North Africa/Middle East

In Southwest Asia lies one of the birthplaces of agriculture. Wild cereals were harvested already in the 10th millennium BC and seed agriculture developed, associated early with the use of ploughs and draught animals [Grigg, 1974]. Intensive agriculture in AD 800 is restricted, however, to the Mediterranean coast and Anatolia, where climate is more favorable, and to the irrigated fields of Egypt and the Fertile Crescent (Figs. 2.2 and 2.3). The latter is the most intensely cultivated region world-wide at the beginning of our reconstruction, with crop fractions of up to 50%. This prominent role, however, is lost during the next few centuries, and a multitude of reasons led to stagnating agriculture also in the other regions of the Middle East and North Africa (Fig. 2.4 c). In Persia and Anatolia, Turkish invasions had negative effects on peasant activity, while North Africa was affected by the Bedouin invasion (11th century), the plague (14th century), and the Mediterranean economic recession (17th century) [McEvedy and Jones, 1978]. In Egypt, all land was already exploited as far as technology allowed. Crop and pasture thus remained at a relatively low extent for many centuries until population gradually grew from the 18th century onwards. With pastoralism being the dominant form of agriculture, much natural grassland was now used for grazing (Fig. 2.5 c). Crop production became more important in the 20th century, associated with a steep increase of population, and with it woody vegetation was reduced.

The long history of cultivation in this region most probably degraded land productivity in many regions, with salinization becoming a common problem in irrigated areas. Permanent agriculture was frequently given up in favor of nomadism in times of economic recession and warfare [Grigg, 1974]. Our persistent estimate thus lies at the higher end of crop estimates, and uncertainties are large for natural and managed grassland areas. Errors in the population estimates play a minor role only — though absolute numbers are still subject to dispute, growth rates are rather similar in all literature estimates.

2.6.3 South Asia and Southeast Asia

The Indian subcontinent experienced peasant settlement in the 4th millennium BC in the Indus valley and around the 1st millennium BC in the Ganges valley [Grigg, 1974]. By AD 800, South Asia was the major player in global crop production with about $4.0 \cdot 10^5$ km² of cultivated land (Fig. 2.4 d). Crop areas grew steadily, though at moderate pace first. Population most certainly has been set back several times throughout the centuries, but historical evidence is sparse [McEvedy and Jones, 1978]. A significant part of the indicated uncertainties must thus be attributed to demographic data. From the 16th to the 19th century agricultural expansion accelerated, significant amounts of forest were cleared for cropland, and grass and shrubland were used for grazing (Fig. 2.5 d). Under European control and after independence, the pattern became more complex with agricultural expansion set off by abandonments in various parts of India [Ramankutty and Foley, 1999].

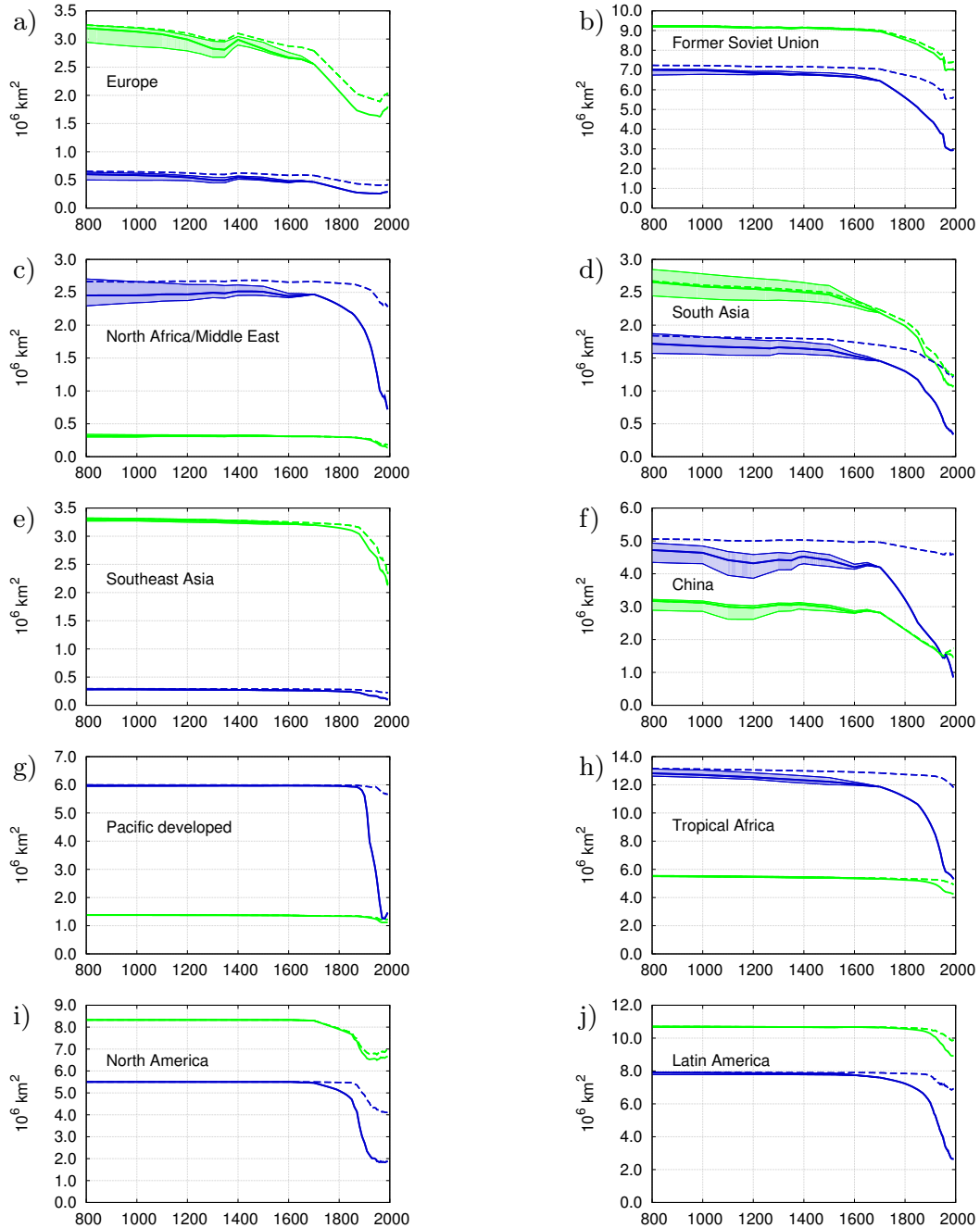


Figure 2.5— Total area of natural vegetation: forest (green) and natural grassland, shrubland, and tundra (blue), for the 10 world regions defined by Houghton et al. [1983] from AD 800 to 1992 (in 10^6 km^2). Shaded area indicates the uncertainty range (see text for explanation). Dashed lines are land cover change due to cropland only.

Compared to the Indian subcontinent, agricultural activity was rather low in Southeast Asia in AD 800 and remained so for the next thousand years. On the Malay Archipelago peasant population has always been concentrated on the southern islands [Grigg, 1974], a pattern reflected in Figs. 2.2 and 2.3. Much of the increase in cropland area that happened in Southeast Asia (Fig. 2.4 e) must be attributed to the spread of wet rice, which had been introduced from China or India about 2000 years ago [Grigg, 1974]. Rice also has a key role in the high expansion rates of crop in the mainland countries in the 19th and 20th century. In recent decades, the Southeast-Asian region has one of the highest deforestation rates globally. Pasture areas are small compared to cropland in Southeast Asia with a total of $3.1 \cdot 10^5$ km² in 1992, but some of the highest stocking rates of the world are found in these countries [Asner et al., 2004].

2.6.4 China

An independent development of seed agriculture took place in Northern China in the 5th and 6th millennia BC including the domestication of pigs, while tropical vegetation was practiced further south [Grigg, 1974]. Based on these traditions, it is not surprising that Chinese crop area was large by AD 800, estimated at $2.1 \cdot 10^5$ km². Large-scale migration from the Yellow River south in the preceding centuries had probably led to a crop pattern similar to today, covering much of the Eastern part of the country. Not reflected in our pattern, however, is the following further concentration of agriculture in the southeastern areas. With it, agricultural methods changed notably, with increasing focus on rice and the introduction of double-cropping. The possible range of crop area prior to the 14th century is thus large, and the persistent estimate is at its lower end (Fig. 2.4 f). Population data contributes only marginally to the uncertainties thanks to meticulous dynastic censuses. Two dramatic events interrupted the otherwise strong growth of population and agriculture: the country lost about a third of its population in the course of the Mongol invasions starting in AD 1211, and again about a sixth of its population in the upheavals after the fall of the Ming Dynasty in 1644 [McEvedy and Jones, 1978]. Thereafter, growth was resumed at unprecedented pace, and half of China's natural forest cover was transformed to cropland.

The $3.4 \cdot 10^5$ km² of pasture in AD 800 is almost exclusively located in Mongolia and Tibet, where herding was the traditional form of agriculture well into the 20th century. The large uncertainties of the estimates should be seen as tribute to nomenclature — nomadism makes it difficult even today to define permanent pastures. The expansion we see is largely at the expense of natural grassland or tundra vegetation (Fig. 2.5 f).

2.6.5 Pacific Developed

A clear break occurs in the late 19th century in the developed countries of the Pacific, with very little agricultural area and dynamics over the preceding millennium and

a steep increase of agriculture — mainly pasture — afterwards (Fig. 2.4 g). In Japan, the agricultural area needed per capita in AD 1700 is extraordinarily small, as fish has been a major part of the traditional diet and the main crop, rice, was cultivated with high nutritional density [Grigg, 1974]. We see notable increases in agriculture only after 1870. After 1945, Australia became the driving force of land cover change in the Pacific developed region. Crop expanded in the 19th century in Southeast Australia, later in Western Australia, affecting grass as well as woody ecosystems. An additional $4.1 \cdot 10^6$ km² of pasture exist in 1992 in Australia, making it the country with the most land area in pasture systems. For a large part natural grasslands were used as pastures, but also shrubland with woody vegetation, which was not always permanently cleared for herding. The reduction in shrubland seen in Fig. 2.5 g for the last century may thus be overestimated when defining pastures as open grassland. New Zealand shows a similar trend in crop and pasture as Australia, though at much smaller absolute numbers.

2.6.6 Tropical Africa

By 1700 the region south of the Sahel was still largely unexplored outside the coastal regions and population numbers and agricultural habits are still a matter of dispute. Vegeticulture must have existed from the 5th millennium BC onwards in West Africa and cereal cultivation developed in the Horn region. The Northern savannas were agriculturally used by the 3rd or 2nd millennium BC [Grigg, 1974]. The Bantu expansion is one of the key factors in spreading cereal cultivation, pastoralism and iron technology throughout much of sub-Saharan Africa [Grigg, 1974, Hanotte et al., 2002], and with it the pattern of agriculture may have been subject to some change especially in the early centuries of our reconstruction. The uncertainty range suggests lower values for cropland and pasture extent to account for the possibility that Bantu culture gradually replaced cultures based on hunting and gathering. Much of the uncertainty in this part of the world, however, is due to contradictory population estimates ranging, e.g., between 25 and 50 million for AD 1000 (see auxiliary material Tab. A.1).

In general, we observe a steady increase of agriculture in all countries of tropical Africa, which comprises the most different cultures, some of which are almost exclusively depending on herding while others mix husbandry with significant cultivation [Vasey, 1992]. Animal husbandry is and has always been a significant sector of agriculture in this part of the world, and pasture features as the dominant type of agriculture in West Africa, the Horn and Southwest Africa in the early centuries of our reconstruction (Fig. 2.3). Grazing focuses on the vast savanna regions and it seems reasonable to assume that their woody fractions are notably affected only during the last two centuries, with the onset of exponential population growth and increasing pressure on ecosystems. Figure 4 h shows that the expansion of pasture came to a halt in the 1960s, while croplands further increased. The pattern of cropland changed to form new centers in South Africa, the Lake Victoria region, and Nigeria, though much of today's crop cover in tropical Africa still remains under low

intensity subsistence farming [Ramankutty and Foley, 1999].

2.6.7 The Americas

While there was a lively dispersal of domesticated plants and animals across the Old World, the Americas developed their very own forms of agriculture. First evidence of plant domestication stems from Meso-America and coastal Peru in the 6th and 5th millennium BC [Grigg, 1974]. In Central and South America, notable cropland intensities developed only within the high cultures, while outside these regions low-intensity swidden cultivation was practiced (Fig. 2.2). Crop areas grew to some $0.8 \cdot 10^5$ km² in our estimates by AD 1500. Pasture at the same time is estimated to be $0.9 \cdot 10^5$ km² and located mainly on the grasslands in the Andes, where some peoples are known to have kept cameloids [Vasey, 1992]. The uncertainty range around these estimates, however, is large despite the small total area, owing to the historians' dispute about pre-Columbian population (Sec. 2.5.3). Significant agricultural areas must have been abandoned with the reduction of the native population by European weapons and diseases, seen as a decrease in crop estimates in Fig. 2.4 j. Under European rule started a large-scale transformation of natural vegetation for crop cultivation as well as for ranching, and agricultural areas were shifted from the West towards the East coast (Figs. 2.2 and 2.3). Much of the natural grasslands of the steppe and savanna is used today for grazing (Vasey [1992], Fig. 2.5 j).

In North America, some clearing of natural vegetation took place in a kind of swidden system, but wild food remained important [Vasey, 1992]. The spatial pattern and the distinct cultures of the different indigenous peoples in North America are not resolved by our global reconstruction, which should thus not be applied in small-scale studies in this part of the world prior to colonization. The new diseases following first European contact brought population growth to a halt, but North America was affected less severely than Central and South America. With the colonization in the 17th century the European form of agriculture was introduced to the East Coast and subsequently spread west. Growth rates of agricultural area are high in the following centuries as a result of both increasing population and the growing dominance of agriculture over hunting and gathering. While the crop maps of Ramankutty and Foley [1999] are based on state-level data from 1850 onwards and are thus able to display this relocation, our algorithm for historical pasture is based on national totals. Some of the grassland in the Great Plains and further west, which Fig. 2.3 classifies as pasture in AD 1800, was thus probably still pristine, and pastures were located further east instead. Robust features, after centuries of very low agricultural activity, are the steep increase of cropland and pasture extent on continental scale during the 18th and 19th century with stagnating numbers in the 20th century.

2.7 Conclusion

This study has presented a consistent approach to reconstruct global historical areas of cropland and pasture for time periods where agricultural data is scarce. Country-based population estimates have been used as proxy for agricultural activity. A method, based on few, basic assumptions, has been developed that allows to consistently translate these population data into estimates of extent of cropland and pasture. Its transparency allows to easily identify possible errors in each region, and we have tried to specify the uncertainties associated with our approach. Data sets for the highest and lowest possible agricultural estimates have been provided that can be used for sensitivity studies in further applications. The reconstruction shows that global land cover change was small between AD 800 and AD 1700 compared to industrial times. Compared to previous millennia, however, land cover change during the preindustrial time period of the last millennium must have been large, and notable fluctuations and distinct histories of agriculture are revealed on regional scales.

There are no global data available that could be used to validate our reconstruction. Local studies can be found for specific time periods, but the subnational scale is not the proper basis for comparison. Except for a few regions, no subnational data were included in our approach, so that meaningful tests can be performed only at the country level or higher. Once independent estimates of historical agricultural extent from proxies such as pollen profiles, archeological evidence, and historical records become available for larger regions, we hope to compare our reconstruction against these estimates. The results of the millennium reconstruction are, however, in general agreement with common knowledge about the history of agriculture, and we are confident that our approach captures the global pattern of changes in agricultural areas and gives a sound approximation of the regional dynamics.

In addition to reconstructing historical agricultural areas, estimates of human-induced changes in natural vegetation cover have also been derived. They provide a better picture of what types of vegetation were transformed to cropland and to pasture. Our estimates show that up to AD 1700 temperate and tropical broadleaf deciduous forests were most severely affected by crop cultivation, while large areas of natural grassland were used as pasture.

The history of agriculture and anthropogenic land cover change is interesting in its own right. Additionally, its knowledge is an essential prerequisite to assess early human impact on the environment. In combination with ecosystem and climate models, geographically explicit data sets like the reconstruction presented in this study can be used to estimate the effects of preindustrial land cover change e.g. on hydrology, nutrient cycles, and regional to global climate. They can thereby contribute to a better understanding of the human role in past changes of the Earth system.

A digital version of the millennium reconstruction of global agricultural areas and land cover is available from the World Data Center for Climate (DOI:

10.1594/WDCC/RECON_LAND_COVER_800-1992). Please contact the authors for further information.

Acknowledgements

The authors would like to thank Pavel Tarasov and Andreas Dix for their valuable suggestions on our reconstruction method. We are grateful to Navin Ramankutty for providing us with the SAGE 5 min and West Africa crop maps and his useful comments on them. We would like to thank Kees Klein Goldewijk for sharing his expert knowledge on historical agriculture and providing us with the HYDE 3.0 version, and Alberte Bondeau for her valuable suggestions on pasture data.

Chapter 3

Radiative Forcing from Anthropogenic Land Cover Change since AD 800

Abstract

We calculate the radiative forcing (RF) from surface albedo changes over the last millennium applying a recently published, population-based reconstruction of anthropogenic land cover change (ALCC). This study thus allows for the first time to assess anthropogenic effects on climate during the preindustrial era at high spatial and temporal detail. We find that the RF is small throughout the preindustrial period on the global scale (negative with a magnitude less than 0.05 W/m^2) and not strong enough to explain the cooling reconstructed from climate proxies between AD 1000 and 1900. For the regional scale, however, our results suggest an early anthropogenic impact on climate: Already in AD 800, the surface energy balance was altered by ALCC at a strength comparable to present-day greenhouse gas forcing — e.g. -2.0 W/m^2 are derived for parts of India for that time. Several other regions exhibit a distinct variability of RF as a result of major epidemics and warfare, with RF changes in the order of 0.1 W/m^2 within just one century.

3.1 Introduction

Anthropogenic land cover change (ALCC) represents one of the most substantial human impacts on the Earth system. The large-scale transformation of natural ecosystems to managed areas alters climate through several pathways: First, biogeochemical cycles are severely disturbed; e.g. ALCC caused about 35% of the anthropogenic CO_2 emissions during the last 150 years [Houghton, 2003]. Second, climate is directly influenced by the modification of the physical properties of the land surface such as albedo, roughness, and evapotranspiration. Modeling studies suggest that through these biogeophysical effects ALCC at mid- and high latitudes

induces a cooling [e.g. Bonan et al., 1992, Claussen et al., 2001, Bounoua et al., 2002]. This is explained by the increase of albedo associated with deforestation, which is caused by the snow masking effect of forest as well as by the higher snow-free albedo of non-forest vegetation. With the strong hydrological cycle in the tropics the reduction of roughness, leaf area, and rooting depth by deforestation reduces the evapotranspiration stronger than in the extra-tropics. The loss of evaporative cooling may thus compensate the albedo effect in the tropics so that ALCC can even lead to a local warming [e.g. Claussen et al., 2001, Bounoua et al., 2002, DeFries et al., 2002]. On the global scale, the opposing biogeophysical effects of ALCC widely cancel each other, but regional climate is significantly influenced by ALCC and may even affect remote areas via teleconnections [e.g. Chase et al., 2000].

While ALCC has been recognized as a key factor for present climate change, its role for historical climate is less clear. Concerning biogeophysical effects, most studies suggest a global cooling as a result of the albedo changes from the dominating midlatitudinal deforestation. The European "Medieval Warm Period" as well as the long-term cooling during the middle of the last millennium may largely be explained by the land cover changes over this period [Govindasamy et al., 2001, Goosse et al., 2006]. Also Brovkin et al. [1999] obtain biogeophysical cooling from historical ALCC, most strongly in the northern mid- and high latitudes. They show that the impact of historical ALCC on climate is of comparable size as concurrent changes of other climate forcings, e.g. solar irradiance and atmospheric CO₂, and is crucial for reproducing historical climate. From these studies we conclude that historical ALCC may have important impacts on regional and possibly global climate through its biogeophysical effects on the atmosphere. However, all previous studies covering the last millennium are based on ad hoc approximations of historical ALCC. In this study, we use a recently published high-resolution reconstruction of ALCC for the last millennium to address the climate impact from historical ALCC at high spatial detail over the course of the history.

For this assessment we apply the radiative forcing (RF) measure, which is calculated as the change in the net shortwave radiation flux at the tropopause after the forcing agent is introduced but prior to any climate feedbacks. In the case of land cover change, the RF is usually determined for the change in surface albedo. Studies have shown that the RF concept is less well applicable to ALCC than to the classic climate forcings such as well-mixed greenhouse gases: First, biogeophysical effects of land cover change other than albedo changes may also impose climate forcings, e.g. changes in evapotranspiration and non-radiative processes [Pielke et al., 2002, Davin et al., 2007]. The albedo effect has, however, been shown to be dominant on global scale [Betts et al., 2007]. Second, the biogeochemical forcing counteracts biogeophysics, with a similar strength on the global mean [Brovkin et al., 2004], but with much less regional heterogeneity. It is, however, usually treated separately from the biogeophysics due to its different nature of processes and impacts and is not considered in this study. Third, the common application of RF to global mean climate may underestimate the impact of ALCC, as ALCC is a spatially highly heterogeneous perturbation where regional effects often differ in sign, so that they

cancel out on global average despite possibly large regional climate impacts. ALCC thus requires a regionally explicit analysis. Nevertheless, the RF concept and its application to albedo changes remain a standard tool to assess the importance of ALCC for climate [Forster et al., 2007], and has frequently been applied to quantify the effects of ALCC on climate for the last 300 years [e.g. Myhre and Myhre, 2003, Betts et al., 2007]. By applying this measure to the entire last millennium, our study allows to consistently compare preindustrial effects of ALCC to publications covering the industrial period.

3.2 Radiative forcing calculations

The RF calculations are performed with the land surface scheme JSBACH [Raddatz et al., 2007] coupled to the climate model ECHAM5 [Roeckner et al., 2003] at a horizontal resolution of T63 (equivalent to about 1.8 degree) with 31 vertical levels. Atmospheric greenhouse gas concentrations, sea ice cover, and sea surface temperature are prescribed to present-day conditions. Computation of the surface shortwave radiation budget includes a spatially-explicit surface albedo calculation for the near infrared as well as the visible range. It depends on the albedo of the soil surface [Rechid et al., 2008], snow cover, and the vegetation composition, in particular the albedo of the canopy and the snow masking of forest. Each grid cell comprises fractions of the three agricultural types (crop, C3 pasture, C4 pasture) and 11 natural vegetation types, each with prescribed canopy albedo and interactive phenology. RF is calculated following the method of Betts et al. [2007] with potential vegetation cover as reference.

Simulations are performed for every hundredth year between AD 800 and 1992, with an additional run for AD 1347, with each simulation comprising 11 years with fixed land cover. Of these, 10 years are used for analysis after one year of spinup. For land cover of the respective years and potential vegetation, spatially aggregated maps of the land cover reconstruction by Pongratz et al. [2008b] are used. This reconstruction is based on published maps of agricultural areas for the last three centuries. For earlier times, a country-based method was applied that uses population data as a proxy for agricultural activity.

3.3 Results

The model simulations yield a global annual mean RF of -0.21 W/m^2 for present vs. potential vegetation cover and of -0.18 and -0.16 W/m^2 since AD 1700 and 1800, respectively, which compares well to the studies summarized in Forster et al. [2007] and Tab. 3.1. Global annual RF is negative and less than 0.04 W/m^2 and 0.05 W/m^2 in magnitude throughout the preindustrial times AD 800 to 1700 and 1800, respectively (Fig. 3.1). Prior to the large-scale deforestation of the tropics, the Northern Hemisphere has always been affected by agricultural expansion more strongly than the Southern Hemisphere. While the latter experienced a steady

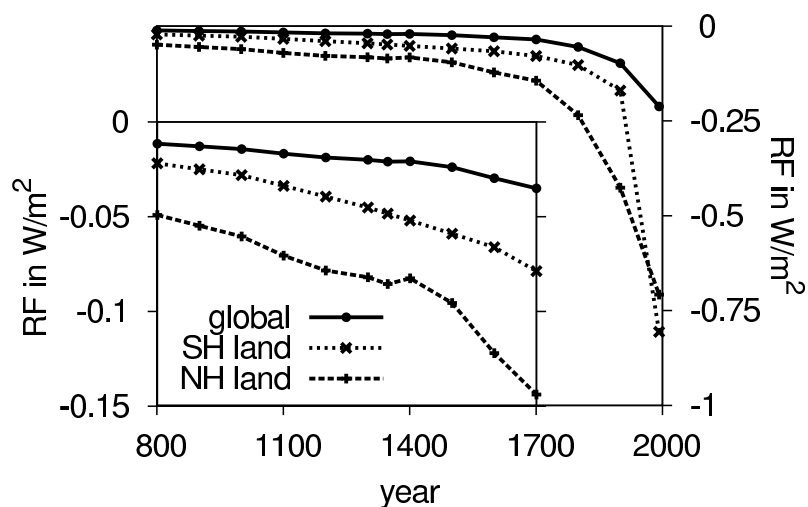


Figure 3.1— Annual mean radiative forcing (RF) in W/m^2 averaged over the globe, Northern Hemisphere land, and Southern Hemisphere land, respectively, for AD 800 to 1700 (inset, left axis) and AD 800 to 1992 (right axis).

Table 3.1— Comparison of global annual mean radiative forcing (RF) from several studies for ALCC. The last column indicates the contribution of the industrial time period relative to the present RF. Reference for present and preindustrial is potential vegetation.

study	present W/m^2	preindustrial W/m^2	industrial W/m^2	fraction %
Betts et al. [2007]	-0.24 (1990)	-0.06 (1750)	-0.18 (1990–1750)	75
Brovkin et al. [2006]	-0.20 (1992)	-0.06 (1700)	-0.14 (1992–1700)	75
this study	-0.21 (1992)	-0.04 (1700)	-0.18 (1992–1700)	83
this study	-0.21 (1992)	-0.05 (1800)	-0.16 (1992–1800)	74

strengthening of RF, epidemics and warfare lead on the Northern Hemisphere to temporary reduction of the strength of RF.

While the global annual mean RF was only -0.01 W/m^2 in AD 800, regional annual values are as low as -2.0 W/m^2 . The strongest forcing at the beginning of the last millennium is simulated for the Indian subcontinent and South China, where large agricultural expansion on previously forested area coincides with high insolation throughout the year (Fig. 3.2). Our results show strong forcings also for the more northern parts of China: negative in summer (JJA) and fall (SON), but positive in winter (DJF) and spring (MAM) when the bare agricultural areas expose more of the dark soil than before deforestation — an effect also simulated for the Black Sea region in spring and autumn. High seasonality of RF also occurs in Europe: although the increase in albedo is highest during winter, when the increased masking of the vegetation by snow takes effect in all northern areas, RF is less than half compared to the summer, where changes in canopy albedo are dominating.

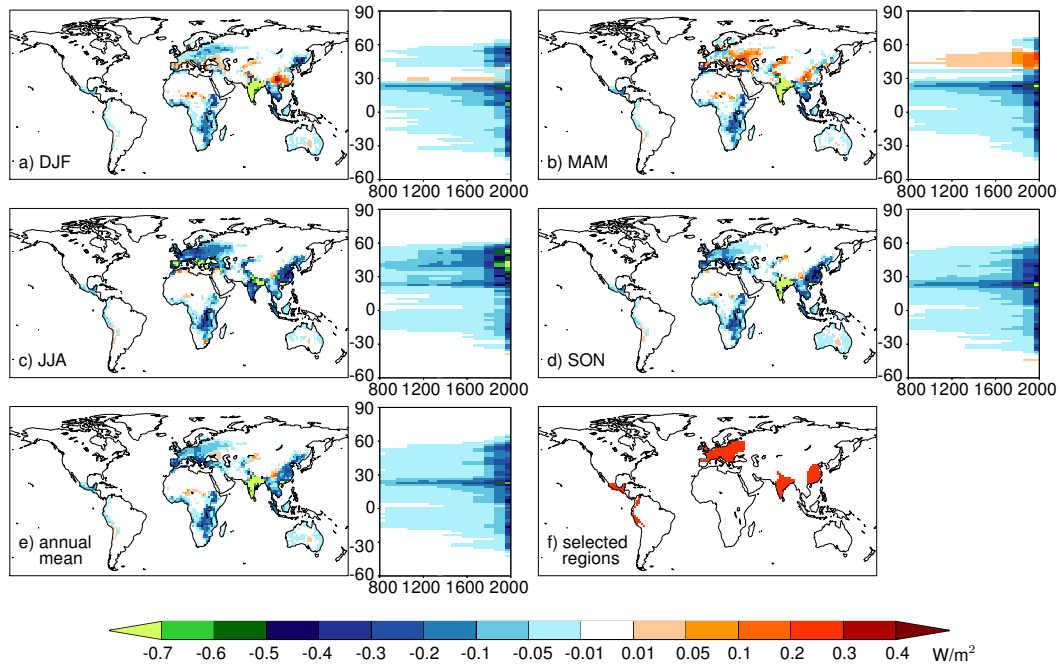


Figure 3.2— (a–d) Seasonal (a–d) and (e) annual mean radiative forcing (RF) in W/m^2 . (left) Map showing RF for the year AD 800; only areas significant at the 95% level are shown. (right) Zonal means of RF for AD 800 to 1992. Note the irregular scale around 0 on the color scale. (f) The red areas indicate the regions of Fig. 3.3.

The already strong forcing further strengthens in South and Southeast Asia during the last millennium (zonal means in Fig. 3.2), similar to Europe, where agriculture further expands into Central Asia in the 19th and 20th centuries. During the recent centuries the colonization of North America increasingly contributes to the decrease of RF in the Northern Hemisphere midlatitudes during winter, summer, and fall. During spring, agricultural expansion in the northern Great Plains increases the positive zonal RF. RF on the Southern Hemisphere grows as a consequence of the Bantu expansion and subsequent agricultural intensification during preindustrial times. Since the 18th century European colonization of South America and Australasia further reduce Southern Hemisphere RF. Tropical deforestation strongly decreases RF in the last century.

3.4 Discussion

The RF from ALCC is small during preindustrial compared to industrial times (Tab. 3.1). The time period 1800–1992 covers 74% and 79% of the changes in global mean RF of the entire agricultural period and of the last thousand years, respectively. The RF from ALCC during industrial times is of the same order of magnitude as solar variability, which amounts to about $0.6 W/m^2$ over the last mil-

lennium, causing temperature variabilities in the order of 0.2 K [Crowley, 2000]. The changes of RF from ALCC during the preindustrial times of the last millennium are one order of magnitude smaller than solar variability, and two orders in comparison with volcanic forcing, as large eruptions typically cause a RF of several W/m^2 [Crowley, 2000]. ALCC, however, differs from the natural forcings in two respects: First, ALCC constitutes a rather permanent forcing, unlike volcanic eruptions. By its persistence over centuries even a small forcing as preindustrial ALCC may significantly affect the long-term energy balance. This notion has been supported by previous studies attributing Northern Hemisphere cooling to ALCC [e.g. Govindasamy et al., 2001, Goosse et al., 2006] and will be discussed in the following. Second, ALCC constitutes a highly heterogeneous forcing and opposing effects in time and space tend to counterbalance on the global and annual mean so that significant regional effects may be masked. Betts et al. [2007], for example, find a cooling of 1–2 K in winter and spring over northern midlatitude agricultural regions as a consequence of ALCC-induced albedo changes. In this study, annual mean values as low as -2.0 W/m^2 are simulated for South Asia in AD 800, which are in the same order of magnitude, though opposite in sign, as the greenhouse gas forcing in present times. Despite small mean values of RF, ALCC may thus have altered regional climate already a thousand years ago. Specific regions further exhibit very distinct histories of agricultural development with partly abrupt changes in RF, as will be illustrated later.

The negative RF in the northern midlatitudes during fall, winter, and most notably summer must be expected to have a cooling effect in accordance with studies by e.g. Betts et al. [2007]. This albedo change has also been suggested by Govindasamy et al. [2001] as the key player in explaining the Northern Hemisphere cooling of about 0.25 K between AD 1000 and 1900 reconstructed from climate proxies [Mann and Bradley, 1999]. In our study, the RF of the Northern Hemisphere decreases by 0.11 W/m^2 during this period, as compared to a RF of 0.28 W/m^2 by Govindasamy et al. [2001]. In contrast to their study, our findings thus suggest that ALCC during this time period cannot be the major cause for the cooling. A main difference is that we apply a detailed land cover reconstruction, while Govindasamy et al. [2001] assume present-day land cover for the year 1900 and potential vegetation in AD 1000 so that deforestation is significantly overestimated.

Ruddiman [2007] suggests that epidemics such as the bubonic plague in the 14th century Europe and the mass mortality in the Americas after European arrival had lowered atmospheric CO_2 concentrations, because agricultural land was abandoned in the course of the many deaths and was regrown by natural vegetation. In Fig. 3.3 a and b we show the RF in these two regions between AD 800 and 1700, indicating the effect of the surface albedo changes associated with the two epidemics. Forest regrows on about 0.18 million km^2 in Europe and weakens the RF by about one third or 0.08 W/m^2 in the indicated area within just one century. In the region of the high cultures of Meso- and South America the RF loses strength from -0.23 to -0.09 W/m^2 between AD 1500 and 1600. Similarly, warfare may affect land cover by their impact on population distribution; the Mongol invasion and the upheavals

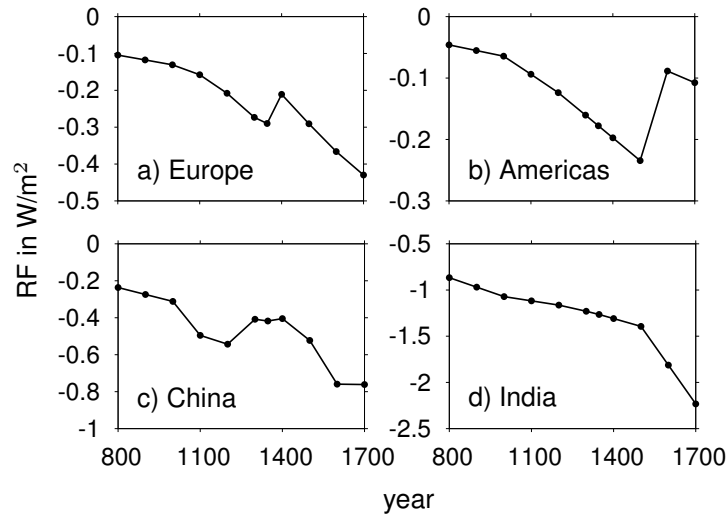


Figure 3.3— Annual mean radiative forcing (RF) in W/m^2 AD 800 to 1700 for the four regions indicated in Fig. 3.2 f.

after the fall of the Ming Dynasty bring agricultural expansion and the decrease of RF in China to a halt in the 13th and the 17th century (Fig. 3.3 c). India is shown for comparison as a region of strong and steady agricultural expansion (Fig. 3.3 d). Although the affected areas may be too small to have caused impacts on global climate, local climate may have been altered significantly. These examples illustrate the importance of using a detailed land cover reconstruction rather than ad hoc interpolation between potential vegetation and land cover maps of the late preindustrial period, as has been done in previous studies, when assessing the effects of historical ALCC on regional climate.

3.5 Conclusions

While ALCC does not seem to be the major cause of large-scale climate changes such as the Northern Hemisphere cooling, this study demonstrates that on a regional scale ALCC has imposed a significant radiative forcing on climate already in preindustrial times. The energy balance has been affected by early agricultural expansion not only in the northern midlatitudes, but even stronger in the northern subtropics. Furthermore, evidence was presented that in order to assess the effects of specific historical events on climate, a land cover reconstruction that captures the regionally distinct evolution of agricultural expansion is needed. This work supports previous studies that have emphasized the spatial heterogeneity of the land cover forcing and the relevance to diverge from the global mean values usually associated with the RF concept [e.g. Pielke et al., 2002] and further stresses the relevance of the seasonal variability. Climate simulations for preindustrial times will help to quantify the

actual climate response to all biogeophysical effects of historical ALCC including feedbacks, and transient simulations over the last millennium should be performed to further include the evolution of land cover CO₂ emissions and their impact on preindustrial climate.

Chapter 4

Effects of Anthropogenic Land Cover Change on the Carbon Cycle of the Last Millennium

Abstract

Transient simulations are performed over the entire last millennium with a general circulation model that couples the atmosphere, ocean, and the land surface with a closed carbon cycle. This setup applies a high-detail reconstruction of anthropogenic land cover change (ALCC) as the only forcing to the climate system with two goals: (1) to isolate the effects of ALCC on the carbon cycle and the climate independently of any other natural and anthropogenic disturbance and (2) to assess the importance of preindustrial human activities. With ALCC as only forcing, the terrestrial biosphere remains a source of carbon throughout the last millennium, with a net release of 96 Gt C and an increase of atmospheric CO₂ by 20 ppm. The biosphere-atmosphere coupling thereby leads to a restorage of 37% and 48% of the primary emissions over the industrial and the preindustrial period, respectively. Due to the stronger coupling flux over the preindustrial period, only 21% of the 53 Gt C preindustrial emissions remain airborne. Despite the low airborne fraction, atmospheric CO₂ rises above natural variability by late medieval times. This suggests that human influence on CO₂ began prior to industrialization. Global mean temperatures, however, are not significantly altered until the strong population growth in the industrial period. Furthermore, we investigate the effects of historic events such as epidemics and warfare on the carbon budget. We find that only long-lasting events such as the Mongol invasion lead to carbon sequestration. The reason for this limited carbon sequestration are indirect emissions from past ALCC that compensate carbon uptake in regrowing vegetation for several decades. Drops in ice core CO₂ are thus unlikely to be attributable to human action. Our results indicate that climate-carbon cycle studies for present and future centuries, which usually start from an equilibrium state around 1850, start from a significantly disturbed state of

the carbon cycle.

4.1 Introduction

The vegetation covering the continents has a decisive influence on the climate. Through the uptake of CO₂ from the atmosphere, plants play a central role in the global carbon cycle. Furthermore, they influence the exchange of energy, water, and momentum between the atmosphere and the land surface. Humankind is altering these processes by transforming areas of natural vegetation to human use in agriculture, forestry, and urbanization (“anthropogenic land cover change”, ALCC). The anthropogenic disturbance of the natural land cover has started thousands of years ago with the expansion of agriculture, and possibly earlier with hunters and gatherers managing woodlands for hunting and traveling. The disturbance has grown to create a human-dominated world today, as 30–50% of the Earth’s land cover are substantially modified by human land use — primarily by the expansion of agriculture [Vitousek et al., 1997]. The recognition is growing that ALCC has an impact on climate and the carbon cycle and needs thorough investigation to understand its pathways of disturbance, its past and future effects, as well as its potential to mitigate climate change [Barker et al., 2007, Denman et al., 2007]. Consequently, land-use modules including carbon cycling are being developed for many terrestrial biosphere or climate models [e.g., McGuire et al., 2001, Strassmann et al., 2008]. They ideally calculate all fluxes endogenously and coupled to the atmosphere and ocean to allow for, e.g., a closed, interactive carbon cycle including biosphere-atmosphere feedbacks. Eventually, the recommendation was given to supply ALCC as spatially explicit information to the climate projections of the next report of the Intergovernmental Panel on Climate Change [Moss et al., 2008].

The influence of vegetation cover and ALCC on the climate is commonly divided into biogeophysical and biogeochemical mechanisms. The first include all modifications of the physical properties of the land surface such as albedo, roughness, and evapotranspiration. Modeling studies suggest that at mid- and high latitudes the increase of albedo is the dominant biogeophysical process of ALCC. Albedo increases as a consequence of deforestation — due to the higher snow-free albedo of non-forest vegetation as well as the snow masking effect of forest [Bonan et al., 1992] — and generally induces a cooling, possibly enforced by the sea ice-albedo feedback [e.g., Betts, 2001, Claussen et al., 2001, Bounoua et al., 2002]. In the tropics, the reduction of evapotranspiration following deforestation leads to a loss of evaporative cooling and counteracts the albedo effect. Tropical deforestation can thus lead to a local warming [e.g., Claussen et al., 2001, Bounoua et al., 2002, DeFries et al., 2002], although its effects on the extra-tropics may be a cooling from the reduced atmospheric content of water vapor acting as a greenhouse gas [e.g., Sitch et al., 2005].

Probably the most important biogeochemical mechanism of ALCC is the influence on the carbon cycle, and the associated impact on the global CO₂ concentration.

Altering atmospheric CO₂, ALCC modifies the Earth’s energy balance and thus climate. ALCC constitutes a source of emissions mainly from the loss of terrestrial biomass. About one third of the anthropogenic CO₂ emissions over the last 150 years are estimated to be the direct consequence of ALCC [Houghton, 2003]. Counteracting the emissions is an increased carbon uptake by both natural and agricultural vegetation, the so-called “residual land sink” [Denman et al., 2007]. Its causes are not well specified and assumed to be, among others, the fertilizing effect of increased atmospheric CO₂, nitrogen deposition, recovery from past disturbances, and climate change [Schimel et al., 2001, and references therein]. The net effect is that the terrestrial biosphere has turned from a source to a sink during the recent decades, thus mitigating anthropogenic greenhouse gas emissions. All these carbon fluxes, however, are very uncertain. The uncertainty range assigned to estimates of ALCC emissions is about $\pm 70\%$ even for the last — best-documented — decades, and propagates to the carbon sink term [Denman et al., 2007]. Difficulties in quantifying and locating ALCC are only one problem beside gaps in process understanding and model differences [McGuire et al., 2001]. Further complexity is added by the interaction of biogeophysical and biogeochemical effects and the two-way coupling of the carbon cycle and the climate.

Primary emissions by ALCC have first been estimated either by simple book-keeping approaches [Houghton et al., 1983] or by spatially explicit simulations of carbon stocks for different time slices by process-oriented models [DeFries et al., 1999, Olofsson and Hickler, 2008]. Primary emissions are now increasingly derived from transient studies, though only for the last three centuries. In these studies, carbon loss, uptake, and the net effect of ALCC on the carbon cycle are simulated. Climate and CO₂ fields may either be prescribed in these simulations [McGuire et al., 2001, Jain and Yang, 2005], in which case no feedbacks from ALCC on the climate are allowed; or they may be calculated interactively. The latter method has been used for past and future ALCC in a range of studies applying Earth system models of intermediate complexity (EMICs) [Gitz and Ciais, 2003, Sitch et al., 2005, Brovkin et al., 2006, Strassmann et al., 2008]. Recently, second-order effects of ALCC were identified, such as the loss of carbon sink capacity by replacing forests with agricultural land [Gitz and Ciais, 2003]. Several studies have focused only on the net effect of potential ALCC scenarios and the resulting influence on climate of the biogeochemical effects in comparison to the biogeophysical ones [e.g., Claussen et al., 2001, Brovkin et al., 2004].

In the present study, we apply a general circulation model (GCM) for the atmosphere and the ocean coupled to a land surface scheme, considering both biogeophysical and biogeochemical effects of ALCC. Our model includes a closed carbon cycle (land, ocean, atmosphere) that evolves interactively with the climate. Feedbacks between the carbon cycle and the climate are thus included in the simulations. We distinguish between source and sink terms and identify further sub-processes of biosphere-atmosphere carbon exchange. A detailed reconstruction of ALCC is applied that indicates areas of cropland, pasture, and natural vegetation for each year since AD 800 [Pongratz et al., 2008b], which allows us to quantify the effects

of ALCC transiently over history. To our knowledge, the combination of method, data, and the length of the simulated time period makes this study the first to assess the effects of ALCC on the carbon cycle and the climate in such detail.

We do not try to simulate a realistic climate evolution as influenced by all natural and anthropogenic forcings, but we try to isolate the impact of ALCC on climate by allowing ALCC as the only forcing to the carbon cycle and climate system. Anthropogenic carbon emissions from fossil-fuel burning and cement production are the most important driver of CO₂ and climate change today, but did not grow significantly larger than ALCC emissions until the 1930s [Houghton, 2003, Marland et al., 2008], and played no role in the preindustrial period. For the preindustrial era, our model results can therefore be expected to represent most of the real impact of human activity. The studies by DeFries et al. [1999], Olofsson and Hickler [2008], Ruddiman [2003, 2007] clearly indicate that significant amounts of carbon were already released in the preindustrial period, but estimates range from 48–320 Gt C. The net effect of preindustrial ALCC is even more disputed, ranging from a key climate forcing [Ruddiman, 2007] to a very small one [Joos et al., 2004]. It has also been suggested that historic events such as warfare and epidemics altered atmospheric CO₂ via their impact on agricultural extent [Ruddiman, 2007], but a thorough investigation has not been undertaken since, until recently, no spatially explicit information on the actual changes of vegetation distribution existed. Our study assesses the effects of historic events over the last millennium and gives new estimates for associated carbon source and sink terms. Including also the carbon cycle in the ocean, we can estimate the amount of carbon that remains in the atmosphere and address the question whether an anthropogenic influence on the carbon cycle, and finally climate, has existed prior to the industrialization.

4.2 Methods

4.2.1 Model

The atmosphere/ocean general circulation model (AOGCM) consists of ECHAM5 [Roeckner et al., 2003] at T31 (approximately 4 degree) resolution with 19 vertical levels representing the atmosphere, and MPI-OM [Marsland et al., 2003] at 3 degree resolution with 40 vertical levels representing the ocean. The two models are coupled daily without flux correction. The carbon cycle model comprises the ocean biogeochemistry model HAMOCC5 [Wetzel et al., 2005] and the modular land surface scheme JSBACH [Raddatz et al., 2007]. HAMOCC5 simulates inorganic carbon chemistry as well as phyto- and zooplankton dynamics in dependence of temperature, solar radiation, and nutrients. It also considers the buildup of detritus, its sinking, remineralization, and sedimentation. JSBACH distinguishes 12 plant functional types (PFTs), including one crop type, which differ with respect to their phenology, morphological and photosynthetic parameters. Their fractional coverage of each grid cell is prescribed from maps annually. For each PFT, the storage of organic carbon on land occurs in five pools: living tissue (“green”), woody material

(“wood”), and a pool storing sugar and starches (“reserve”) for the vegetation carbon, and two soil carbon pools with a fast (about 1.5 years) and a slow turnover rate (about 150 years).

For this study ALCC was implemented in JSBACH as follows: The change in the cover fractions of PFTs is prescribed from the maps described below and linearly interpolated from annual changes to a daily timestep. With changes in the cover fractions, carbon is relocated between the pools. The vegetation carbon of PFTs with decreasing area is either directly released to the atmosphere, or relocated to the two soil pools. Carbon release directly to the atmosphere happens, e.g., when forest is cleared by fire, and a fraction of 50% of the vegetation carbon is chosen in this study as flux to the atmosphere. The choice of this value is not critical for the present analysis: The timescale of our study is multi-centennial and thus larger than the slowest turnover rate of the carbon pools, so that all vegetation carbon lost is eventually transferred to the atmosphere. The amount of ALCC carbon per m^2 and day directly released to the atmosphere from the three vegetation pools is calculated as

$$F_{\triangleright A} = \sum_{i \in a-} (c_i^{\text{old}} - c_i^{\text{new}}) \cdot (f_{G \triangleright A} C_{G,i} + f_{W \triangleright A} C_{W,i} + f_{R \triangleright A} C_{R,i}), \quad (4.1)$$

where $f_{G \triangleright A}$, $f_{W \triangleright A}$, and $f_{R \triangleright A}$ denote the fractions of carbon released to the atmosphere due to ALCC for the three vegetation carbon pools (green, wood, and reserve, respectively). $c_i^{\text{old}} - c_i^{\text{new}}$ denotes the daily change in cover fraction of the i -th PFT that loses area ($a-$) due to ALCC, and $C_{G,i}$, $C_{W,i}$, and $C_{R,i}$ denote the carbon densities of the three vegetation pools. For the relocation of vegetation carbon to the two soil pools, the carbon from the green and reserve pools is transferred to the fast soil pool in each grid cell, while the carbon from the wood pool is transferred to the slow soil pool. The long decay time of the slow soil pool implicitly includes the storage of carbon in long-term human use. The ALCC carbon fluxes to the fast and slow pool are calculated as

$$F_{\triangleright F} = \sum_{i \in a-} (c_i^{\text{old}} - c_i^{\text{new}}) \cdot [(1 - f_{G \triangleright A}) C_{G,i} + (1 - f_{R \triangleright A}) C_{R,i}] \quad (4.2)$$

$$F_{\triangleright S} = \sum_{i \in a-} (c_i^{\text{old}} - c_i^{\text{new}}) (1 - f_{W \triangleright A}) C_{W,i}. \quad (4.3)$$

Vegetation carbon is therefore lost from a PFT only due to the decrease of its area, while its carbon densities are unaffected. The carbon lost is then transferred to the respective soil carbon pools of the expanding PFTs, distributed proportionally to their new cover fractions, and the PFT carbon densities adjusted accordingly. This scheme describes the temporal evolution of land carbon storage for agricultural expansion as well as abandonment consistently.

4.2.2 ALCC data

As ALCC forcing, the reconstruction of global agricultural areas and land cover by Pongratz et al. [2008b] is applied. It contains fractional maps of 14 vegetation types at an annual timestep and a spatial resolution of 0.5 degree. The agricultural types considered are cropland, C3, and C4 pasture. The reconstruction merges published maps of agriculture from AD 1700 to 1992 and a population-based approach to quantify agriculture for each country for the time period AD 800 to 1700. With this approach the general expansion of agriculture is captured as well as specific historic events, such as epidemics and wars, that are likely to have caused abandonment of agricultural area in certain regions due to their impact on population numbers. The uncertainty associated with the chosen approach, with respect to the uncertainty of population data and of agrotechnological development, was assessed in two additional datasets for AD 800 to 1700, which indicate the upper and lower range of possible agricultural extent.

A map of potential vegetation with 11 PFTs was used as background to the agricultural reconstruction with different allocation rules for cropland and pasture. Most previous studies that included pasture interpreted the expansion of pasture as deforestation or reduced all natural vegetation equally, not taking into account that in history humans used natural grasslands for pastures rather than clearing forested area [e.g., Houghton, 1999], thus overestimating ALCC. The ALCC reconstruction applied here implemented the preferential allocation of pasture on natural grasslands.

ALCC other than caused by the change in agricultural extent, e.g., shifting cultivation and wood harvest on areas that are not subsequently used for agriculture, is not taken into account in this study. However, forestry for wood production is expected to have only a small effect on the net carbon balance, as harvest in most cases tends to be compensated by regrowth [Houghton, 2003]. The same effect makes the distinction of agricultural area as either permanent or part of a system of shifting cultivation less important. In this study, all agriculture is treated as permanent. An extension of the agricultural and land cover maps into the future follows the A1B scenario [Nakicenovic et al., 2000], superimposing changes in agricultural extent from the scenario maps on the ALCC map of 1992, the last map available from the ALCC reconstruction.

4.2.3 Simulation protocol

The model is spun up for more than 4000 years under CH_4 , N_2O , solar, orbital, and land cover conditions of the year AD 800 until the carbon pools are in equilibrium. The final atmospheric CO_2 concentration is 281 ppm. Three simulations branch off from this equilibrium (Tab. 4.1): A 1300-year-long control simulation (named *ctrl*) keeps all forcings constant at the year AD 800 state, while two transient simulations run until the year 2100 applying ALCC as the only forcing (*LC*). The first applies the middle-range (*best-guess*) ALCC reconstruction with the aim to capture the

Table 4.1— Description of model simulations. All simulations with ALCC as land cover maps have been performed twice, for best-guess ALCC and for high land cover dynamics.

acronym	target quantity	coupling	land cover maps	climate
<i>ctrl</i>	control simulation	full coupling	constant AD 800	control
<i>LC</i>	net emissions	full coupling	ALCC	ALCC-driven
<i>L</i>	primary emissions ($L - ctrl$) coupling flux ($L - LC$)	offline	ALCC	control
<i>C</i>	loss of sink capacity ($(LC - C) - (L - ctrl)$)	offline	constant AD 800	ALCC-driven

impact of ALCC realistically; the second applies the lower-range ALCC reconstruction (*high land cover dynamics*) with the aim to give an upper limit of possible ALCC emissions and impact on climate and the carbon cycle for the preindustrial period. The transient runs simulate both biogeochemical and biogeophysical effects of ALCC and all atmosphere-ocean-biosphere feedbacks. They deliberately neglect natural and anthropogenic forcings other than ALCC, such as changes in the orbit, in the volcanic and solar activity, and the emissions from fossil-fuel burning. With this setup, it is thus possible to isolate the effect of ALCC on the climate and the carbon cycle.

In addition to the coupled simulations described above, the carbon pools are re-calculated offline with the aim to separate the primary effect of ALCC on the carbon balance, i.e. prior to any feedbacks arising from the coupling with the climate and the atmospheric and marine part of the carbon cycle. In offline simulations any land cover history can be combined with any climate description. Derived from a coupled simulation, climate enters the offline simulation in the form of net primary productivity (NPP), leaf area index (LAI), soil moisture, and soil temperature and thus also includes physiological as well as climatic effects of changes in atmospheric CO₂. Two offline simulations are performed: In simulation *L*, the effects of ALCC were re-calculated under the climate of the control simulation. $L - ctrl$ then isolates the primary emissions of ALCC prior to any feedbacks. The loss of carbon due to ALCC which is determined in this way, the “primary emissions”, is directly comparable to book-keeping approaches such as by [Houghton et al. \[1983\]](#), which neglect any interactions between climate, CO₂, and the terrestrial carbon pools. $L - LC$, on the other hand, isolates the coupling flux, i.e. the influence that climate and CO₂ exert on carbon uptake and release by the biosphere. In the second offline simulation, *C*, the carbon pools are re-calculated for constant land cover of the year AD 800 under the climate and CO₂ from the coupled transient simulation. The difference between $LC - C$ and $L - ctrl$ quantifies the difference of primary emissions created under changing climate as compared to those created under the stable control climate.

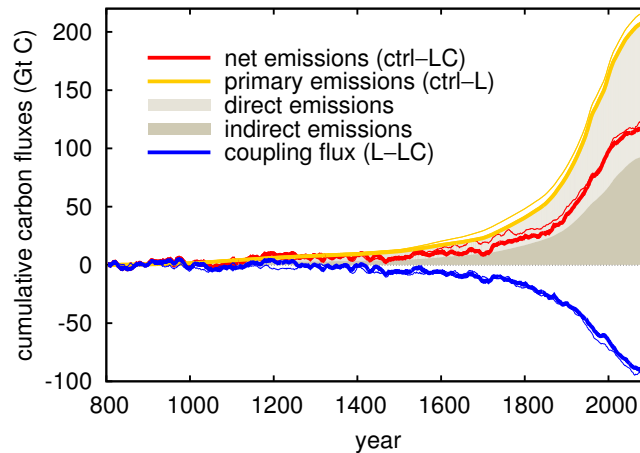


Figure 4.1— Global land-atmosphere carbon fluxes, cumulative since AD 800. Positive values indicate release to the atmosphere. Thick lines are results for the best-guess ALCC reconstruction, thin lines for the high land cover dynamics. The shaded areas split up the best-guess primary emissions into direct (light) and indirect (dark) emissions. Simulations ctrl, L, LC as explained in Tab. 4.1. Values are 10-years running means.

4.3 Primary emissions and carbon cycle feedback

4.3.1 Overview

With ALCC as only forcing, the land biosphere remains a net source of carbon throughout the last millennium (Fig. 4.1). It loses 96 Gt C between AD 800 and 2000 (see Tab. 4.2 for the preindustrial, industrial, and future period). This results from a loss of vegetation carbon only partly offset by a gain in soil carbon, similar as in previous studies [e.g., Jain and Yang, 2005] (Fig. 4.2, $LC - ctrl$). Primary emissions are significantly higher than the net emissions, with 161 Gt C. The difference of 65 Gt C is the consequence of the coupling flux: The primary emissions alter climate and increase atmospheric CO_2 concentration (see Sec. 4.4.1). These changes enhance carbon uptake by the biosphere, in particular via CO_2 fertilization. As a consequence, 40% of the primary emissions over the last millennium are buffered by the biosphere.

4.3.2 Spatial patterns

The spatial distribution of the primary emissions, the coupling flux and the net emissions are shown separately for the preindustrial (AD 800–1850), the industrial (1850–2000), and the future (2000–2100) period in Fig. 4.3. The maps for the net emissions contrast clearly the regions where agricultural expansion was strong during the respective time period and emissions are higher than the terrestrial sink, and those regions where carbon uptake from the coupling flux is stronger, usually the remaining pristine regions. In the preindustrial period, emissions arise primarily

Table 4.2— Atmosphere-biosphere carbon fluxes as described in the text, in Gt C accumulated over the respective time periods with 30-years running mean. Positive values indicate fluxes to atmosphere. NEP is net ecosystem productivity.

flux	time period			
	800–1850	1850–2000	2000–2100	800–2000
primary emissions	52.6	108.3	47.7	160.9
— direct emissions	30.4	63.7	21.5	94.1
— indirect emissions	22.2	44.6	26.2	66.8
coupling effect	-25.2	-39.6	-27.0	-64.8
— on NEP	-25.3	-41.4	-27.9	-66.7
— on direct emissions	-0.2	-1.8	-0.9	-2.0
net emissions	27.4	68.7	20.7	96.0
loss of sink capacity	-0.3	-4.0	-4.3	-4.3

from Europe, India, China, and, in the last preindustrial centuries, North America, while a shift into tropical regions can be observed for the industrial times. Some regions show similar emissions for preindustrial and industrial times, but it needs to be kept in mind that the time span is very different (1050 vs. 150 years). The future scenario is characterized by reforestation in the midlatitudes and further emissions from the tropics. The strength of loss per converted area depends mainly on the biomass density. Negative emissions arise in some regions, where in the model cropland is more productive than the natural vegetation. The coupling flux shows an uptake of carbon in most areas, especially in the tropics. Only in few regions a carbon loss is simulated, which is probably a result from a climate change that is unfavorable for the prevailing vegetation. Apart from these areas, the change in CO₂, not a change in climate, seems to be the key factor for carbon uptake. The dominance of CO₂ fertilization for terrestrial carbon uptake cannot be proven with the present setup, but has been shown by previous studies [e.g., [Jain and Yang, 2005](#), [Raddatz et al., 2007](#)] and is also suggested here, since the relative increase in NPP is homogeneous over all latitudes (not shown) and the climate signal is weak, especially in preindustrial times (see [Sec. 4.4.2](#)).

4.3.3 Primary emissions

Our quantification of the primary emissions for the preindustrial and industrial period is compared to previous studies in [Tab. 4.3](#). We simulate primary emissions of 53 Gt C for the years AD 800 to 1850; approximately 10 Gt C must be added to take into account the emissions prior to AD 800 (assuming that the same amount of carbon is emitted per m² of agricultural expansion prior to 800 as averaged for 800 to 1850). Our estimates thus fall within the range given by [DeFries et al. \[1999\]](#) and [Olofsson and Hickler \[2008\]](#). The values by [Olofsson and Hickler \[2008\]](#) may overestimate emissions since they implemented agricultural expansion entirely as

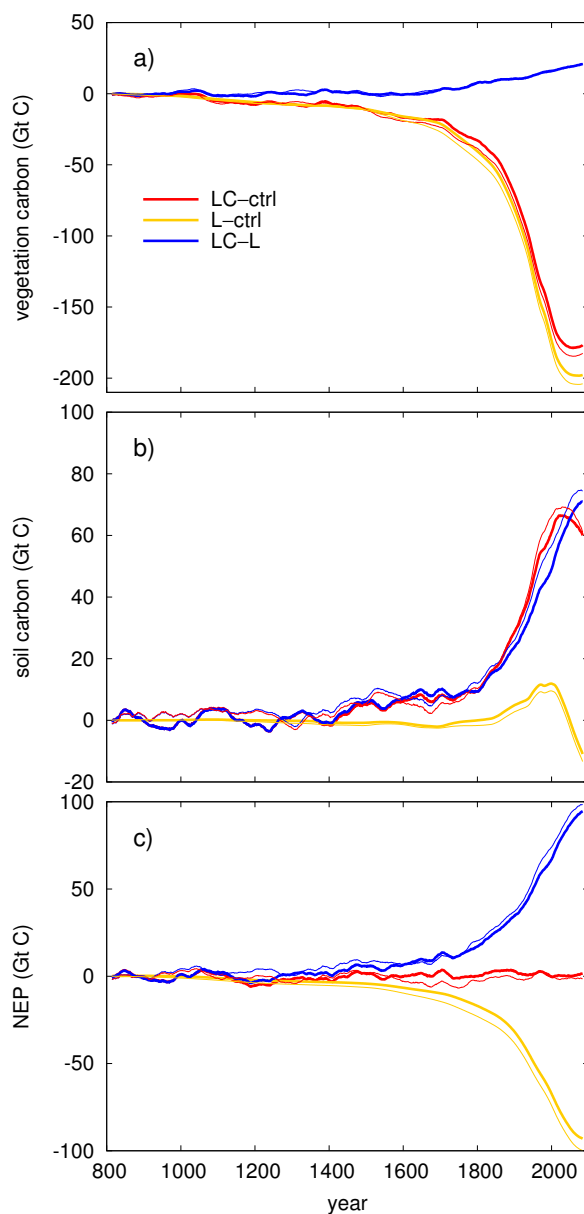


Figure 4.2— Accumulated changes since AD 800: (a) vegetation carbon pools, (b) soil carbon pools, (c) NEP. Thick lines are results for the best-guess ALCC reconstruction, thin lines for the high ALCC dynamics. Simulations ctrl, L, LC as explained in Tab. 4.1. Values are 30-years running means.

deforestation. Our estimates are lower than the ones by Ruddiman [2003, 2007], who, however, takes into account several additional emission processes including some unrelated to ALCC, such as coal burning in China. The uncertainty estimate from the simulation with high land cover dynamics indicates that our primary emissions

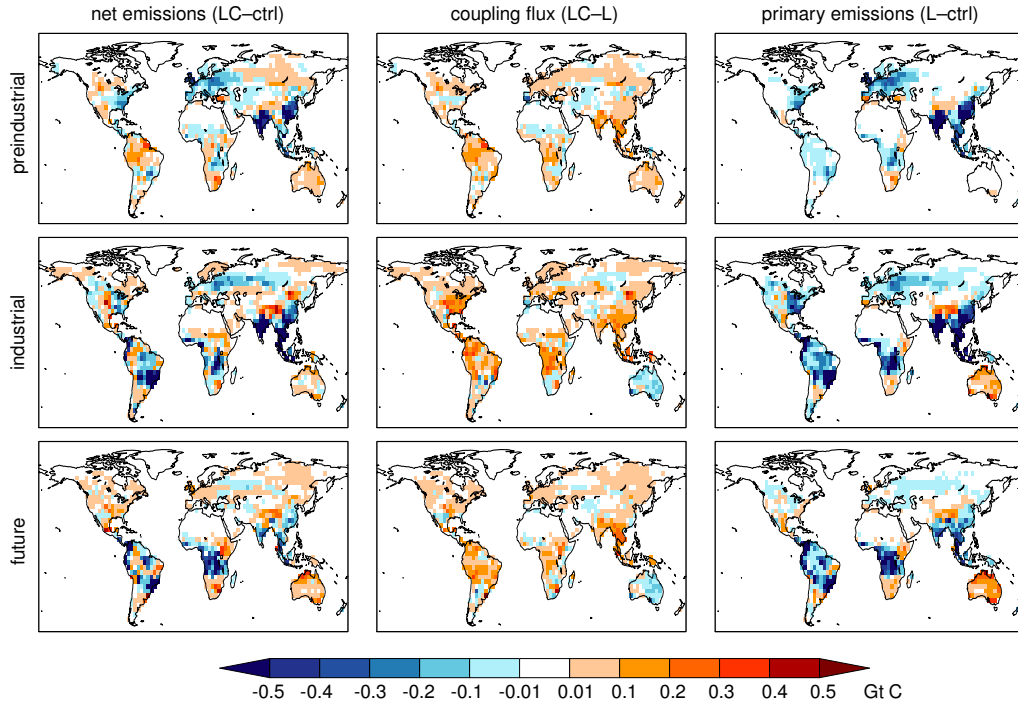


Figure 4.3— Net emissions, coupling flux, and primary emissions of ALCC accumulated over the given time interval: preindustrial (AD 800–1850), industrial (AD 1850–2000), and future period (AD 2000–2100). Units are Gt C taken up in each grid cell. Simulations ctrl, L, LC as explained in Tab. 4.1.

may be up to 8 Gt C or 15% higher over preindustrial times, which would also lead to a larger net carbon loss (Fig. 4.1). For the industrial period, we simulate primary emissions of 108 Gt C. This value is similar to other studies, though at the lower end, because most studies include additional processes such as wood harvest and shifting cultivation (Olofsson and Hickler [2008] include non-permanent agriculture in their high estimate, and DeFries et al. [1999] uses Houghton [1999] for the industrial value, including thus wood harvest).

The primary emissions are composed of two parts (Fig. 4.1): (a) A direct, instantaneous release of carbon to the atmosphere from the vegetation biomass during the process of conversion (accounting for 94 of the 161 Gt C emissions from AD 800 to 2000). This implicitly includes respiration of plant products in short-term human use, e.g. as domestic fuel. (b) Indirect emissions from the decrease in net ecosystem productivity (NEP; defined as $NPP - R_h$, where R_h is heterotrophic respiration) (67 of the 161 Gt C). This implicitly includes respiration of plant products in long-term human use, e.g. as construction wood. NEP decreases since the decrease of NPP — the result of the ALCC-related change in area of differently productive PFTs — is not entirely balanced by a decrease of R_h . R_h decreases less than expected for the equilibrium state due to (1) additional plant material added to the soil pools

Table 4.3— Primary emissions of this study in comparison to previous estimates. Values are in Gt C and cumulative over the indicated time periods, with 30-years running mean for this study. Estimates of emissions prior to AD 800 in this study are estimated by assuming that the same amount of carbon is emitted per m² of agricultural expansion prior to AD 800 as averaged for AD 800 to 1850.

study	preindustrial	industrial	until present
DeFries et al. [1999]	48–57 (until 1850)	124 (1850–1990)	182–199 (until 1987)
Ruddiman [2003]	320 (4000 B.C.–1800)	–	–
Ruddiman [2007]	120–137 (–)	–	–
Olofsson and Hickler [2008]	114 (4000 B.C.–1850)	148 (1850–1990)	262 (4000 B.C.–1990)
Olofsson and Hickler [2008] permanent ag. only	79 (4000 B.C.–1850)	115 (1850–1990)	194 (4000 B.C.–1990)
this study	53 (800–1850)	108 (1850–2000)	161 (800–2000)
this study	63 (until 1850)	108 (1850–2000)	171 (until 2000)

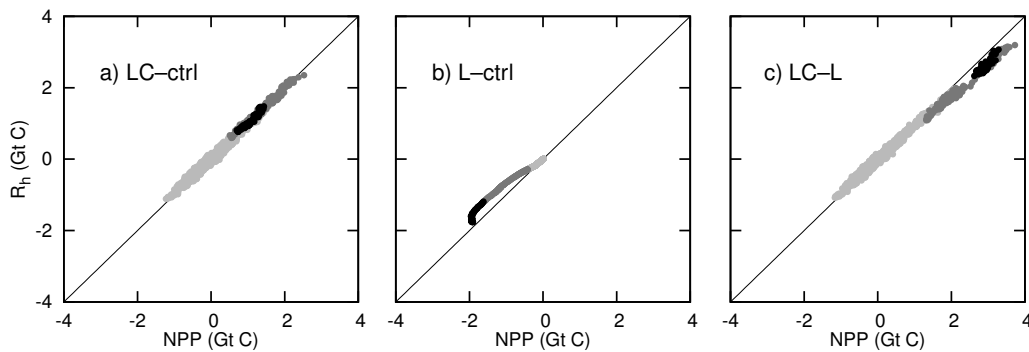


Figure 4.4— Changes in soil respiration R_h over changes in net primary productivity NPP. Gray shades indicate the time period: preindustrial (light), industrial (medium), future (dark). Simulations ctrl, L, LC as explained in Tab. 4.1. Values are 50-years running means.

from the converted natural vegetation and (2) excess soil organic matter from past conversions, which accumulates due to the time lag of R_h to NPP. The disequilibrium between NPP and R_h is depicted in Fig. 4.4: Fig. 4.4 a shows the changes in the transient coupled simulation, where both NPP and R_h increase, but no apparent disequilibrium occurs. The change in land cover alone, however, decreases NPP stronger than R_h (Fig. 4.4 b) due to the additional and excess soil organic matter. The disequilibrium vanishes in the future afforestation scenario. The coupled simulation seems to be in balance because the disequilibrium with respect to primary emissions is balanced by a disequilibrium with respect to the coupling flux: with altered climate and increased CO_2 but unchanged land cover, NPP increases stronger than R_h due to the time lag of R_h to NPP (Fig. 4.4 c). The latter disequilibrium has been called an “intriguing possibility” by Denman et al. [2007] in the context of a tropical forest sink.

The indirect emissions lead to an increase of soil carbon in the long term (Fig. 4.2), though this only slightly compensates the loss of vegetation carbon. The increased transfer of plant material to the soil pools, especially of woody parts with slow decomposition rates, leads to “committed” future carbon emissions beyond the instantaneous ALCC. This committed flux becomes the dominant source of emissions in the afforestation scenario of the future (Tab. 4.2).

4.3.4 Coupling flux

The quantitative estimates of the coupling flux in this study cannot be compared directly to previous studies, as those include changes in CO_2 from fossil-fuel burning in addition to ALCC emissions. While those studies assume that present CO_2 lies 70–100 ppm over the preindustrial level, CO_2 in our study rises only by 20 ppm (thus close to the 18 ppm found by Brovkin et al. [2004] in a comparable EMIC study). In particular due to lower CO_2 fertilization the coupling flux in our study is thus

lower than found e.g. by Gitz and Ciais [2003], Denman et al. [2007]. In our study, the coupling flux is even too weak to turn the biosphere into a net carbon sink, indicating that the sink capacity of the biosphere as observed for the last decades could not be achieved if atmospheric CO₂ was not additionally increased by fossil-fuel burning. As described before, the coupling flux leads to carbon uptake because of an increasing disequilibrium between NPP and heterotrophic respiration (Fig. 4.4 c). The absorbed carbon is primarily stored in the soil carbon pools (Fig. 4.2).

The coupling flux increases NEP stronger, though only marginally, than has been determined above as overall strength of the coupling flux from the difference in total terrestrial carbon. The small counteracting effect is the coupling effect on the direct emissions: with the coupling to the altered climate and increased CO₂, more carbon is stored in the vegetation than would be under the control climate and unaltered CO₂ — and more carbon is thus released in the conversion of vegetation with ALCC. This effect amounts to only 2 Gt C until 2000.

Gitz and Ciais [2003] were the first to quantify the “land-use amplifier effect” (“replaced sinks/sources” in Strassmann et al. [2008]). This denotes the effect that ALCC “acts to diminish the sink capacity of the terrestrial biosphere by decreasing the residence time of carbon when croplands have replaced forests”. In other words, the additional biosphere sink that arises under rising CO₂ is not as large as would be under natural vegetation, because storage in woody biomass ceases (carbon turnover rates are thus higher for cropland). Gitz and Ciais [2003] estimate that this effect may be as high as 125 Gt C over the 21st century for the A2 scenario. Calculation of the land-use amplifier effect in our study that most closely imitates their setup is to determine the loss of NEP for $LC - C$. For ALCC over the industrial period, this yields 49 Gt C. This cumulative flux, however, is composed of two parts: Only one part is the actual loss in additional sink from increased turnover rates that is intended to be quantified. The other part are indirect emissions from past ALCC. By comparing one simulation with static to one with transient land cover, both under changing CO₂ and climate, Gitz and Ciais [2003] implicitly include in the land-use amplifier effect the indirect emissions. In our simulation, indirect emissions amount to 45 Gt C, derived from the changes in NEP for $L - ctrl$ (Tab. 4.2). The indirect emissions have to be subtracted from the 49 Gt C in order to isolate the loss of additional sink capacity, which then amounts to only 4 Gt C. The relative difference between indirect emissions and loss of sink capacity is certainly not as high in the setup by Gitz and Ciais [2003] as here, since their study has a stronger increase of CO₂ by also including fossil-fuel burning, and the underlying ALCC is different. Still, with its analysis of sub-fluxes, our study suggests that a significant fraction of the land-use amplifier effect results from the indirect emissions and thus from past ALCC, rather than from the change in current turnover rates.

4.4 Anthropogenic influence on the preindustrial carbon cycle and climate

During the preindustrial period, a lower fraction of the emissions remains in the atmosphere than during the industrial period (Tab. 4.4): biospheric uptake amounts to 48% of the emissions over the preindustrial period, as compared to only 37% for the industrial, fossil-fuel-free, period in this study. The difference to the industrial period is even greater when a realistic industrial period is considered that includes fossil-fuel burning: then, only 26–34% of the emissions are taken up by the biosphere, because of the additional emissions from fossil-fuel combustion (Tab. 4.4). This difference in strength of biospheric uptake between the industrial and preindustrial period is mostly the result of a stronger coupling flux in the latter. The slow and more linear increase of emissions gives the land biosphere more time for CO₂ uptake, and CO₂ fertilization is more efficient at low CO₂ concentrations. The relative uptake by the ocean is almost unaffected and remains at around one third.

4.4.1 Anthropogenic contribution to Holocene CO₂ increase

As a consequence of the strong buffering of primary emissions by the biosphere and the low airborne fraction of CO₂ in the preindustrial period, the simulations show an only slow increase of atmospheric carbon content, despite significantly altered carbon pools of the ocean and the land biosphere several centuries earlier already (Fig. 4.5). Atmospheric carbon increases by 11.5 or 13.4 Gt C over the time period 800 to 1850 (5 or 6 ppm) for the best-guess ALCC and high land cover dynamics, respectively. When we assume the same airborne fraction prior to AD 800 as for 800 to 1850 and calculate the change in atmospheric carbon proportionally to agricultural expansion, ALCC prior to 800 would add roughly 2.1 or 1.1 Gt C (1 or 0.5 ppm, best-guess ALCC and high land cover dynamics, respectively). If we accounted fully for the net emissions prior to AD 800, atmospheric CO₂ may have risen above natural variability prior to AD 800 already. However, especially the ocean uptake must be expected to have been even more efficient in the early period of the Holocene, both because uptake by dissolution is higher with lower CO₂ release and because carbonate compensation gets effective at the millennial timescale [Archer et al., 1997]. It seems thus plausible to neglect these small early net emissions. In this case, atmospheric carbon content has not increased beyond natural variability until the late medieval times, when net emissions grew larger than the natural variability in land-atmosphere CO₂ exchange (see Fig. 4.5). This happens rather independently of the ALCC scenario, since the largest differences between the scenarios occur only later with stronger population growth in the 16th and 17th century.

With an increase of atmospheric CO₂ by 5–6 ppm by AD 1850, our estimates of the anthropogenic contribution to the Holocene rise in CO₂ are similar to the ones by Ruddiman [Ruddiman, 2003, 2007]. Ruddiman suggests in his “early anthropogenic hypothesis” that preindustrial ALCC emissions increase CO₂ by at least 9 ppm — of which about half are resulting from ALCC — and are responsible, via

Table 4.4— Comparison of our results to previous studies: uptake of anthropogenic CO₂ emissions by land, atmosphere, and ocean including sediments. Values are in Gt C and %, respectively, accumulated over the respective time periods with 30-years running mean. ALCC and fossil-fuel emissions are those considered in the studies. For [Bolin et al. \[2001\]](#), [Sabine et al. \[2004\]](#), the mid-range values were adopted.

study	time period	emissions			uptake		
		ALCC	fossil fuel	land	ocean	atmosphere	
Bolin et al. [2001]	1850–1998	136	270	110 (27%)	120 (30%)	176 (43%)	
House et al. [2002]	1800–2000	200	280	166 (34%)	124 (26%)	190 (40%)	
Gitz and Chais [2003]	1850–1998	139	269	110 (29%)	116 (30%)	157 (41%)	
Sabine et al. [2004]	1800–1994	140	244	101 (26%)	118 (31%)	165 (43%)	
this study	800–1850	53	0	25 (48%)	17 (31%)	11 (21%)	
this study	1850–2000	108	0	40 (37%)	37 (34%)	31 (29%)	
this study	2000–2100	48	0	27 (56%)	20 (41%)	1 (3%)	

4.4 Anthropogenic influence on the preindustrial carbon cycle and climate 71

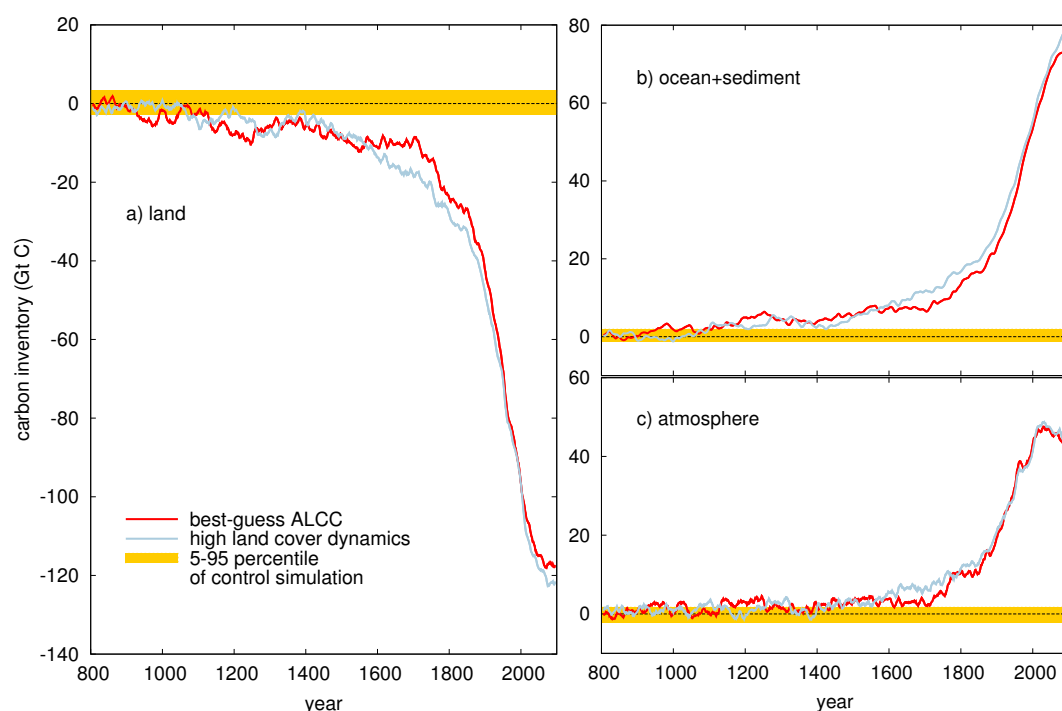


Figure 4.5— Change in the carbon stored globally on land, the ocean and sediment, and the atmosphere. Red lines are results for the best-guess ALCC reconstruction, blue lines for the high ALCC dynamics. The yellow area indicates the 5–95 percentile of the control simulation. Values are 10-years running means.

several feedbacks, for the anomalous CO_2 increase during the Holocene of 40 ppm. A discrepancy arises, however, when one considers that much of the anomaly in Ruddiman's study has been built up already in the early preindustrial period, while less than half of the net emissions indicated above for AD 800 to 1850 in our study occur before 1700. This discrepancy may be explained by the difference in method and data: Ruddiman derives his estimates by assuming one global terrestrial carbon stock and one global value for the per-capita use of agricultural areas, which is simplified in comparison to the present study that applies a spatially and temporally detailed reconstruction of ALCC and that explicitly models terrestrial carbon coupled to the atmosphere and ocean. Especially the coupling of the biosphere to atmospheric CO_2 and to the ocean seems to be a major improvement, since it proves to be the reason why preindustrial primary emissions become effective only to the small part of 21%. The present study further cannot support Ruddiman's hypothesis that the ALCC-induced release of CO_2 increased temperatures which in turn triggered an outgassing from the ocean. In our study, surface temperatures do not rise significantly in preindustrial times (Sec. 4.4.2) and the ocean remains a carbon sink throughout the last millennium. Since the present study indicates a substantially smaller anthropogenic influence on the global carbon cycle than the early

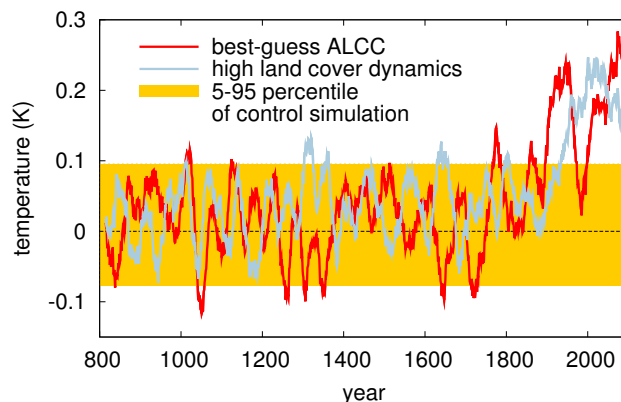


Figure 4.6— Change in the global mean surface temperature. Red lines are results for the best-guess ALCC reconstruction, blue lines for the high ALCC dynamics. The yellow area indicates the 5–95 percentile of the control simulation. Values are 30-years running means.

anthropogenic hypothesis, it supports studies that suggested additional reasons like temporally limited post-glacial vegetation regrowth and carbonate compensation to explain the CO_2 anomalies (see, e.g., Claussen et al. [2005] for a discussion).

4.4.2 Effect of ALCC on global mean temperatures

A significant impact of ALCC on global mean surface temperature does not occur until the industrial period, when temperature starts to rise beyond the natural variability (Fig. 4.6). Changes are small not only because of the low airborne fraction of CO_2 and thus small greenhouse effect, but also because biogeophysical and biogeochemical effects are counteracting each other. The anthropogenic influence on global mean temperature thus begins even later than on atmospheric CO_2 .

4.4.3 Epidemics and warfare

In addition to the hypothesis of CO_2 rising anomalously during the Holocene, Rudiman [2007] also suggests that 1–2 ppm of several sudden CO_2 drops of up to 8 ppm, which are reconstructed from ice core records, can be explained by epidemics. Epidemics as well as warfare have the potential to change land cover since natural vegetation regrows on those agricultural areas that have been abandoned in the course of the many deaths. Through this, previously released CO_2 could again be sequestered. The land cover reconstruction applied in this study indicates, for example, a forest regrowth on about 0.18 million km^2 as a consequence of the Black Death, which arrived in Europe in 1347 and killed about one third of the population [McEvedy and Jones, 1978]. Other such historic events during the last millennium are the conquest of Middle and South America by the Europeans and both the

4.4 Anthropogenic influence on the preindustrial carbon cycle and climate 73

Mongol invasion in China and the upheavals after the fall of the Ming Dynasty.

Although the conquest of Middle and South America led to a mass mortality by epidemics as well as direct warfare (the ALCC reconstruction used in this study assumes that 66% of the 40 million people died), this event does not imply large areas of regrowing vegetation and alters global carbon fluxes only negligibly. With total cumulative emissions of below 0.3 Gt C AD 800 to 1500 this region contributes only 2% to global emissions; even a sequestration of the entire 0.3 Gt C would be compensated by global emissions within 6 years and could therefore not be detected in ice core records. The reason for the few regrowing areas is mainly the assumption of a low per-capita use of agricultural land by the native Americans, but uncertainties are high in this region; for details see [Pongratz et al. \[2008b\]](#). Regrowth happens on larger areas, however, during the epidemics and warfare in Europe and China.

As explained in [Sec. 4.3.3](#), ALCC does not only imply instantaneous, but also indirect future emissions from changes in NEP, which arise due to the imbalance of the soil carbon pools after ALCC. The strength of the indirect emissions of past ALCC as compared to the carbon sequestered in regrowing vegetation determines whether farm abandonment turns a region into a carbon sink or not; transient simulations are essential to capture this process. The Black Death and the 17th century upheavals in China, for example, bring emissions from NEP changes to zero or close to it, but do not lead to negative emissions, i.e. carbon uptake from regrowth ([Fig. 4.7](#)). The amount of carbon sequestered in the regrowing vegetation is thus balanced by the indirect emissions. For the Mongol invasion, on the other hand, NEP increases after two decades and leads to an overall carbon sink. We must thus distinguish two kinds of events: In weak events indirect emissions from past ALCC keep a region as carbon source despite declining agricultural area, while in strong, long-lasting events the increase of NEP with vegetation regrowth turns a region into a carbon sink. In all events, direct emissions vanish of course during the time of agricultural decline.

Even if a region becomes a carbon sink, the global impact of such historic events remains small: even during the Mongol invasion the global emission rates decrease, but do not get negative ([Fig. 4.7](#)). Other areas in the world with unperturbed agricultural expansion outdo the regional carbon uptake. This is valid, according to our simulations, even if we take into account the uncertainty of relevant parameters such as turnover rates of soil carbon: If we assume as a maximum estimate of carbon uptake that the entire area returns to its state of AD 800 within 100 years (the approximate time of tree maturing) after the epidemic or war, global emissions over the following 100 years always compensate the maximum regional regrowth. From this study, it thus seems implausible that regrowth on abandoned agricultural areas following epidemics and warfare, as suggested by [Ruddiman \[2007\]](#), caused the CO₂ drops reconstructed from ice core data. Not taken into account so far, however, is the global coupling flux, which restores almost half of the primary emissions ([Sec. 4.4](#)). It amounts to about 12 Mt C per year averaged over 800 to 1500, and 48 Mt C per year 1500 to 1700. These values are close to the respective minima in global primary emissions, so that global carbon sequestration may indeed temporarily occur. The

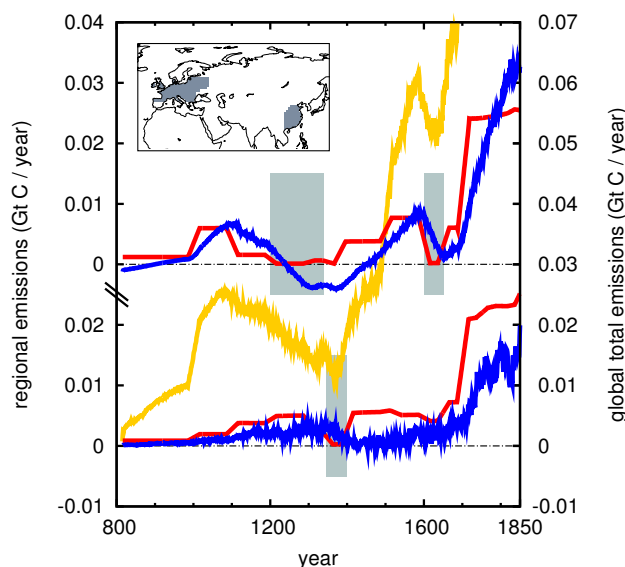


Figure 4.7— Direct emissions (red) and indirect emissions from changes in NEP (blue) for China (top) and Europe (bottom). The gray boxes indicate the time periods of decreasing regional population. On the right axes in yellow, global total primary emissions are given. Values are 30-years running means.

coupling flux is, however, highly variable even on a centennial timescale, imposing a high variability also on the atmospheric response, as seen in Fig. 4.5 c. Drops in CO_2 of several ppm may thus indeed occur, but can entirely be explained by natural variability.

4.5 Conclusions

For the first time, transient simulations are performed over the entire last millennium that apply a general circulation model with closed marine and terrestrial carbon cycle. With this setup we quantify the effects of ALCC on the carbon cycle and climate isolated from other natural and anthropogenic forcings. For the preindustrial period, the simulated results are expected to be close to a realistic simulation, since ALCC is the only anthropogenic forcing and the only major natural forcing — volcanoes — acts on a short timescale only. For the industrial period, the simulated results are significantly different from observations. By neglecting the emissions from fossil-fuel burning, the increase of atmospheric CO_2 is smaller than observed, with consequences on the strength of feedbacks, e.g., lower CO_2 fertilization.

Results show that without additional CO_2 fertilization from fossil-fuel burning, the biosphere does not turn into a carbon sink and leads to net emissions of 96 Gt C over the last millennium. The underlying primary emissions are 108 and 53 Gt

C for the industrial and preindustrial period, respectively. We have quantified the feedback of CO₂ emissions on land carbon uptake to be high especially during the preindustrial era: Here, the biosphere-atmosphere coupling reduces the impact of ALCC by 48%. Together with ocean uptake, only 21% of the emissions remain airborne. This keeps the human impact on atmospheric CO₂ small over much of the preindustrial times, which is in agreement with estimates by [Olofsson and Hickler \[2008\]](#), [Strassmann et al. \[2008\]](#). However, by late medieval times atmospheric CO₂ rises above natural variability. Our study thus suggests that with respect to global CO₂ concentration, the “Anthropocene” began prior to the industrialization.

We also investigated the effects of rapid changes in ALCC as occurred in several regions over the last millennium due to epidemics and warfare. Indirect emissions from past ALCC can be overcome by carbon storage in regrowing vegetation only for events of long-lasting impact on population numbers. Only then regional carbon uptake occurs. The concurrent agricultural expansion in other regions, however, renders these events ineffective on the global scale. Such events thus cannot be the major cause for observed drops in global CO₂, as had been suggested by previous studies. It seems more likely that local climate has been altered due to the fast changes in biogeophysical fluxes [[Pongratz et al., 2009](#)].

This study applies an estimate of maximum ALCC to give an upper limit of possible human impact with respect to uncertainties in reconstructing land cover. Primary emissions are higher in this case, but the net effect on CO₂ and global mean temperature is little altered. The only forcing taken into account is the change in agricultural extent. Other types of ALCC such as deforestation for wood harvest are not included, but, as explained, are unlikely to have a major impact on our results. The long timescale further reduces the influence of uncertain parameters such as the decomposition rates of carbon released during ALCC. Largely unknown, however, are preindustrial land management practices in their impact on the carbon cycle. Low-tillage practices, for example, are known to reduce CO₂ fluxes from soils [e.g., [Reicosky et al., 1997](#)], but base data to follow changes in management techniques globally and through the last millennium does not exist. Since the largest emissions arise from vegetation carbon and since restorage occurs mainly on natural areas, we expect our results to be generally robust.

The present study is relevant beyond the historical perspective in several points. First, an analysis of sub-fluxes suggests that a large fraction of the land-use amplifier effect results from the indirect emissions and thus from past ALCC, rather than from the change in current turnover rates. Our analysis does not suggest that there is less importance of including this effect in estimates for future climate change, but it indicates that a second process acts next to the change in turnover rates. Being indirect emissions, this second process may either be reported as part of the primary (“book-keeping”) emissions, or as part of the land-use amplifier effect, but must not be double-counted. It further is highly dependent on the assumptions made concerning the decay time of soil carbon on a decadal timescale. Model comparison and sensitivity studies should in the future aim at quantifying both processes separately with the associated uncertainty ranges.

Second, this study has found an anthropogenic influence on atmospheric CO₂ by late medieval times, and has indicated significant changes in the land and ocean carbon content even earlier. The carbon balance has already for this reason been considerably out of equilibrium for many centuries. Furthermore, one third of the ALCC emissions until today have already been released by the end of the preindustrial era. This early disturbance of the carbon balance does not only imply a legacy of the past by increasing the potential for anthropogenic climate change already prior to industrialization. It also implies that the beginning of the simulation period usually applied for climate projections may be too late — our results indicate that climate-carbon cycle studies for present and future centuries, which usually start from an equilibrium state around 1850, start from a significantly disturbed state of the carbon cycle, possibly distorting model calibration against the industrial period.

Acknowledgements

We thank Elke Stehfest for her help in extending the agricultural maps into the future, and Victor Brovkin and Katharina Six for helpful discussions. The simulations of this study were carried out as part of the “Community Simulations of the Last Millennium” (<http://www.mpimet.mpg.de/en/wissenschaft/working-groups/millennium.html>); we would like to thank all participants. We gratefully acknowledge Reiner Schnur for setting up and performing the simulations. These were carried out at the German Climate Computing Center (DKRZ).

Chapter 5

Biogeophysical Contributions to the Effects of Anthropogenic Land Cover Change

Abstract

The biogeophysical effects of historical anthropogenic land cover change (ALCC) are compared consistently to the biogeochemical effects on climate. For this, several simulations with a coupled atmosphere/ocean general circulation model are performed transiently over the last millennium applying ALCC as the only forcing. Biogeophysical effects are found to exert only a weak influence on global mean temperature (-0.03 K) due to offsetting regional and seasonal effects, and teleconnections. Regionally, they may cause significant temperature changes in the 20th century, but not during the preindustrial era. The rise in CO_2 from ALCC emissions (about 20 ppm AD 800 to present) is therefore the driving force of the simulated global warming of 0.13–0.15 K. Biogeophysical effects do further not contribute to the global restorage of carbon in the biosphere. The biosphere therefore mitigates ALCC emissions only via its response to increased CO_2 . The weak climate response to biogeophysical effects contrasts with high radiative forcing from surface albedo changes; if radiative forcing is used as estimate for global mean temperature, temperature change would be overestimated by a factor of 4–5. The dominance of the biogeochemical effects of ALCC has consequences also for the potential of climate change mitigation: If historical ALCC were reversed, most regions, including the northern mid- to high latitudes, would contribute a cooling signal. This study highlights the need for an integrated assessment of the different pathways of biosphere-atmosphere interaction to determine past and future effects of ALCC.

5.1 Introduction

Anthropogenic land cover change (ALCC) represents one of the few climate forcings for which it is still not known whether they impose a global net cooling or warming effect. The analysis of ALCC is complex because it affects biosphere-atmosphere fluxes through a multitude of partially counteracting processes. These processes are generally grouped into biogeophysical and biogeochemical mechanisms. Biogeophysical mechanisms describe the influence on climate by the modification of the physical properties of the land surface such as albedo, roughness, and evapotranspiration. Modeling studies suggest that through these biogeophysical effects, ALCC at mid- and high latitudes induces a cooling [e.g., [Bonan et al., 1992](#), [Claussen et al., 2001](#), [Bounoua et al., 2002](#)]. This is explained by the increase of surface albedo associated with deforestation, which is caused by the snow masking effect of forest as well as by the higher snow-free albedo of non-forest vegetation. The difference is particularly large during the winter and spring season for areas with snow cover, where albedo may change from 0.2 for forest to 0.8 on an open field [[Robinson and Kukla, 1984](#)]. With the strong hydrological cycle in the tropics, the reduction of roughness, leaf area, and rooting depth by deforestation reduces the evapotranspiration stronger than in the extra-tropics. Changes in plant physiology may therefore dominate over the albedo effect in the tropics so that ALCC can even lead to a local warming [e.g., [Claussen et al., 2001](#), [Bounoua et al., 2002](#), [DeFries et al., 2002](#)]. The loss of evapotranspiration in the tropics may again have a cooling effect on the extra-tropics due to the reduced atmospheric content of water vapor acting as greenhouse gas [e.g., [Ganopolski et al., 2001](#), [Sitch et al., 2005](#)]. On the global scale, the opposing biogeophysical effects of ALCC partially cancel each other, but regional climate is significantly influenced by ALCC and may even affect remote areas via teleconnections [e.g., [Chase et al., 2000](#)]. Past studies on the biogeophysical effects of historical ALCC have either performed transient simulations with Earth system models of intermediate complexity (EMICs) [[Brovkin et al., 1999](#), [Bertrand et al., 2002](#), [Bauer et al., 2003](#), [Matthews et al., 2003](#)], or equilibrium simulations with general circulation models (GCMs) [[Chase et al., 2000](#), [Betts, 2001](#), [Zhao et al., 2001](#), [Bounoua et al., 2002](#), [Davin et al., 2007](#)].

Probably the most important biogeochemical mechanism of ALCC is the influence on the carbon cycle, and the associated impact on the global CO₂ concentration. Altering atmospheric CO₂, ALCC modifies the Earth's energy balance and thus climate. ALCC constitutes a source of emissions mainly from the loss of terrestrial biomass. About one third of the anthropogenic CO₂ emissions over the last 150 years are estimated to be the direct consequence of ALCC [[Houghton, 2003](#)]. Counteracting the emissions is an increased carbon uptake by both natural and agricultural vegetation, the so-called "residual land sink" [[Denman et al., 2007](#)]. Uptake of CO₂ by the ocean constitutes another sink of ALCC emissions. Coupled simulations that isolated the effects of ALCC quantified an increase of atmospheric CO₂ of about 20 ppm over the last millennium after ocean uptake and biospheric restorage ([Brovkin et al. \[2004\]](#), Chapter 4). While the biogeophysical effects of ALCC have

a more regional impact on climate, the altered carbon fluxes are felt globally since atmospheric CO₂ is well mixed.

The overall picture so far is that with respect to ALCC most studies agree on (1) a global mean cooling from biogeophysical effects with pronounced cooling in the highly cultivated midlatitudes of Eurasia and counteracting biogeophysical effects in the tropics, and (2) a global warming from an increased atmospheric CO₂ concentration. Most studies have just addressed single aspects and do thus not allow for complete conclusions. Some studies, however, have contrasted biogeophysical and biogeochemical effects for certain scenarios: Claussen et al. [2001] have performed sensitivity studies of complete deforestation and afforestation in zonal belts, finding that tropical deforestation tends to warm the planet due to dominating biogeochemical mechanisms, while in mid and high northern latitudes biogeophysical processes of deforestation lead to a global cooling. Betts [2000], Bala et al. [2007] determined that there is no gain for climate protection if abandoned agricultural areas in the northern midlatitudes are reforested. Studies using EMICs have analyzed both individually and in combination biogeophysical and biogeochemical effects of historical ALCC: Matthews et al. [2004] for the last 150, and Brovkin et al. [2004] for the last 1000 years. It needs to be noted that the latter study did not rely on reconstructed land cover prior to AD 1700, but linearly interpolates between a state of potential vegetation in the year AD 1000 and AD 1700. Nevertheless, these two publications may be the most complete studies for the actual influence of ALCC on climate: First, they address both mechanism groups consistently with the same data and method. Second, they have a long enough history, which is crucial for atmospheric CO₂, since primary emissions may accumulate in the atmosphere over time. The two studies agree in (1) an overall cooling caused by biogeophysical mechanisms and a warming caused by biogeochemical mechanisms and (2) a similar magnitude of both effects. However, their conclusions concerning the net effect of biogeophysical and biogeochemical mechanisms are contradicting: While Brovkin et al. [2004] find a net cooling of -0.05 K over the last millennium, Matthews et al. [2004] suggest a net warming of about 0.14 K over the last 150 years. In the present study we try to give an improved estimate of the strength of the two individual effects and determine the sign of the net effect. We go beyond the previous studies in two important aspects: (1) We apply a detailed reconstruction of ALCC over the last millennium. The reconstruction includes ALCC due to cropland and pasture with sub-grid information and specific allocation rules for agriculture on the different types of natural vegetation. (2) We couple our land surface scheme to a general circulation model (GCM) for the atmosphere and the ocean. This allows a comparatively high spatial resolution, which is crucial to capture realistically the effects of such a heterogeneous forcing as ALCC. Unlike the two EMIC studies, this model further takes into account natural internal variability, which is important to make statements concerning the significance of ALCC-induced climate changes in relation to internal climate variability.

5.2 Model and data

The atmosphere/ocean general circulation model (AOGCM) consists of ECHAM5 [Roeckner et al., 2003] at T31 (approximately 4 degree) resolution with 19 vertical levels representing the atmosphere, and MPI-OM [Marsland et al., 2003] at 3 degree resolution with 40 vertical levels representing the ocean. The two models are coupled daily without flux correction. The closed carbon cycle is simulated in the ocean biogeochemistry model HAMOCC5 [Wetzel et al., 2005] and the modular land surface scheme JSBACH [Raddatz et al., 2007]. HAMOCC5 simulates inorganic carbon chemistry as well as phyto- and zooplankton dynamics in dependence of temperature, solar radiation, and nutrients. It also considers the buildup of detritus, its sinking, remineralization, and sedimentation. JSBACH distinguishes 12 plant functional types (PFTs), including one crop type, which differ with respect to their phenology, morphological, and photosynthetic parameters. Their fractional coverage of each grid cell is prescribed from maps annually. For each PFT, the storage of organic carbon on land occurs in five pools: living tissue, woody material, and a pool storing sugar and starches for the vegetation carbon, and two soil carbon pools with a fast (about 1.5 years) and a slow turnover rate (about 150 years). ALCC alters the pool carbon contents by relocating vegetation carbon to the soil and soil carbon between the PFTs of decreasing and expanding area (Sec. 4.2.1).

For the present study, the model code is changed such that the biogeophysical effects of ALCC are isolated: Carbon pools do not experience a change in cover fractions, i.e. there is no ALCC-related relocation of carbon. Furthermore, ALCC consequences on plant productivity are not allowed, i.e. gross primary productivity, autotrophic, and heterotrophic respiration are calculated as if the PFT distribution remained at the year AD 800. For this, canopy conductances for CO₂ and for water are treated differently: All variables depending on canopy conductance for CO₂ are calculated using the land cover map of AD 800, while transpiration, depending on canopy conductance for water, is calculated as usual on the prescribed ALCC maps. The prescribed ALCC maps are also used as usual for the calculations of morphological and phenological variables such as albedo and roughness length.

As ALCC forcing, the reconstruction of global agricultural areas and land cover by Pongratz et al. [2008b] is applied. It contains fractional maps of 14 vegetation types at an annual timestep and a spatial resolution of 0.5 degree. The agricultural types considered are cropland, C3 pasture, and C4 pasture. The reconstruction merges published maps of agriculture from AD 1700 to 1992 and a population-based approach to quantify agriculture for each country for the time period AD 800 to 1700. With this approach the general expansion of agriculture is captured as well as specific historic events, such as epidemics and wars. An extension of the agricultural and land cover maps into the future follows the A1B scenario [see Nakicenovic et al., 2000], superimposing changes in agricultural extent from the scenario maps on the ALCC map of 1992, the last map available from the ALCC reconstruction.

Four simulations branch off from the equilibrium state of the year AD 800 that all

exclude any changes in greenhouse gases other than the interactively calculated CO₂. They further exclude any changes in natural and anthropogenic forcings other than ALCC, i.e. changes in solar, orbital, volcanic forcings, and fossil-fuel-related CO₂ emissions are not permitted. With this setup, it is thus possible to isolate the effect of ALCC on climate. Apart from a 1300-year-long control simulation (named *ctrl*), two transient simulations run until the year 2100 applying ALCC as the only forcing (*LC*): The first applies the middle-range (*best-guess*) ALCC reconstruction, the second applies the lower-range ALCC reconstruction (*high land cover dynamics*), with the aims to give a best estimate and an upper limit of possible ALCC effects on the carbon cycle and related climate change for the preindustrial period. These simulations assess the combined biogeochemical and biogeophysical effects of ALCC and all atmosphere-ocean-biosphere feedbacks. A third transient simulation (*LC_{Ph}*) applies the middle-range ALCC reconstruction to simulate exclusively the biogeophysical effects of ALCC including feedbacks. The difference $LC_{Ch} = LC - LC_{Ph}$ approximates the climate response to exclusively the biogeochemical effects of ALCC.

In addition to the coupled simulations described above, the carbon pools are re-calculated offline with the aim to separate the primary effect of ALCC on the carbon balance prior to any feedbacks arising from the coupling with the climate and the atmospheric and marine part of the carbon cycle. In offline simulation *L*, the effects of ALCC were re-calculated under the climate of the control simulation. $L - ctrl$ then isolates the primary CO₂ emissions of ALCC prior to any feedbacks. $L - LC$ and $L - LC_{Ph}$, on the other hand, isolates the carbon flux induced by coupling the biosphere to the atmosphere (“coupling flux”) — under climate and CO₂ altered by both biogeophysical and biogeochemical effects and by biogeophysical effects only, respectively.

The following sections analyze the biogeophysical effects of ALCC as simulated in our model and compare them to the full influence on climate and the carbon cycle from both biogeophysical and biogeochemical effects as described in Chapter 4. They further give a synopsis of these effects in view of the mitigation potential of ALCC, and revisit the radiative forcing concept introduced in Chapter 3. Some figures that provide additional detail on the biogeophysical effects that is less relevant in the context of this Chapter will be found in Appendix B.

5.3 Climate response to ALCC

The full or “net” effect of combined biogeophysical and biogeochemical mechanisms of ALCC is a global warming. It becomes significant during the last centuries simulated in this study where ALCC is particularly strong (Fig. 5.1 a). This net effect includes a small biogeophysical cooling, which, on the global mean, remains mostly within the limits of internal variability throughout history and future. When determining the biogeochemical response as difference between the net effect and the biogeophysical response, it leads thus to a warming slightly higher than the net effect. Averaged over the 20th century, a global and annual mean surface temper-

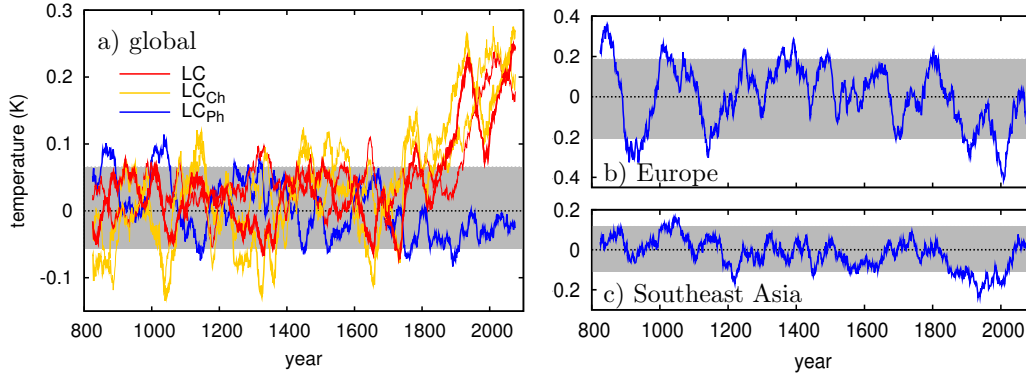


Figure 5.1— (a) Changes in global mean annual surface temperature from ALCC. LC_{Ph} : biogeophysical effects. LC_{Ch} : biogeochemical effects. LC : net effect. Thick lines are best-guess ALCC, thin lines are high land cover dynamic. The shaded area indicates the 5–95 percentile of the control simulation for the net effect. (b–c) Biogeophysical effects for Europe (land area 0–50°E, 40–60°N) and Southeast Asia (land area 67–120°E, 10–40°N). All values are 50-years running mean.

ature change of -0.03 K is found as response for the biogeophysical mechanisms, a warming of 0.15 and 0.13 K for the net effect (for best-guess ALCC and high land cover dynamics, respectively), and a consequent warming of 0.18 and 0.16 K for the biogeochemical mechanisms (Tab. 5.1). While the entire land area is more strongly affected by the biogeochemical warming than the ocean, the biogeophysical cooling is particularly pronounced over the agricultural areas. The table further compares our findings to the two previous studies that isolated the biogeophysical and biogeochemical responses. The net temperature rise found in the present study is close to the estimate by Matthews et al. [2004], who also found a strongly dominating biogeochemical response as the present study does. While our biogeochemical response is close to the estimate by Brovkin et al. [2004] in absolute values, our biogeophysical response is substantially smaller than both previous studies suggested. The next two sections will describe in more detail the two individual model responses and their spatial patterns.

5.3.1 Biogeophysical mechanisms

The weak global and annual mean response to the biogeophysical mechanisms of ALCC of -0.03 K contrasts sharply with its regional importance. In Europe, North America, China, and India annual mean temperature is decreased by 0.3 – 0.5 K, while a warming is simulated for smaller regions in the tropics and subtropics (Fig. 5.2 a). The cooling in northern mid- and high latitudes is largely driven by an increase of surface albedo (Fig. 5.3, averages over agricultural land). A strong snow-masking effect is discernible in the seasonal analysis in App. B.1, leading to cooling of up to 0.9 K in Northeast Europe in winter (compared to 1 – 2 K found e.g. by Betts [2001]). The albedo effect is dominating in the mid- and high latitudes on the annual mean

Table 5.1— Changes in annual surface temperature in K from ALCC averaged over the 20th century. The upper panel indicates results for global mean temperature from this study and previous studies for comparison. The lower panel separates changes in surface temperature for land, ocean, and agricultural area as found in this study. Values in brackets indicate results from the simulation with high land cover dynamics.

Simulation	Brovkin et al. [2004]	Matthews et al. [2004]	global
LC_{Ph}	-0.26	-0.16	-0.03
LC_{Ch}	0.18	0.30	0.18 (0.16)
LC	-0.05	0.15	0.15 (0.13)

Simulation	land	ocean	agric. area
LC_{Ph}	-0.04	-0.03	-0.10
LC_{Ch}	0.27 (0.24)	0.15 (0.14)	0.31 (0.25)
LC	0.22 (0.19)	0.12 (0.11)	0.21 (0.15)

over hydrological aspects also because transpiration effects are seasonally offsetting: As described in Pitman et al. [submitted], in the model applied here, the slower phenological growth of cropland as compared to the natural vegetation tends to transfer soil water from the spring to the summer season, with respective drying and warming of the lower atmosphere in spring as compared to wetter and cooler conditions in summer. ALCC in tropical regions, on the other hand, leads to a warming, which has also been found in previous studies [e.g., Bounoua et al., 2002]. The tropical warming is mostly induced by a loss of evaporative cooling throughout the year (Fig. 5.3), initiated by a reduction of net primary productivity (NPP) with the conversion of tropical forest to agriculture, and a reduction of roughness length (not shown). In addition to a decrease of the latent heat flux the warming is enforced by decreased cloud cover (not shown), counteracting the increase of surface albedo. This climate response is similar in the southern subtropics. In the northern subtropics, however, which are dominated by India, an increase in albedo and evaporation act in the same direction to cause strong cooling on land.

From the regional and seasonal description of effects, two important reasons for the weak global and annual mean response found in this study for the biogeophysical mechanisms of ALCC are already given: offsetting seasonal and regional responses over agricultural areas, with changing importance of albedo and hydrology. A third reason are teleconnections, leading to significant warming over the ocean and land areas remote from ALCC. A feeling for the importance of teleconnections can be gained by comparing temperature averaged over agricultural land against that averaged over all land or global area in Fig. 5.3. Clearly, the warming in the northern high latitudes is induced by teleconnections and offsets much of the cooling over agricultural area at 50–60°N. The offsetting of the albedo-driven cooling by hydrological warming and teleconnections seems to be stronger in ECHAM5/JSBACH/MPI-OM/HAMOCC5 than in EMICs: None of the 6 EMICs used in the intercomparison

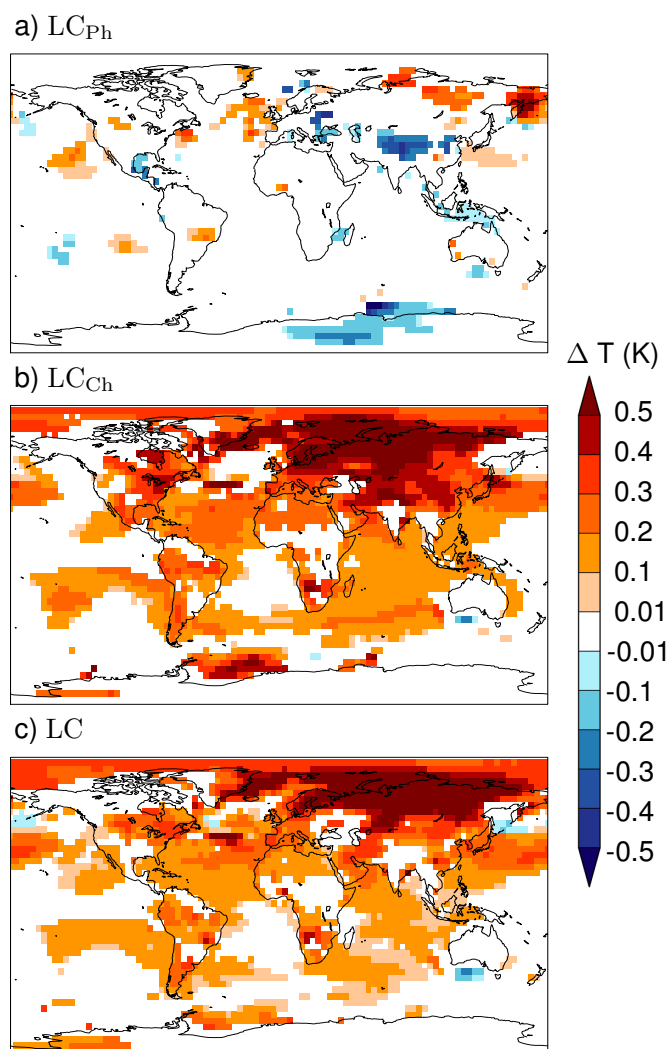


Figure 5.2— Change in annual surface temperature from ALCC averaged over the 20th century. LC_{Ph} : biogeophysical effects; LC_{Ch} : biogeochemical effects; LC : net effect. Shown are only areas significant at the 95% level of a Student's t-test.

study by Brovkin et al. [2006], for example, yielded a notable warming in the tropics, while all exhibited larger changes in albedo and a stronger associated cooling (global and annual mean of -0.13 to -0.25 K) (see Fig. B.2 for a comparison of this study to the EMIC study). This discrepancy may arise from the general differences between GCMs and EMICs or specifics of the setup of the EMIC study (the study, for example, overestimates ALCC by assuming potential vegetation in the year AD 1000), rather than from the specific characteristics of the model applied in this study, since the results of this study are much closer to other GCM studies: The global and annual mean cooling found in the GCM study by Betts [2001] for

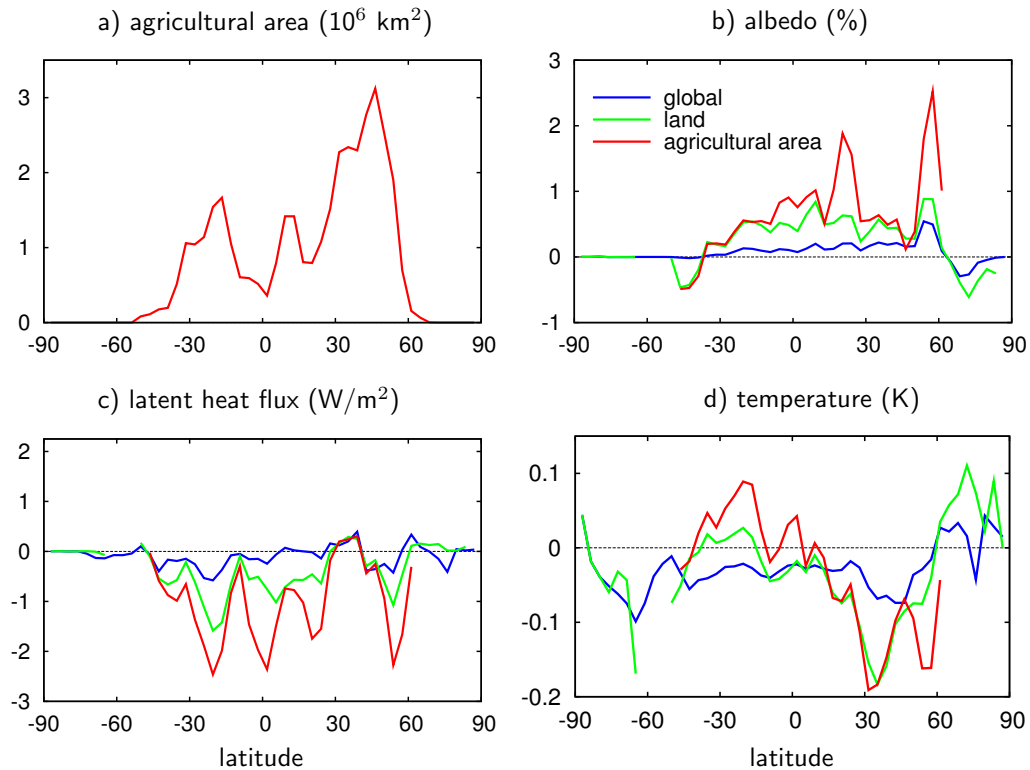


Figure 5.3— (a) Zonal integral of changes in agricultural area since AD 800 (20th century average); (b–d) annual mean changes induced from biogeophysical effects of ALCC (simulation LC_{Ph}) averaged zonally and over the 20th century for (b) surface albedo, (c) latent heat flux, (d) surface temperature. The different lines indicate averages over the globe, the land area, and agricultural area (cut at 62° N), respectively.

ALCC until today is 0.02 K, and tropical and extra-tropical effects largely cancel each other on the global mean also in the GCM study by [Bounoua et al. \[2002\]](#). The discrepancy may, however, be enforced by model-specific parameterizations: Biogeophysical effects of ALCC are known to be very sensitive to model parameterizations, including the implementation of ALCC, the representation of crop phenology, and PFT-dependent values of albedo and roughness [[Pitman et al., submitted](#)]. In particular the difference between models with respect to the change in albedo due to ALCC has repeatedly been identified as a main source of difference in model results [[Matthews et al., 2003](#), [Myhre and Myhre, 2003](#), [Matthews et al., 2004](#)]. In a similar setup, the model applied here yielded the smallest areas that exhibit significant summer temperature changes in comparison to 6 other land surface models [[Pitman et al., submitted](#)].

The weak biogeophysical response found in this study for the 20th century is consistent with no significant changes in global mean temperature also for earlier

times (Fig. 5.1 a). The tropical warming from changes in the latent heat flux plays a much smaller role in the preindustrial period since tropical deforestation is a phenomenon mostly of recent decades, but also the midlatitudinal cooling is not pronounced. Even for Europe, where substantial cooling occurs in the 20th century, this effect is not discernable in earlier centuries (Fig. 5.1 b), although Europe was one of the centers of preindustrial agriculture [Pongratz et al., 2008b]. The large internal variability in these latitudes conceals any earlier climate signal; with a dynamic ocean, the present study captures the entire internal variability. Also in the second region of strong cooling in the 20th century, Southeast Asia, no significant climate response to biogeophysical mechanisms of ALCC is found for the preindustrial period (Fig. 5.1 c). Similarly, no significant cooling for more than single decades is found for the Northern Hemisphere mean temperature (not shown), with a 20th century cooling of -0.03 K. Since the biogeochemical aspects of ALCC are related to warming only, one can thus conclude that there is no indication that ALCC has substantially contributed to the long-term Northern Hemisphere cooling found in temperature reconstructions (see Sec. 1.4) and simulated as, at least partially, an effect of ALCC by Govindasamy et al. [2001], Bauer et al. [2003], Brovkin et al. [2006].

5.3.2 Biogeochemical mechanisms

The temperature response to the biogeochemical mechanisms of ALCC is driven by a rise of atmospheric CO_2 from ALCC emissions, which has been simulated in Chapter 4 to be about 20 ppm over the last millennium for *LC*. The spatial pattern of the response of surface temperature resembles those from observed climate change over the last decades, with a strong warming in northern high latitudes due to the sea ice-albedo feedback (Fig. 5.2 b). Driven by the atmospheric concentration of the well-mixed CO_2 , the temperature response is unrelated to local effects of ALCC; thus, strong local biogeophysical effects imprint on the spatial pattern of the net temperature response, as seen e.g. in Eastern Europe/Central Asia and also in parts of India. The latter is one of the few areas, where biogeophysical effects “win” over the biogeochemical effects so that the net effect of ALCC results in a cooling, although the signal is not statistically significant.

5.4 Biogeophysically-induced changes in the carbon cycle

Changes in the carbon storage on land are, as explained in Chapter 4, the net effect of primary emissions from ALCC on the one hand, and a restorage of carbon in the biosphere on the other hand. These effects are calculated from the coupled and offline simulations described before. Carbon restorage occurs due to the coupling of the biosphere to the atmosphere, when changes in atmospheric CO_2 and climate can influence plant productivity. In the coupled simulation including both biogeochemical and biogeophysical effects, a strong coupling flux has been found of 37%

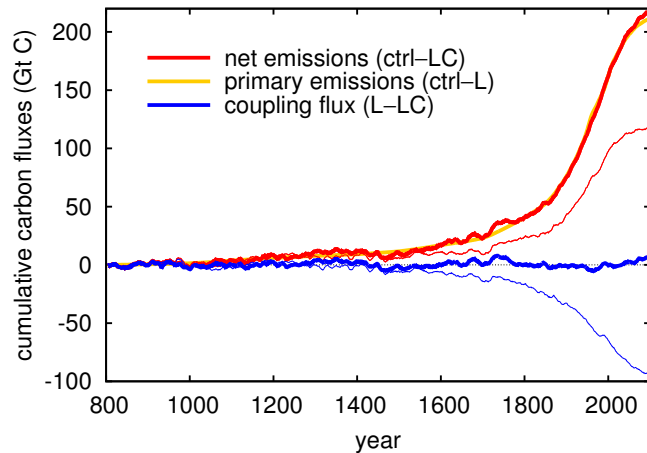


Figure 5.4— Global land-atmosphere carbon fluxes, cumulative since AD 800. Positive values indicate release to the atmosphere. Thick lines are results for the simulation with biogeophysical effects only (LC_{Ph}), thin lines are results for the simulation with biogeophysical and biogeochemical effects (LC , best-guess ALCC). Note that the curves for primary emissions are behind the curve for net emissions of ($ctrl - LC_{Ph}$).

and 48% for the industrial and preindustrial period, respectively, initiated probably by CO_2 fertilization (see Sec. 4.3). We can now quantify the contribution of those climate changes that were induced by the biogeophysical mechanisms of ALCC.

On the global mean, ALCC does not contribute to restorage of carbon via its biogeophysical effects. Primary emissions and net emissions of ALCC are similar, indicating a zero coupling flux (Fig. 5.4). This is consistent with a stable CO_2 concentration in LC_{Ph} , fluctuating around the average value of the control simulation of 281 ppm (Fig. 5.5 c). This also indicates that the biogeophysical effects of ALCC do not contribute to the rise in CO_2 observed for the last centuries. Regionally, some carbon storage does, however, occur (Fig. 5.6). These regional carbon storages are induced by climate change, which may be favorable for carbon uptake as in the case of Eastern Europe (higher water availability in summer), or unfavorable for carbon uptake as in the case of Australia (decreased rainfall). Overall, however, also the regional coupling fluxes are small as compared to those under additional CO_2 emissions from ALCC (compare Fig. 4.3 and Fig. B.3). This shows that the coupling flux observed for simulation LC is predominantly driven by the increase of CO_2 , either directly via CO_2 fertilization, or indirectly via the associated climate change, but not by the biogeophysical effects of ALCC.

5.5 Relevance of the radiative forcing concept

In Chapter 3, a very common measure used to quantify the importance of ALCC as climate forcing has been introduced: radiative forcing (RF) from ALCC-induced changes in surface albedo. RF, ΔF , can be related to the change in global mean

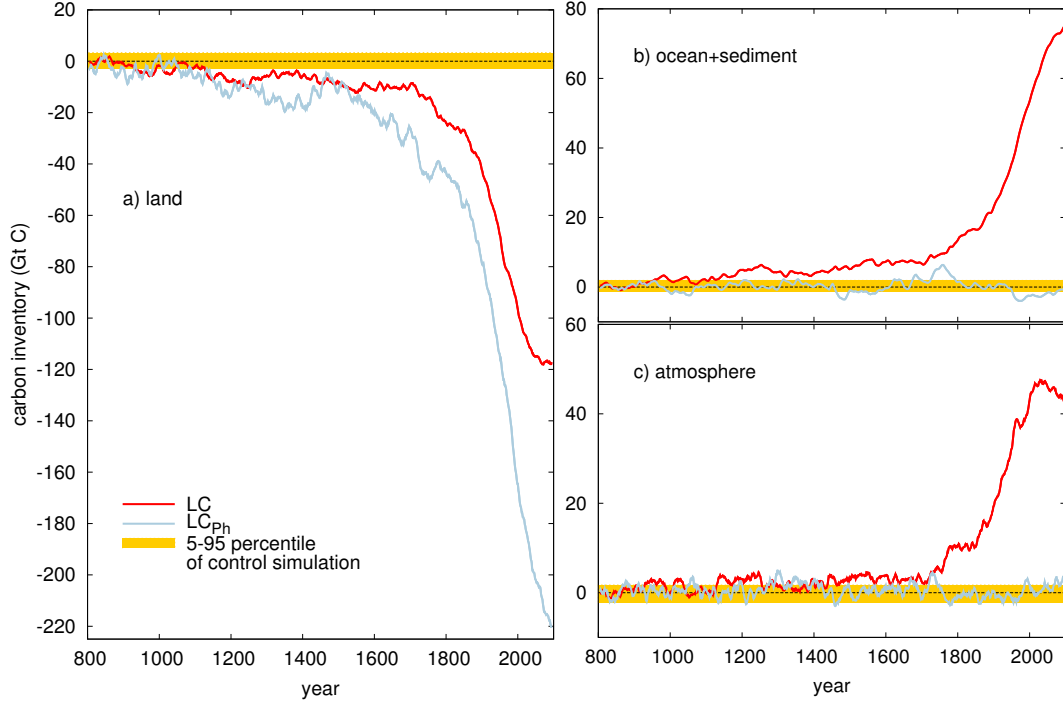


Figure 5.5— Change in the carbon stored globally on land, the ocean and sediment, and the atmosphere. Red lines are results for simulation LC including both biogeophysical and biogeochemical effects of ALCC. Blue lines are results for simulation LC_{Ph} including only biogeophysical effects. Both simulations apply the best-guess ALCC reconstruction. The yellow area indicates the 5–95 percentile of the control simulation. Values are 10-years running means. This figure compares with Fig. 4.5; note the different scale for (a) land.

surface temperature, ΔT , via the climate sensitivity parameter λ (see Sec. 1.5),

$$\Delta T = \lambda \cdot \Delta F . \quad (5.1)$$

This RF is meant to represent the global mean climate response to biogeophysical effects of ALCC and is used as such e.g. in the reports by the Intergovernmental Panel on Climate Change. In Chapter 4, the CO_2 emissions from ALCC and the associated increase in CO_2 have been quantified. Though often subsumed as fossil-fuel-dominated anthropogenic emissions, this is the second important pathway of direct ALCC influence on temperature. The RF for ALCC-induced changes in CO_2 , ΔF_{CO_2} , can be estimated via the increase in atmospheric CO_2 , ΔC , in the two LC simulations (best-guess ALCC and high land cover dynamics) after uptake by land and ocean, using the relationship [Myhre et al., 1998]

$$\Delta F_{\text{CO}_2} = 5.35 \cdot \ln(1 + \Delta C/C_0) . \quad (5.2)$$

Here, C_0 is the CO_2 concentration at the beginning of the simulations.

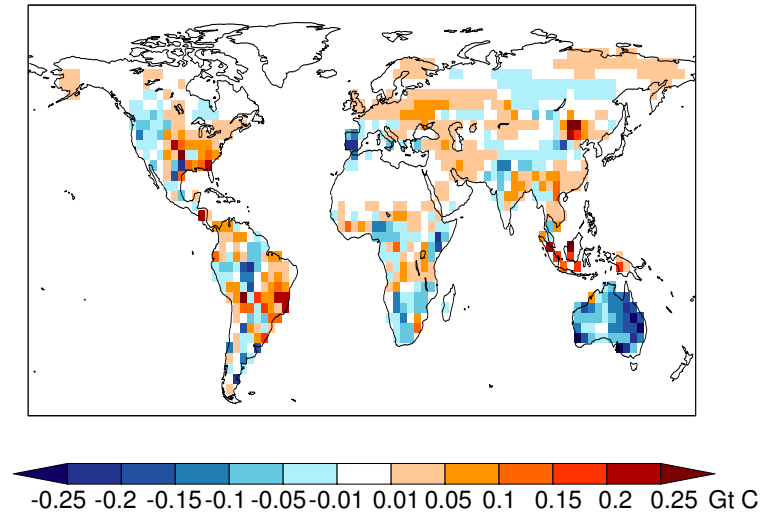


Figure 5.6— Coupling flux of ALCC derived from simulations ($L - LC_{Ph}$) accumulated over the industrial period (AD 1850–2000). Units are Gt C taken up in each grid cell.

In the present Chapter now, the individual temperature responses to biogeophysical and biogeochemical mechanisms have been quantified. Together with the RF for albedo changes and for CO_2 , this allows a synopsis of the relation of forcings and climate responses, and an assessment of the relevance of the RF concept with respect to both biogeophysical and biogeochemical mechanisms of ALCC as evaluated consistently with the same data and model.

Fig. 5.7 depicts RFs and temperatures for the biogeochemical, biogeophysical, and net effect, from the 18th century onwards when clear trends in global mean temperatures emerge. The RF for albedo changes since AD 800 and CO_2 are of opposite sign, but on the same order of magnitude, creating a total RF from adding the two effects that is distinct from any of the two components. For temperatures, however, the full climate response follows closely the biogeochemical response, with both full and biogeochemical response being predominantly driven by the RF of CO_2 . The underlying reason is the weak dependence of temperature change from biogeophysical effects of ALCC on RF from albedo changes. The temperature-RF dependence for CO_2 in the 20th century is 0.7 and 0.6 K/(W/m²) for best-guess ALCC and high land cover dynamics, respectively (this dependence would equal λ of Eq. 5.2 if it were derived from an equilibrium study, not a transient study as here). Applying this temperature-RF dependence, a biogeophysical cooling of 0.12–0.14 K would be expected from the albedo RF, but temperature decreases only by 0.03 K. In the model used here, the RF concept as commonly applied to surface albedo changes thus overestimates the climatic importance of the biogeophysical effects of ALCC by a factor of 4–5 as compared to the importance of CO_2 . As expected from the description of biogeophysical temperature response above, the regions con-

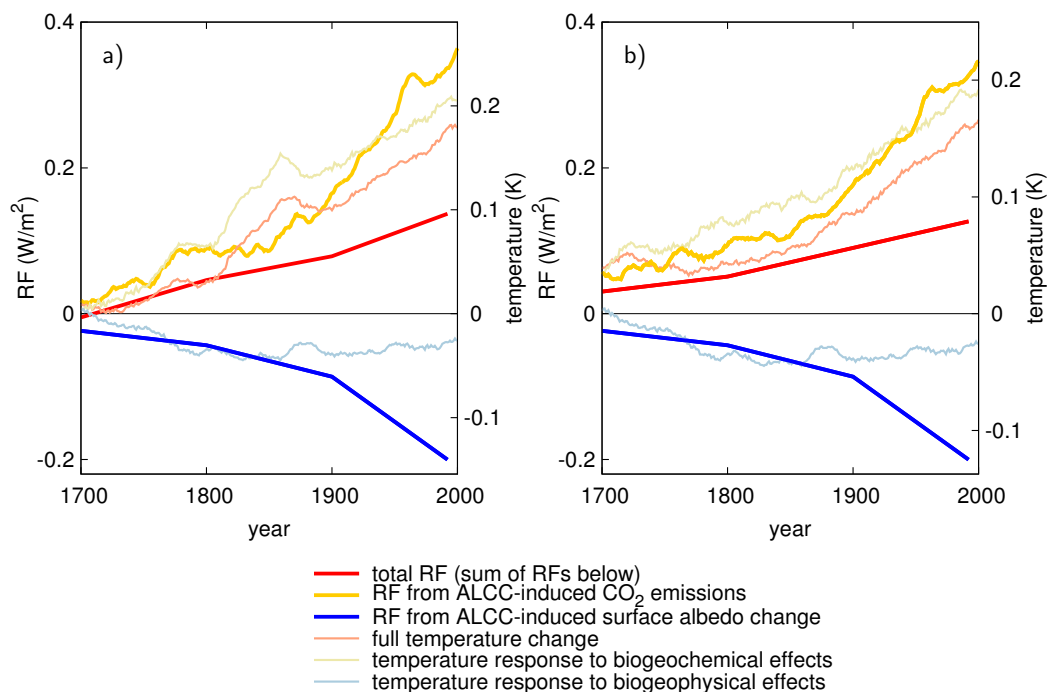


Figure 5.7— Comparison of changes in radiative forcing since AD 800 (RF, left axis, 10-years running mean for CO₂) to temperature change (right axis, 200-years running mean). (a) Biogeochemical and total/full curves for best-guess ALCC, (b) biogeochemical and total/full curves for high land cover dynamics. The temperature axis is scaled relative to the RF axis via the temperature-RF dependence for CO₂ in the 20th century (0.7 and 0.6 K/(W/m²) for (a) and (b), respectively). Depicted is only the time period following 1700, when clear temperature trends emerge.

tributing most to the forcing-response discrepancy are the tropical regions, where the temperature-RF dependence is an order of magnitude lower than the one for CO₂ (Fig. 5.8). Temperature in the northern mid- to high latitudes, on the other hand, is more sensitive to the RF with changes up to 0.25 K/(W/m²). The spatial pattern may also cause the dependence of biogeophysical temperature response to RF from albedo changes to be stronger until the 19th century: Until then, agriculture centered in particular in Europe, India, and China, where the temperature response is indeed a cooling; tropical deforestation, on the other hand, which alters climate via evapotranspiration rather than via albedo, occurred mainly in the 20th century. However, internal variability of temperature is too large for a definite statement.

The overestimation of the biogeophysical temperature response from albedo RF is qualitatively similar to the findings by Davin et al. [2007], who quantify a climate sensitivity parameter that is lower as compared to CO₂ forcing by a factor of 0.5 and 0.3 for ALCC-induced RF from albedo changes and from changes in both albedo and water vapor, respectively. The reasons for a reduced temperature response to RF from albedo changes are assumed to be (1) the spatial distribution of ALCC,

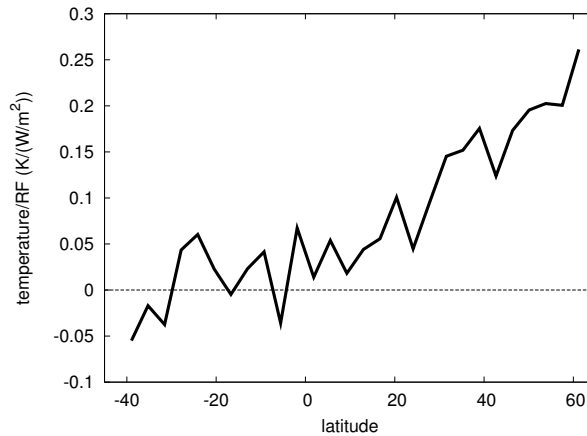


Figure 5.8— Quotient of change in surface temperature (average over the 20th century) from simulation LC_{Ph} and change in RF from surface albedo changes (average over 1900 and 1992 minus AD 800). Shown are zonal averages over all those grid points where RF is negative with a magnitude greater than 0.5 W/m^2 .

with little changes in the high latitudes where via cryospheric feedbacks climate sensitivity is enforced [Hansen et al., 1997, Davin et al., 2007], and (2) changes in the partitioning of the turbulent heat fluxes, from latent towards more sensible heat, warming the lower atmosphere [Pielke et al., 2002, Kleidon, 2006, Davin et al., 2007]. The present study supports in particular the latter suggestion, finding a biogeophysical warming in the tropics from reduced evaporative cooling, and a consequently very weak temperature-RF dependence in these regions. Furthermore, it shows that the net temperature response to ALCC is indeed predominantly driven by the CO_2 emissions from ALCC.

5.6 Historical ALCC in the context of climate mitigation

Reforestation and afforestation have been suggested as tools to mitigate climate change, as carbon would be stored in the (re-)growing trees [UNFCCC, 1998]. It has also been noted that the appraisal of the climate mitigation potential of a region based solely on its carbon sequestration potential may be insufficient, since forestation influences climate also via the biogeophysical mechanisms [Betts, 2000, Claussen et al., 2001, Bala et al., 2007]. Depending on their location, intended cooling or unintended warming may be the final consequence of forestation projects. Betts [2000] for example noted that such unintended warming may occur from coniferous carbon plantations in the boreal zone, and that the cooling potential of such plantations in the temperate latitudes may be overestimated. Similarly, Sitch et al. [2005] simulated for the B1 scenario (large-scale future temperate reforestation) an overall

warming similar to the A2 scenario (large-scale tropical deforestation) due to strong biogeophysical warming. All mentioned studies except for [Betts \[2000\]](#) performed coupled simulations, which is problematic in the mitigation context since CO₂ emissions mix in the atmosphere to give a local temperature signal that is not caused by local, but by global CO₂ emissions. All mentioned studies except for [Sitch et al. \[2005\]](#) further performed idealized experiments only in which extreme scenarios of complete deforestation and forestation over certain latitudinal bands were assumed. This theoretical consideration of the overall impact of maximum forestation on climate can be contrasted to the question of the actual overall impact of ALCC until present. For this purpose, the contribution of ALCC at each grid point to global climate change is estimated as described in the following 5 paragraphs.

First, the contribution of ALCC at each grid point to global climate change via the biogeophysical mechanisms is assessed. For this, the change of RF from albedo changes between the years AD 800 and 1992 from Chapter 3 is used (Fig. 5.9 a). Though, as described in Sec. 5.5, RF from albedo changes may not be a good approximation of the overall climate response to biogeophysical effects, it is advantageous to use it here: As long as it is not clear whether the model applied in this study has a too weak biogeophysical climate response or the other models a too strong one (Sec. 5.3.1), it is more objective to rely on a measure that is similar across models, which RF from albedo changes is (see Chapter 3). By using this measure as representation of the biogeophysical effects, a conservative, upper estimate of the biogeophysical effects possibly counteracting RF from CO₂ is given.

Second, the contribution of ALCC at each grid point via the biogeochemical mechanisms is assessed. The method is as follows: Using Eq. 5.2, the primary emissions from AD 800 until 1992 determined from the simulations *L - ctrl* (best-guess ALCC) can be translated into the RF from CO₂ emissions for each grid point. The grid-point based usage of Eq. 5.2, however, introduces an error: Instead of calculating the RF of the global CO₂ increase of 20 ppm, the RF is calculated for each grid point individually and summed to give the global RF. This introduces an error because RF does not depend linearly on CO₂. An error estimate (App. C) shows, however, that the error is below 4% and can therefore be neglected in this analysis.

Primary emissions are scaled down to yield the RF as determined from the increase in atmospheric CO₂ in Sec. 5.5 on the global mean. This is the same as subtracting proportionally to the primary emissions of each grid point the global ocean uptake over history as simulated in *LC* (best-guess ALCC), and the carbon restorage on land due to the coupling effect as derived from *L - LC*. The reader should note that the described method of subtracting terrestrial carbon uptake from primary emissions does not duplicate the method of Sec. 4.3, where the coupling flux has already been subtracted from primary emissions, but in a spatially explicit form also for the coupling flux, to yield a map of net emissions. The underlying reason why the map of net emissions cannot be used here is that we need to clearly distinguish between effects of ALCC that can be attributed to ALCC in a specific location and those that cannot. Attributable effects are changes in carbon storage that are

caused directly by the local ALCC, and include primary emissions that depend on the strength and type of ALCC a grid point is undergoing and the carbon thereby lost at this grid point. Effects not attributable to ALCC of a specific location include the coupling flux, which is initiated by primary emissions only via the pathway of atmospheric CO₂; atmospheric CO₂, however, is globally well mixed and integrates over the emissions of all grid points, its effects on carbon uptake are therefore detached from the local source of CO₂. Therefore, the terrestrial carbon uptake due to the coupling effect needs to be globally summed and subtracted proportionally to the local primary emissions, independent of where it actually occurs. This principle also applies to ocean uptake (here, it is obvious that the (ocean) map of carbon uptake cannot sensibly be subtracted from the (land) map of carbon emissions). Since both ocean and terrestrial carbon uptake are carbon sinks that are initiated by ALCC, they need to be taken into account as counteracting the primary emissions in order to quantify the net effect of ALCC on CO₂.

Overall, the estimate derived here for RF from ALCC-induced increase in atmospheric CO₂ reflects the historical effect of ALCC including the transient history of carbon source and sink terms. This more closely simulates the true temporal evolution of ALCC-induced changes in carbon fluxes than previous equilibrium studies. With this method, the individual contribution of each grid point to the global RF from CO₂ is determined and shown in Fig. 5.9 b.

The map of RF from CO₂ emissions until present is added to the map of RF from present albedo changes to yield the total RF shown in Fig. 5.9 c. Note that the content of this map is quite different from Fig. 5.2 c, which showed the temperature change from the coupled simulation: The present approach allows to assess the contribution of ALCC in an individual grid cell to global climate change. Fig. 5.2 c, on the contrary, shows the net temperature change caused by the biogeochemical and biogeophysical effects of ALCC, but not as intended in this section as being attributable to ALCC of a specific location — the biogeophysical effects (Fig. 5.2 a) clearly include teleconnections that are caused by remote, not localized ALCC, and the biogeochemical effects (Fig. 5.2 b) mainly capture the climate response to the globally well-mixed CO₂.

In Fig. 5.9 c, global mean RF is 0.35 W/m² for CO₂, -0.20 W/m² for albedo, and 0.15 W/m² total RF (compare Fig. 5.7). Most regions exhibit a positive total RF, indicating that there, the increase of atmospheric CO₂ by historical ALCC in a grid point has had a larger radiative effect than the increase in surface albedo resulting from the same ALCC. These regions include Europe, India, China, and regions with tropical forest. Some regions exhibit a negative total forcing due to either of two reasons: (1) the increase in albedo induces a larger forcing than CO₂ emissions, as on the U.S. West Coast, in Central Asia, the Eastern Amazon, and West Africa; or (2) the increase in albedo and changes in carbon stocks act in the same direction, since ALCC leads to carbon sequestration, as in Australia, South and East Africa, the Pampas, and Mexico. Only in these few regions of negative total forcing may local ALCC have had a mitigating effect on global warming in the past.

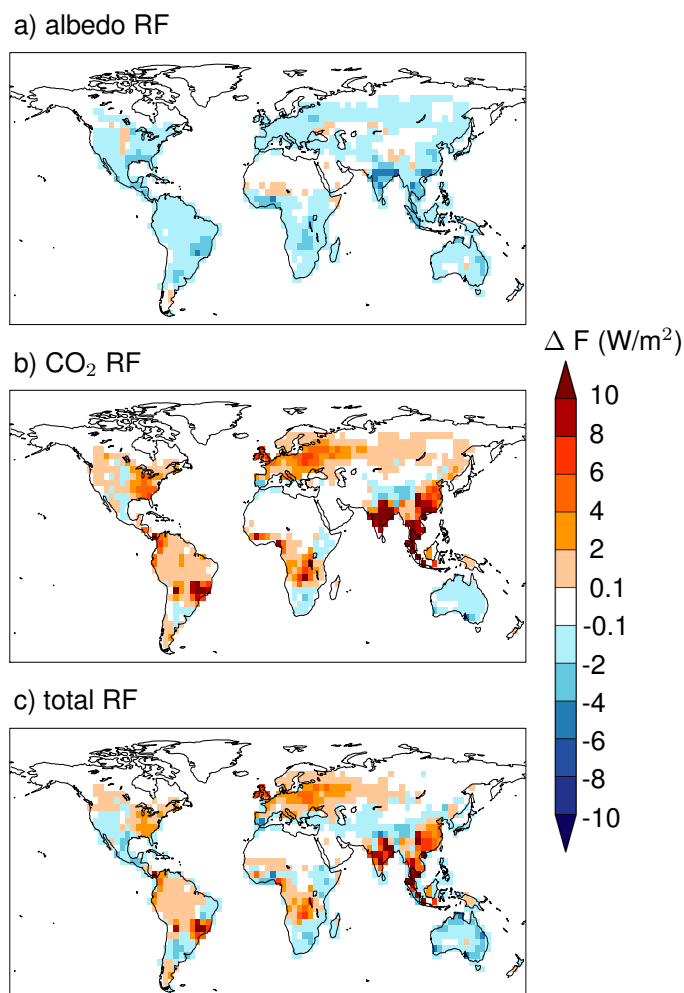


Figure 5.9— Comparison of radiative forcing (RF), ΔF : (a) RF from ALCC-induced surface albedo changes AD 800–1992, data as described in Chapter 3; (b) RF from ALCC-induced CO₂ emissions AD 800–1992; (c) total RF as sum of (a) and (b).

What does this conversely mean for future mitigation potential? Reversing ALCC of the last millennium would, on a timescale long enough to let the ocean outgas what it had taken up of ALCC emissions, simply reverse the total RF of Fig. 5.9 c. This means that most regions would have a cooling potential when reversing them to their vegetation cover of AD 800. In the transient history, however, this may not be the most plausible scenario: On a short timescale and with small changes in atmospheric CO₂ ocean uptake would continue at an unchanged rate (approximately 0.2 Gt C per year over the last 50 years of our simulation). Via the time lag in ocean response past ALCC would thereby add on the carbon sequestration potential of reversing ALCC. Depending on how long ocean uptake continues, the total RF would become

more negative and might even render those regions effective for climate mitigation where past ALCC led to cooling.

It may be appropriate that previous studies have warned that the climate change mitigation potential may be overestimated when we assume future scenarios in which, after replacing boreal coniferous forest with crops, agricultural area is again reforested (although currently, only 7% of agricultural expansion or 23% of deforestation affects evergreen coniferous forest, Sec. 2.4). However, the mitigation potential seems to be less overestimated when we look at the effects of past ALCC, the reversion of which is possibly the more realistic scenario as first step for future mitigation. The ALCC over the past has only in few regions lead to a cooling radiative effect.

5.7 Summary and conclusions

This study has isolated the climate response to the biogeophysical effects of ALCC from that to the biogeochemical effects. Both responses were simulated in the same coupled atmosphere/ocean GCM, which allows to compare the responses consistently without differences in ALCC implementation and model parameterization. Applying a GCM allows a higher spatial resolution than previous EMIC studies, which is more adequate for a forcing as heterogeneous as ALCC. The setup further allows to compare signals to natural internal variability. By running the model transiently over the last millennium, we could estimate the coupled response, including feedbacks, to the evolving strength of ALCC over the last millennium. A disadvantage of this study certainly is the fact that biogeochemical effects are not simulated independently, but are derived as residual of a fully-coupled simulation and one allowing only biogeophysical mechanisms. Therefore, the effect identified as contribution from biogeochemical mechanisms may also include possible synergies. However, in an EMIC study determining independently biogeophysical, biogeochemical, and full model response, [Claussen et al. \[2001\]](#) found that synergies are much smaller than pure contributions, which is also supported by the studies by [Brovkin et al. \[2004\]](#), [Matthews et al. \[2004\]](#). Hence, one of the three responses may also in our study be approximated as residual of the two others. Considering that the biogeophysical response of the EMICs differs substantially from GCMs, this remains, however, an open question until more GCM studies have been performed.

This study has found a global temperature change due to biogeophysical effects that is small as compared to the temperature response under both biogeophysical and biogeochemical consequences of ALCC, namely -0.03 K as opposed to 0.13 – 0.15 K. While in Europe and Southeast Asia some regions show significant cooling in the 20th century, changes are nowhere significant, as compared to internal variability, during the preindustrial era. Warming from ALCC-induced CO_2 emissions is thus little dampened by biogeophysical cooling and leads to a significant warming in the industrial period. The Northern Hemisphere cooling simulated is substantially smaller than found in previous studies and unlikely to have driven the long-term cooling leading to the “Little Ice Age”. A similar conclusion has been drawn in

Chapter 3 based on estimates of RF from albedo changes only, and is confirmed here by the coupled model response.

The small biogeophysical cooling contradicts high estimates of RF from ALCC-induced albedo changes. This contradiction indicates that RF from albedo changes is not an appropriate measure for the global impact of ALCC on climate, for which the concept has been applied [Forster et al., 2007]. The present study thereby supports previous studies [Pielke et al., 2002, Davin et al., 2007], which have pointed out the importance of biogeophysical effects other than albedo. The usage of the “climate efficacy” concept [Hansen et al., 2005] has been proposed as solution. The climate efficacy is defined as ratio between the climate sensitivity to a given forcing such as ALCC and the climate sensitivity to CO₂ and can be introduced as correcting factor to the RF-temperature relationship. However, as shown above the temperature/RF-quotient depends strongly on the location of ALCC; the climate efficacy must therefore be expected to change with time as the spatial distribution of ALCC changes. For ALCC, coupled climate simulations and comparison to other forcings based on temperature change therefore seem the best tool to assess the climatic importance.

In addition to biogeophysical effects, the present study has estimated the temperature response to ALCC emissions consistently with the same model and data. Both on the global mean and for most regions, the forcing from CO₂ emissions is the driving force behind ALCC-induced temperature change. The dominance of the biogeochemical effects of ALCC also has consequences for the potential of climate change mitigation: When returning to a state of natural vegetation, most regions, including the northern mid- to high latitudes, would contribute a cooling signal to climate change mitigation.

The carbon storage is found to be not affected by ALCC via its biogeophysical mechanisms on the global scale, and is little affected on the regional scale. This indicates that only by CO₂ emissions, ALCC alters climate and atmospheric composition in a way that causes a global feedback on the carbon cycle — this feedback had been identified as substantially counteracting primary emissions by biospheric restorage in Ch. 4. The biogeophysical effects of ALCC on carbon fluxes are, however, dependent on the climate scenario: This study has shown that in a climate altered only by ALCC, the biogeophysical effects induce weak regional carbon sources and sinks, which cancel each other on the global scale. This picture may change under the currently observed climate state of rising CO₂ and global warming: While the albedo changes and their radiative effects are not directly depending on atmospheric CO₂ concentration and temperature, or may become even weaker with less snow cover, the reduction of evapotranspiration and consequent warming in the tropics due to ALCC may become stronger. Increasing temperature may tip the respiration-photosynthesis balance of tropical forest in the direction of net emissions [Clark, 2004], especially when associated by a reduction in precipitation [Rödenbeck et al., 2003]. Biogeophysical effects can then be expected to counteract the biogeochemically-induced coupling flux simulated in this study for the tropical forest. All these considerations, however, are subject to large uncertainties concern-

ing the complex interplay of temperature and moisture effects on photosynthesis and heterotrophic respiration [Clark, 2004].

This study has given a synopsis of different pathways, via which ALCC influences climate, from several perspectives: the influence on climate, the impact on the carbon cycle, and the forcing-response relationship. It has highlighted the need for an integrated assessment of all terrestrial feedbacks on climate across different scales. Although on the global mean, biogeochemically-induced warming seems to be the dominating effect of historical ALCC, biogeophysical effects are strongly offsetting this signal on the regional scale. Often, the latter one is more relevant, e.g. when living conditions and agricultural productivity are concerned. High spatial detail should therefore be an emphasis also in future studies. It is crucial to apply the integrated approach to historical ALCC in order to understand the past evolution of climate, but also to accurately predict the future evolution and the mitigation potential of ALCC scenarios.

Acknowledgements

I thank Victor Brovkin for providing me with the data of the EMIC intercomparison study.

Chapter 6

Summary and Conclusion

6.1 Summary of methods

This thesis has assessed the influence of anthropogenic land cover change (ALCC) on the carbon cycle and the climate of the last millennium, with a special focus on the, so far little-studied, preindustrial period. The methodological steps taken by the author in this study are summarized in the following.

As a first step and prerequisite to the following modeling study, the climate perturbation under investigation has been quantified: Agricultural extent and the resulting changes in natural vegetation have been reconstructed globally with a population-based approach, building on published maps for the last 300 years. Regional specifics such as changes in cultures were integrated as far they could reasonably be derived from literature. Uncertainties associated with this approach have been quantified using both modern and historical records. The resulting datasets are being tested and applied in several projects outside this study (e.g., NCAR: Paleoclimate Reconstructions, NASA GISS: Modeling Paleo-Climates, University of Oxford: Millennium European Climate, Stanford Graduate School of Business). This dataset has then been applied as only forcing to a comprehensive climate model to assess several aspects of biosphere-climate interactions in isolated and combined form: First, the ECHAM5/JSBACH-model has been modified to simulate radiative forcing (RF) from surface albedo changes. Second, from coupled simulations using ECHAM5/JSBACH/MPI-OM/HAMOCC5 (the simulations were carried out with help of the Millennium Group), the coupled climate response has been analyzed, with special focus on the carbon cycle. To our knowledge, these are the first transient simulations over a millennial timescale using a comprehensive climate model that includes the closed carbon cycle. Third, this same model setup was applied to isolate the biogeophysical effects of ALCC (the simulations were carried out with help of the Millennium Group). For this, the biosphere-atmosphere coupling was modified in the model code. Overall, this study relied on model results from 154 years simulated at T63 resolution with ECHAM5/JSBACH and 5200 years at T31 resolution with ECHAM5/JSBACH/MPI-OM/HAMOCC5 (excluding approximately 4000 years of model spinup).

6.2 Main findings concerning the beginning of the Anthropocene

As explained in Chapters 1, 3, 4, and 5, there is no consensus in the scientific community on whether humankind influenced significantly the climate prior to the large-scale burning of fossil-fuels in the industrial era. This study has investigated this topic at unprecedented detail with respect to both input datasets and model setup. The main findings are:

1. Cropland and pastures have been quantified to have increased from 2.8 (1.3–5.1 ·10⁶ km²)¹ to 7.7 ·10⁶ km² between AD 800 and 1700, causing a deforestation of 2.1 (1.2–2.6 ·10⁶ km²)¹ (Chapter 2).
2. Surface albedo change from ALCC imposed a radiative forcing on the preindustrial energy balance that is, on the global scale, one to two orders of magnitude smaller than both the concurrent natural forcings and its strength during the industrial period. It is thus unlikely to be the major driver of climate variations such as the long-term Northern Hemisphere cooling including the “Little Ice Age”. In this respect, the present study contradicts earlier studies like Brovkin et al. [1999], Govindasamy et al. [2001], Bauer et al. [2003], Goosse et al. [2006] (Chapter 3).
3. On the regional scale, RF estimates suggest a human-induced climate change: In “hot spots” such as India, the energy balance was altered at the same strength as present-day CO₂ forcing (Chapter 3). However, the signal in the coupled climate including other biogeophysical processes and feedbacks remains within natural internal variability over the preindustrial period even in the hot-spot regions (Chapter 5).
4. This study gives a new, more comprehensive estimate of preindustrial primary emissions: primary emissions are simulated to amount to 53–61 Gt carbon (C) AD 800–1850 (excluding an estimated 10 Gt C for the earlier millennia) — 33–36% of the ALCC emissions until present (161–169 Gt C) (Chapter 4). This compares to emissions from fossil-fuel combustion of 321 Gt C [Marland et al., 2008].
5. A high restorage of carbon by the biosphere occurs over the preindustrial period due to the coupling to climate and CO₂ (48% of the primary emissions), most likely due to CO₂ fertilization. As a consequence, the airborne fraction of CO₂ amounts to only 21% (Chapter 4).
6. The strong coupling flux keeps the human impact on atmospheric CO₂ lower than would be expected from the amount of primary emissions alone. Nevertheless, the atmospheric CO₂ concentration is significantly altered by ALCC

¹The uncertainties around the best-guess estimate are compiled from Sec. 2.4 and 2.5. Any ranges given in the following refer to the best-guess and upper estimate of deforestation.

prior to industrialization: an increase by 5–6 ppm is simulated for AD 800 to 1850 (Chapter 4).

7. With a CO₂ increase by 5–6 ppm in this study for AD 800 to 1850, of which only about half developed prior to 1700, our estimate of a human impact on atmospheric CO₂ is lower than suggested by the “early anthropogenic hypothesis” — at least 9 ppm were suggested by [Ruddiman, 2007]. A major advantage of the present study, and reason for the lower estimate, is the interactive simulation of oceanic carbon uptake and carbon restorage in the biosphere (Chapter 4).
8. Unlike previously suggested, historic events are unlikely to have imprinted on CO₂ as reconstructed from ice core records. The reasons are (1) indirect emissions from past ALCC (inhibiting regional carbon sequestration for all events except for the long-lasting Mongol invasion) and (2) concurrent emissions from other parts of the world. Both effects have not been taken into account in previous studies. The internal variability of the model suggests that CO₂ drops of several ppm may well be explained by internal variability instead (Chapter 4).
9. Global mean temperature is likely to have not been significantly altered by ALCC during the preindustrial period (Chapters 4 and 5).
10. The model study suggests that, historically, warming from biogeochemical effects of ALCC was stronger than cooling from biogeophysical effects concerning global mean temperature (Chapter 5).

In summary, the present study suggests that the Anthropocene did indeed begin prior to industrialization as far as atmospheric CO₂ is concerned. An anthropogenic climate change with respect to global mean temperature, on the other hand, cannot be identified. The smaller amount of preindustrial emissions and the long timescale over which they were emitted leaves the overall climate impact much smaller than during the industrial period, despite a significant disturbance of subsystems (e.g., terrestrial carbon stocks).

6.3 Main findings beyond the historical aspect

1. An analysis of sub-fluxes suggests that a large fraction of the land-use amplifier effect results from the indirect emissions and thus from past ALCC, rather than from the change in current turnover rates. The change in turnover rates is not to be considered less important in estimates of future climate change, but it is complimented by a second process. Being indirect emissions, this second process may either be reported as part of the primary (“book-keeping”) emissions, or as part of the land-use amplifier effect, but must not be double-counted (Chapter 4).

2. There exists a legacy of preindustrial ALCC to the industrial period: This study has found an anthropogenic influence on atmospheric CO₂ by late medieval times, and has indicated significant changes in the land and ocean carbon content even earlier. It has further quantified a small loss of the additional sink capacity due to ALCC over the preindustrial period. Due to all these factors, the potential for anthropogenic climate change has been increased already prior to industrialization (Chapter 4).
3. As consequence of the previous point, the carbon balance has been considerably out of equilibrium for many centuries prior to the Industrial Revolution. This implies that the beginning of the simulation period usually applied for climate projections may be too late: Most climate-carbon cycle studies for present and future centuries initialize their model from an equilibrium state around 1850. However, at that point the carbon cycle was already in a significantly disturbed state, as the present results indicate. This discrepancy may distort model calibration against the industrial period (Chapter 4).
4. There further exists a legacy of any past ALCC beyond its instantaneous action: This study has shown how indirect emissions continue several decades beyond the end of ALCC due to the disequilibrium between NPP and heterotrophic respiration. This counteracts carbon storage in regrowing vegetation, which has been exemplarily shown for several historic events. It also implies that any mitigation efforts building on reforestation will lead to a carbon sink only with a certain time lag (Chapter 4).
5. This study has reassessed the radiative forcing (RF) concept. It supports previous studies in that RF from surface albedo changes gives an incomplete indication of the full biogeophysical climate response. Going beyond this, the present study estimates consistently with the same model and data additionally the biogeochemical effects on climate, which are found to dominate both the climate response driven by albedo changes and by all biogeophysical effects (Chapter 5).
6. This study has assessed the mitigation potential of forestation from the historical perspective, by quantifying the local contribution to the global net radiative forcing from albedo effects and CO₂ emissions (Chapter 5). The reversion of past ALCC would in most regions, including the mid- to high latitudes, lead to a cooling radiative effect.

6.4 Next steps to be taken

Expanding inclusiveness. This study has assessed ALCC as limited to the transformation of natural vegetation to agricultural areas. Other aspects of ALCC to be possibly included in similar modeling studies are wood harvest, the influence of shifting cultivation, and the interdependence of humans and fire (usage of fire for

hunting, fire suppression). As described before, these aspects are most likely of subordinate influence compared to the ALCC treated in this study. Further ALCC processes to be possibly included, beyond the biogeophysical effects on climate and biosphere-atmosphere exchange of carbon via CO₂, are methane (CH₄) emissions, impacts on nitrogen and other nutrient cycles, dust and aerosol emissions from open soils and fires, changes in the hydrological cycle caused by irrigation, and soil erosion, salinization, and desertification.

Many of these missing model processes may be accounted for within the next years. However, data availability for the historical period will be a severe obstacle. A strong interaction across the disciplines of archeology, reconstruction of human activity via proxies such as pollen or charcoal, history, ecology, and modeling is needed. In particular the global scale poses a problem: Many of the mechanisms of human interference cannot be isolated from global cycles, so that statements about human influence on a specific region are impossible even if all regional data were available.

Statistical analysis. More rigorous statistics should be applied to detect human influence in regions and times where it is small in comparison to natural internal variability. This is the case, e.g., for the regional effects of biogeophysical mechanisms during the preindustrial period. This “signal-to-noise” problem may be amplified by the fact that the model applied in the present study tends to overestimate rather than underestimate internal variability, in particular due to a too strong representation of El Niño/Southern Oscillation (ENSO) [Jungclaus et al., 2006]. Due to the internal variability in the climate system and its non-linear evolution, the detectability of a human fingerprint may further be facilitated by ensemble studies, i.e. several experiments of the same forcing, but with slightly different initial conditions. Ensemble studies could be particularly useful for studies on the effect of historic events such as warfare and epidemics. These events alter the anthropogenic forcing on a short timescale, so that the forcing’s effect is more easily concealed by natural variability than the general trend of agricultural expansion on the millennial timescale.

Validation of biogeophysical model response. A detailed evaluation of the ECHAM5/JSBACH model should indicate how accurately the biogeophysical response to ALCC is simulated and attribute errors to individual processes. The model is currently participating in a model intercomparison study for biogeophysical impacts of ALCC on regional and global climate (“Land-Use and Climate, Identification of robust impacts”, LUCID). Early results of the intercomparison study highlight the largely different response of atmosphere-biosphere models to the same perturbation [Pitman et al., submitted]. A validation against observational data, however, has yet to be performed. As stated above, a validation of historical climate effects of a perturbation against observational data is not feasible, especially when these effects shall be quantified in an isolated form from other forcings, unrelated to

real climate. However, databases such as FLUXNET (www.fluxnet.ornl.gov) could be used indirectly: By validating the model response for two different land cover maps against measurement stations in close proximity and with comparable environmental conditions, the change in climate variables from one land cover type to another, represented as temporal evolution in the model, can be assessed in the spatial domain via observations. We would also like to better understand which processes lead to the different climate responses across models — if it is rather the response to changes in surface albedo or to changes in the hydrological cycle. The two effects both act with different signs in individual regions and seasons and may often counteract each other. The model responses towards changes in albedo and hydrological cycle can be separated in a similar setup as it has been used in Chapter 5 to split up biogeophysical and biogeochemical mechanisms; stomatal conductance for CO₂ and for water were treated differently in this setup, with the first experiencing no ALCC, while the second did. Similarly, stomatal conductance for water could also be excluded from experiencing ALCC, so that only albedo changes are allowed to act on climate. This would not only reveal the relative importance of changes in albedo and hydrology, but also whether radiative forcing from albedo changes would at least be a good measure for the climate response to albedo changes.

Comparison against observational data. This study has delivered an important step towards a more complete understanding of the driving forces behind climate change: It has quantified and analyzed one of the two dominant anthropogenic forcings, ALCC. This has been done over a time period long enough (1) to allow the accumulation of the forcing (in particular with respect to atmospheric CO₂), and (2) to cover different strengths of the forcing and its variability. Therefore, the changing importance of ALCC in comparison to the other natural and anthropogenic climate forcings can be assessed, most notably to solar variability, orbital forcing, volcanic eruptions, and changes in greenhouse gas concentration from fossil-fuel combustion. Once similar quantifications of these other forcings have been conducted, as isolated and combined studies, all forcings can be consistently compared against each other in their importance for long-term climate trends and short-term climate variability, both globally and regionally. Model results for the combination of all known forcings can eventually be compared against reconstructed climate for the last millennium to assess the comprehensiveness of our understanding of past and present climate change.

Appendix A

Auxiliary material to the millennium land cover reconstruction

The auxiliary material contains the data used for the assessment of uncertainty and validity of the millennium land cover reconstruction for the time period AD 800 to 1700, viz. (1) different estimates of population and (2) changes in per-capita agricultural areas.

Table A.1— Alternative population estimates (in million) on continental scale for the years AD 1000, 1500 and 1700. Except for the Americas, the estimates of this study and McEvedy and Jones (1978) are identical.

Reference	AD 1000	AD 1500	AD 1700
Europe and FSU			
This study	39.1	85.1	125.0
Clark 1967	44.2	73.8	111.8
Durand 1977 (mean)	45.5	79.0	126.8
Durand 1977 (low)	36.0	70.0	107.8
Durand 1977 (high)	5.0	88.0	145.8
McEvedy and Jones 1978	—	—	—
Biraben 1979	43.0	84.0	125.0
Maddison 2001	39.0	87.7	126.8
Asia and Australasia			
This study	186.4	277.2	411.8
Clark 1967	173.0	227.0	416.0
Durand 1977 (mean)	189.5	304.0	443.0
Durand 1977 (low)	134.0	226.0	385.0
Durand 1977 (high)	245.0	382.0	501.0
McEvedy and Jones 1978	—	—	—
Biraben 1979	152.0	245.0	436.0
Maddison 2001	183.4	284.4	402.4
Africa			
This study	32.3	46.6	61.3
Clark 1967	50.0	85.0	100.0
Durand 1977 (mean)	37.5	54.0	79.0
Durand 1977 (low)	25.0	36.0	58.0
Durand 1977 (high)	50.0	72.0	100.0
McEvedy and Jones 1978	—	—	—
Biraben 1979	38.0	87.0	107.0
Maddison 2001	33.0	46.0	61.0
The Americas			
This study	13.2	41.1	14.4
Clark 1967	13.0	41.0	13.0
Durand 1977 (mean)	37.5	47.5	16.5
Durand 1977 (low)	22.0	32.0	11.0
Durand 1977 (high)	53.0	63.0	22.0
McEvedy and Jones 1978	9.0	14.0	13.0
Biraben 1979	18.0	42.0	12.0
Maddison 2001	12.9	19.8	13.3

Appendix B

Supplementary figures for biogeophysical mechanisms

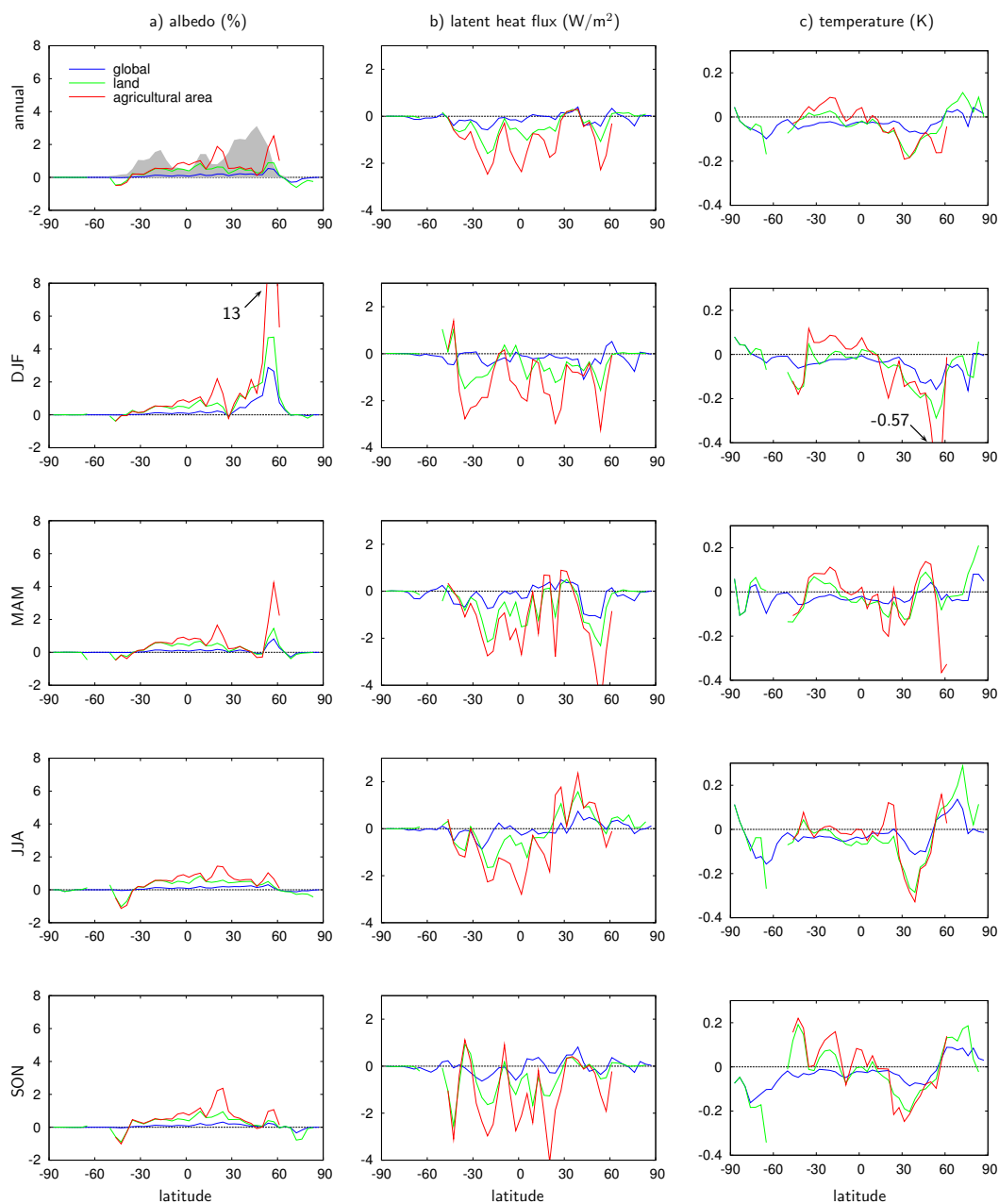


Figure B.1— Changes induced from biogeophysical effects of ALCC averaged zonally and over the 20th century for (a) surface albedo, (b) latent heat flux, (c) surface temperature. The shaded area in the first figure indicates the agricultural area per latitude in million km^2 . Rows from top to bottom: annual mean, winter (DJF), spring (MAM), summer (JJA), and fall mean (SON).

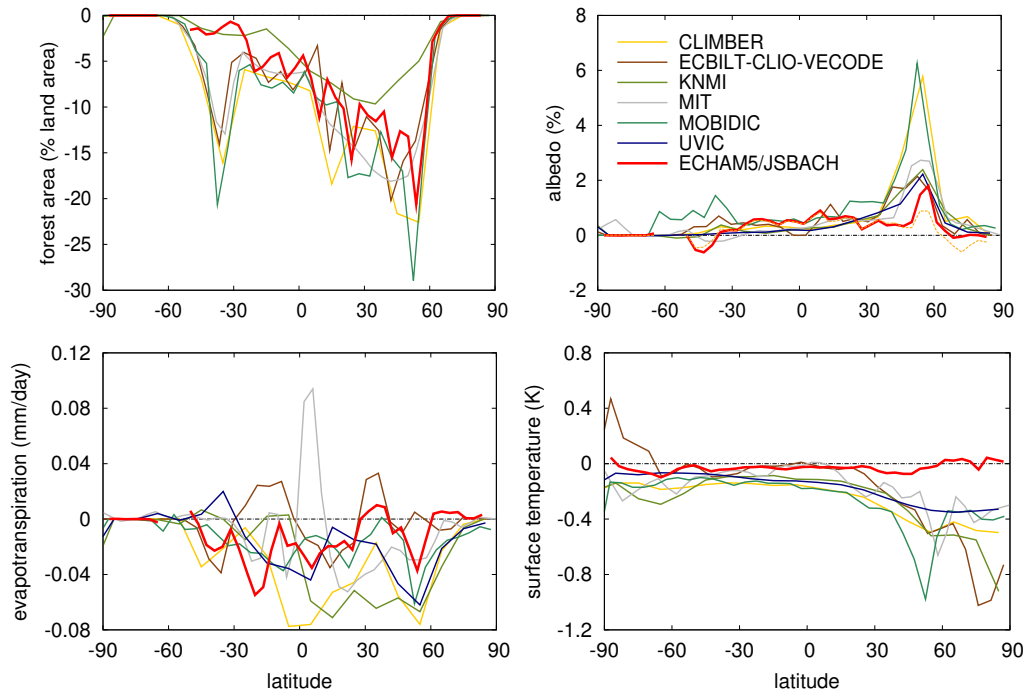


Figure B.2— Comparison of simulation results with ECHAM5/JSBACH/MPI-OM/HAMOCC5 (ECHAM5/JSBACH in the following) to 6 Earth system models of intermediate complexity (EMICs). Data for ECHAM5/JSBACH from simulations described in Chapter 5, data for EMICs from Brovkin et al. [2006]. Shown are annual mean values averaged zonally over land or the globe as indicated. The variables depicted are changes between the averaged 20th century and the control simulation for AD 800 for ECHAM5/JSBACH, and changes between the final and initial 10-years average in a simulation going from AD 1000 with an assumed state of potential natural vegetation to 1992 for the EMICs. (a) Deforested area in percent of land area (note that if 1992, not 20th century average values were taken, ECHAM5/JSBACH would have slightly larger deforested area; note further that EMICs assume potential vegetation for the beginning of their simulation in the year AD 1000, while ECHAM5/JSBACH starts from a reconstructed land cover map in the year AD 800); (b) surface albedo over land (note that for the EMICs, daily albedo values were averaged over the year with the same weight, which emphasizes winter conditions. In Chapter 5 and for the orange line for ECHAM5/JSBACH, albedo is calculated by dividing 100-year sums of reflected and incoming radiation, which follows more closely the definition of climate-relevant albedo.); (c) evapotranspiration over land (same as latent heat flux except for units); (d) global mean surface temperature.

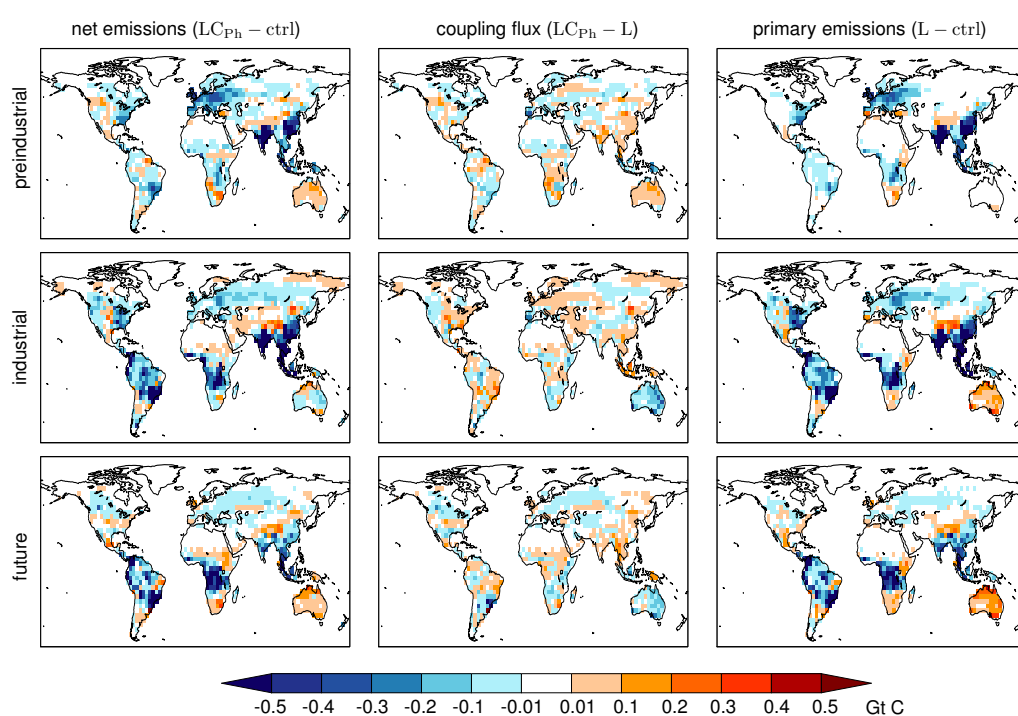


Figure B.3— Net emissions, coupling flux, and primary emissions of ALCC for simulation LC_{Ph} , which simulates the climate response to the biogeophysical effects of ALCC, accumulated over the given time interval: preindustrial (AD 800–1850), industrial (AD 1850–2000), and future period (AD 2000–2100). Other simulation acronyms are described in Tab. 4.1. Units are Gt C taken up in each grid cell. The scale is chosen such that this figure is directly comparable to Fig. 4.3.

Appendix C

Error estimate for local radiative forcing from emissions

The radiative forcing ΔF resulting from CO₂ emissions ΔC (in ppm) is given by

$$\Delta F = 5.35 \frac{\text{W}}{\text{m}^2} \cdot \ln \left(1 + \frac{\Delta C}{C_0} \right), \quad (\text{C.1})$$

where $C_0 = 281$ ppm is the CO₂ concentration at the beginning of the simulation. Let ΔC_i be the emissions from one pixel i , and let n be the number of pixels considered. Then, $\Delta C = \sum_{i=1}^n C_i$, and the radiative forcing resulting from the sum of the emissions is given by

$$\Delta F = 5.35 \frac{\text{W}}{\text{m}^2} \cdot \ln \left(1 + \sum_{i=1}^n \frac{\Delta C_i}{C_0} \right). \quad (\text{C.2})$$

In Chapter 5, an approximation of Eq. C.2 is used, in which the radiative forcings resulting from single pixels are summed:

$$\Delta \tilde{F} = \sum_{i=1}^n \left[5.35 \frac{\text{W}}{\text{m}^2} \cdot \ln \left(1 + \frac{\Delta C_i}{C_0} \right) \right]. \quad (\text{C.3})$$

The error made by this approximation is estimated as follows. Subtracting Eq. C.2 from Eq. C.3 yields the error e :

$$e = 5.35 \frac{\text{W}}{\text{m}^2} \cdot \left[\sum_{i=1}^n \ln \left(1 + \frac{\Delta C_i}{C_0} \right) - \ln \left(1 + \sum_{i=1}^n \frac{\Delta C_i}{C_0} \right) \right]. \quad (\text{C.4})$$

Since $\ln(1+x)$ is a concave function (its slope is decreasing with increasing x), the first term of Eq. C.4 is larger than the second one and therefore e is positive. Since it is $\ln(1+x) \leq x$, an upper bound on e can be given by

$$\begin{aligned} e \leq e_{max} &= 5.35 \frac{\text{W}}{\text{m}^2} \cdot \left[\sum_{i=1}^n \frac{\Delta C_i}{C_0} - \ln \left(1 + \sum_{i=1}^n \frac{\Delta C_i}{C_0} \right) \right] \\ &= 5.35 \frac{\text{W}}{\text{m}^2} \cdot \left[\frac{\Delta C}{C_0} - \ln \left(1 + \frac{\Delta C}{C_0} \right) \right]. \end{aligned} \quad (\text{C.5})$$

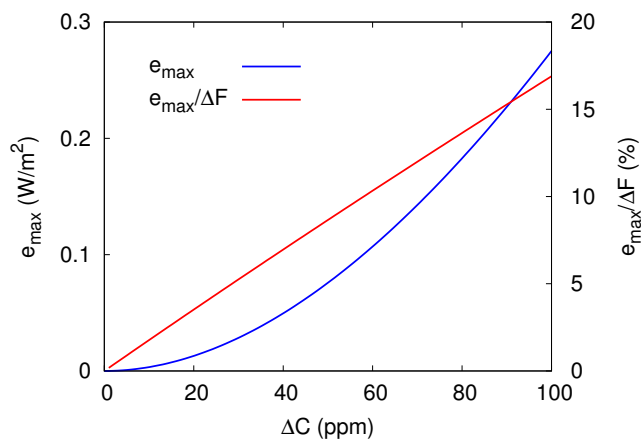


Figure C.1— Maximum error in W/m^2 (left axis) and in % (right axis) from the error estimate to local radiative forcing from CO_2 emissions.

Therefore, the error e is smaller than the error resulting from linearly approximating $\ln(1+x)$ by the linear function x . Figure C.1 plots e_{\max} and the relative error $e_{\max}/\Delta F$ for values of $\Delta C = 0 \dots 100$ ppm. The relative maximum error is 4% at $\Delta C = 20$ ppm and 17% at 100 ppm, the true error is consequently even smaller.

List of Figures

1.1	Map of anthropogenic land cover change until present	9
1.2	The world's population	13
2.1	Scheme for reconstructing agricultural areas and land cover	24
2.2	Maps of historical cropland	36
2.3	Maps of historical pasture	37
2.4	Total area of crop and pasture for world regions AD 800–1992	39
2.5	Total area of natural vegetation for world regions AD 800–1992	41
3.1	Global and hemispherical radiative forcing AD 800–1992	50
3.2	Maps for AD 800 and zonal means of radiative forcing AD 800–1992	51
3.3	Changes in radiative forcing during epidemics and warfare	53
4.1	Global land-atmosphere carbon fluxes AD 800–2100	62
4.2	Changes in vegetation and soil carbon pools and NEP AD 800–2100	64
4.3	Maps of net emissions, primary emissions, and coupling flux	65
4.4	Disequilibria of soil respiration vs. NPP	67
4.5	Carbon inventory for land, ocean, and atmosphere AD 800–2100	71
4.6	Change in global mean temperature AD 800–2100	72
4.7	Carbon fluxes during epidemics and warfare	74
5.1	Temperature changes from different ALCC mechanisms AD 800–2100	82
5.2	Maps of temperature change for different ALCC mechanisms	84
5.3	Zonal plots of changes in albedo, latent heat flux, and temperature	85
5.4	Global land-atmosphere carbon fluxes due to biogeophysical mechanism	87
5.5	Carbon inventory AD 800–2100 for biogeophysical simulation	88
5.6	Map of coupling flux due to biogeophysical mechanism	89
5.7	Comparison of radiative forcings to temperature responses	90
5.8	Zonal plot of temperature/radiative forcing	91
5.9	Maps of radiative forcing for albedo, CO ₂ , and total forcing	94
B.1	Seasonal zonal plots of changes in albedo, latent heat flux, and temperature	110

B.2	Comparison with EMICs for biogeophysical effects	111
B.3	Maps of net emissions, coupling flux, and primary emissions for biogeophysical simulation	112
C.1	Error estimate to local radiative forcing from emissions	114

List of Tables

2.1	Estimated global extent of land cover types AD 800–1992	29
3.1	Comparison of (pre-)industrial radiative forcing across studies	50
4.1	Description of model simulations for carbon studies	61
4.2	Global atmosphere-biosphere carbon fluxes for different eras	63
4.3	Primary emissions from anthropogenic land cover change	66
4.4	Carbon uptake by land, ocean, and atmosphere	70
5.1	Temperature changes in comparison to previous studies	83
A.1	Alternative population estimates	106
A.2	Changes in per-capita agricultural area	107

Bibliography

- R.C. Allen. Economic structure and agricultural productivity in Europe, 1300–1800. *European Review of Economic History*, 3:1–25, 2000.
- M. Andreae and P.J. Crutzen. Atmospheric aerosols: biogeochemical sources and role in atmospheric chemistry. *Science*, 276(5315):1052–1058, 1997.
- M.O. Andreae and P. Merlet. Emission of trace gases and aerosols from biomass burning. *Global Biogeochem. Cycles*, 15(4):955–966, 2001.
- D. Archer, H. Kheshgi, and E. Maier-Reimer. Multiple timescales for neutralization of fossil fuel CO₂. *Geophys. Res. Lett.*, 24(4):405–408, 1997.
- G.P. Asner, A.J. Elmore, L.P. Olander, R.E. Martin, and A.T. Harris. Grazing systems, ecosystem responses, and global change. *Ann. Rev. Environ. Resources*, 29:261–299, 2004.
- G. Bala, K. Caldeira, M. Wickett, T.J. Phillips, D.B. Lobell, C. Delire, and A. Mirin. Combined climate and carbon-cycle effects of large-scale deforestation. *PNAS*, 104(16):6550–6555, 2007.
- T. Barker, I. Bashmakov, A. Alharthi, M. Amann, L. Cifuentes, J. Drexhage, M. Duan, O. Edenhofer, B. Flannery, M. Grubb, M. Hoogwijk, F.I. Ibitoye, C.J. Jepma, W.A. Pizer, and K. Yamaji. Mitigation from a cross-sectoral perspective. In B. Metz, O.R. Davidson, P.R. Bosch, R. Dave, and L.A. Meyer, editors, *Climate Change 2007: Mitigation. Contribution of Working Group III to the Fourth Assessment Report of the Intergovernmental Panel on Climate Change*, pages 619–690. Cambridge University Press, Cambridge, United Kingdom and New York, NY, USA, 2007.
- E. Bauer and M. Claussen. Analyzing seasonal temperature trends in forced climate simulations of the past millennium. *Geophys. Res. Lett.*, 33:L02702, doi:10.1029/2005GL024593, 2006.
- E. Bauer, M. Claussen, and V. Brovkin. Assessing climate forcings of the Earth system for the past millennium. *Geophys. Res. Lett.*, 30(6):1276, doi:10.1029/2002GL016639, 2003.

- F.A. Bazzaz. The response of natural ecosystems to the rising global CO₂ levels. *Annual Rev. Ecol. System.*, 21:167–196, 1990.
- A. Berger. Milankovitch theory and climate. *Rev. Geophys.*, 26:624–657, 1988.
- C. Bertrand, M.F. Loutre, M. Crucifix, and A. Berger. Climate of the last millennium: a sensitivity study. *Tellus*, 54A:221–244, 2002.
- R.A. Betts. Offset of the potential carbon sink from boreal forestation by decreases in surface albedo. *Nature*, 408:187–190, 2000.
- R.A. Betts. Biogeophysical impacts of land use on present-day climate: near-surface temperature change and radiative forcing. *Atmos. Sci. Lett.*, 1: doi:10.1006/asle.2001.0023, 2001.
- R.A. Betts, P.D. Falloon, K. Klein Goldewijk, and N. Ramankutty. Biogeophysical effects of land use on climate: Model simulations of radiative forcing and large-scale temperature change. *Agric. For. Meteorol.*, 142:216–233, 2007.
- J.N. Biraben. Essai sur l'évolution du nombre des hommes. *Population*, 34(1):13–25, 1979.
- B. Bolin, R. Sukumar, P. Ciais, W. Cramer, P. Jarvis, H. Khesghi, C.A. Nobre, S. Semenov S, and W. Steffen. Global perspective. In R.T. Watson, I.R. Noble, B. Bolin, N.H. Ravindranath, D.J. Verardo, and D.J. Dokken, editors, *Land Use, Land-Use Change, and Forestry - A Special Report of the IPCC*. Cambridge University Press, Cambridge, United Kingdom and New York, NY, USA, 2001.
- G. Bonan. *Ecological Climatology*, chapter Land use and land-cover change, pages 433–469. Cambridge University Press, Cambridge, 2002.
- G.B. Bonan, D. Pollard, and S.L. Thompson. Effects of boreal forest vegetation on global climate. *Nature*, 359:716–718, 1992.
- E. Boserup. *The conditions of agricultural growth*. Aldine, Chicago, 1965.
- L. Bounoua, R.S. DeFries, G.J. Collatz, P.J. Sellers, and H. Khan. Effects of land cover conversion on surface climate. *Climatic Change*, 52:29–64, 2002.
- V. Brovkin, A. Ganopolski, M. Claussen, C. Kubatzki, and V. Petoukhov. Modelling climate response to historical land cover change. *Glob. Ecol. and Biogeogr.*, 8:509–517, 1999.
- V. Brovkin, S. Sitch, W. von Bloh, M. Claussen, E. Bauer, and W. Cramer. Role of land cover changes for atmospheric CO₂ increase and climate change during the last 150 years. *Global Change Biol.*, 10:1253–1266, 2004.

- V. Brovkin, M. Claussen, E. Driesschaert, T. Fichefet, D. Kicklighter, M.F. Loutre, H.D. Matthews, N. Ramankutty, M. Schaeffer, and A. Sokolov. Biogeophysical effects of historical land cover changes simulated by six Earth system models of intermediate complexity. *Clim. Dyn.*, 26:587–600, 2006.
- V. Brovkin, T. Raddatz, C.H. Reick, M. Claussen, and V. Gayler. Global biogeophysical interactions between forest and climate. *Geophys. Res. Lett.*, submitted.
- E.C. Brown de Colstoun, R.S DeFries, and J.R.G. Townshend. Evaluation of ISLSCP Initiative II satellite-based land cover data sets and assessment of progress in land cover data for global modeling. *J. Geophys. Res.*, 111:D22S07, 2006.
- T.N. Chase, R.A. Pielke Sr., T.G.F. Kittel, R.R. Nemani, and S.W. Running. Simulated impacts of historical land cover changes on global climate in northern winter. *Clim. Dyn.*, 16:93–105, 2000.
- C. Clark. *Population growth and land use*. Macmillan, London, 2nd edition, 1967.
- D.A. Clark. Tropical forests and global warming: slowing it down or speeding it up? *Front. Ecol. Environ.*, 2(2):73–80, 2004.
- M. Claussen. Does land surface matter in climate and weather? In P. Kabat, M. Claussen, P.A. Dirmeyer, J.H.C. Gasha, L.B. de Guenni, M. Meybeck, R.A. Pielke Sr., C.J. Vörösmarty, R.W.A. Hutjes, and S. Lütkeemeier, editors, *Vegetation, Water, Humans and the Climate*, pages 5–153. Springer, Berlin, 2004.
- M. Claussen, V. Brovkin, and A. Ganopolski. Biogeophysical versus biogeochemical feedbacks of large-scale land cover change. *Geophys. Res. Lett.*, 28(6):1011–1014, 2001.
- M. Claussen, V. Brovkin, R. Calov, A. Ganopolski, and C. Kubatzki. Did humankind prevent a Holocene glaciation? *Climatic Change*, 69:409–417, 2005.
- Commission of the European Communities. *Biofuels progress report: Report on the progress made in the use of biofuels and other renewable fuels in the member states of the European Union*. COM(2006) 845 final, Brussels, 2006.
- A.C. Crombie. *Von Augustinus bis Galilei. Die Emanzipation der Naturwissenschaft*. dtv, Wissenschaftliche Reihe, München, 1977.
- T.J. Crowley. Causes of climate change over the past 1000 years. *Science*, 289: 270–277, 2000.
- P.J. Crutzen and E.F. Stoermer. The “Anthropocene”. *IGBP Newsletter*, 41:17–18, 2000.
- E.L. Davin, N. de Noblet-Ducoudré, and P. Friedlingstein. Impact of land cover change on surface climate: Relevance of the radiative forcing concept. *Geophys. Res. Lett.*, 34:L13702, 2007.

- R.S. DeFries, C.B. Field, I. Fung, G.J. Collatz, and L. Bounoua. Combining satellite data and biogeochemical models to estimate global effects of human-induced land cover change on carbon emissions and primary productivity. *Global Biogeochem. Cycles*, 13(3):803–815, 1999.
- R.S. DeFries, L. Bounoua, and G.J. Collatz. Human modification of the landscape and surface climate in the next fifty years. *Global Change Biol.*, 8:438–458, 2002.
- R.S. DeFries, J.A. Foley, and G.P. Asner. Land-use choices: balancing human needs and ecosystem function. *Front. Ecol. Environ.*, 2(5):249–257, 2004.
- K.L. Denman, G. Brasseur, A. Chidthaisong, P. Ciais, P.M. Cox, R.E. Dickinson, D. Hauglustaine, C. Heinze, E. Holland, D. Jacob, U. Lohmann, S. Ramachandran, P.L. da Silva Dias, S.C. Wofsy, and X. Zhang. Couplings Between Changes in the Climate System and Biogeochemistry. In S. Solomon, D. Qin, M. Manning, Z. Chen, M. Marquis, K.B. Averyt, M. Tignor, and H.L. Miller, editors, *Climate Change 2007: The Physical Science Basis. Contribution of Working Group I to the Fourth Assessment Report of the Intergovernmental Panel on Climate Change*. Cambridge University Press, Cambridge, United Kingdom and New York, NY, USA, 2007.
- J. Diamond. *Guns, Germs, and Steel*. W. W. Norton & Company, New York, London, 1999.
- I. Douglas. Human settlements. In W.B. Meyer and B.L. Turner II, editors, *Changes in Land Use and Land Cover: A Global Perspective*, pages 149–170. Cambridge University Press, Cambridge, 1994.
- J.D. Durand. Historical estimates of world population: An evaluation. *Popul. Develop. Rev.*, 3(3):253–296, 1977.
- J. Feddema, K. Oleson, G. Bonan, L. Mearns, W. Washington, G. Meehl, and D. Nychka. A comparison of a GCM response to historical anthropogenic land cover change and model sensitivity to uncertainty in present-day land cover representations. *Clim. Dyn.*, 25:581–609, 2005.
- F. Fehsenfeld, J. Calvert, R. Fall, P. Goldan, A.B. Guenther, C.N. Hewitt, B. Lamb, S. Liu, M. Trainer, H. Westberg, and P. Zimmermann. Emissions of volatile organic compounds from vegetation and the implications for atmospheric chemistry. *Global Biogeochem. Cycles*, 6:389–430, 1992.
- J.A. Foley, C. Delire, N. Ramankutty, and P. Snyder. Green Surprise? How terrestrial ecosystems could affect earth’s climate. *Front. Ecol. Environ.*, 1:38–44, 2003.
- J.A. Foley, R.S. DeFries, G.P. Asner, C. Barford, G. Bonan, S.R. Carpenter, F.S. Chapin, M.T. Coe, G.C. Daily, H.K. Gibbs, J.H. Helkowski, T. Holloway, E.A.

- Howard, C.J. Kucharik, C. Monfreda, J.A. Patz, I.C. Prentice, N. Ramankutty, and P.K. Snyder. Global consequences of land use. *Science*, 309:570–574, 2005.
- Food and Agricultural Organization (FAO). FAOSTAT: Land use. *FAO Statistics Division*, 2007.
- P. Forster, V. Ramaswamy, P. Artaxo, T. Berntsen, R. Betts, D.W. Fahey, J. Haywood, J. Lean, D.C. Lowe, G. Myhre, J. Nganga, R. Prinn, G. Raga, M. Schulz, and R. Van Dorland. Changes in atmospheric constituents and in radiative forcing. In S. Solomon, D. Qin, M. Manning, Z. Chen, M. Marquis, K.B. Averyt, M. Tignor, and H.L. Miller, editors, *Climate Change 2007: The Physical Science Basis. Contribution of Working Group I to the Fourth Assessment Report of the Intergovernmental Panel on Climate Change*, pages 129–234. Cambridge University Press, Cambridge, United Kingdom and New York, NY, USA, 2007.
- J.N. Galloway, W.H. Schlesinger, H. Levy II, A. Michaels, and J.L. Schnoor. Nitrogen fixation: Anthropogenic enhancement-environmental response. *Global Biogeochem. Cycles*, 9(2):235–252, 1995.
- A. Ganopolski, V. Petoukhov, S. Rahmstorf, V. Brovkin, M. Claussen, A. Eliseev, and C. Kubatzki. CLIMBER-2: a climate system model of intermediate complexity. Part II: validation and sensitivity tests. *Clim. Dyn.*, 17:735–751., 2001.
- P. Gepts. Crop domestication as a long-term selection experiment. *Plant Breeding Reviews*, 24(2):1–43, 2004.
- V. Gitz and P. Ciais. Amplifying effects of land-use change on future atmospheric CO₂ levels. *Global Biogeochem. Cycles*, 17(1):doi:10.1029/2002GB001963, 2003.
- H. Goosse, O. Arzel, J. Luterbacher, M.E. Mann, H. Renssen, N. Riedwyl, A. Timmermann, E. Xoplaki, and H. Wanner. The origin of the European “Medieval Warm Period”. *Clim. Past*, 2:99–113, 2006.
- B. Govindasamy, P.B. Duffy, and K. Caldeira. Land use changes and Northern Hemisphere cooling. *Geophys. Res. Lett.*, 28(2):291–294, 2001.
- D.B. Grigg. *The agricultural systems of the world - an evolutionary approach*. Cambridge Geographical Studies. Cambridge University Press, New York, 1974.
- H. Haberl, K.H. Erb, F. Krausmann, V. Gaube, A. Bondeau, C. Plutzer, S. Gingrich, W. Lucht, and M. Fischer-Kowalski. Quantifying and mapping the human appropriation of net primary production in earth’s terrestrial ecosystems. *Proc. Natl. Acad. Sci.*, 104(31):12942–12947, 2007.
- O. Hanotte, D.G. Bradley, J.W. Ochieng, Y. Verjee, E.W. Hill, and J.E.O. Rege. African pastoralism: genetic imprints of origins and migrations. *Science*, 296(5566):336–339, 2002.

- J. Hansen, M. Sato, and R. Ruedy. Radiative forcing and climate response. *J. Geophys. Res.*, 102:6831–6864, 1997.
- J. Hansen, M. Sato, R. Ruedy, L. Nazarenko, A. Lacis, G.A. Schmidt, G. Russell, I. Aleinov, M. Bauer, S. Bauer, N. Bell, B. Cairns, V. Canuto, M. Chandler, Y. Cheng, A. Del Genio, G. Faluvegi, E. Fleming, A. Friend, T. Hall, C. Jackman, M. Kelley, N.Y. Kiang, D. Koch, J. Lean, J. Lerner, K. Lo, S. Menon, R.L. Miller, P. Minnis, T. Novakov, V. Oinas, Ja. Perlwitz, Ju. Perlwitz, D. Rind, A. Romanou, D. Shindell, P. Stone, S. Sun, N. Tausnev, D. Thresher, B. Wielicki, T. Wong, M. Yao, and S. Zhang. Efficacy of climate forcings. *J. Geophys. Res.*, 110:D18104, 2005.
- M.C. Hansen, S.V. Stehman, P.V. Potapov, T.R. Loveland, J.R.G. Townshend, R.S. DeFries, K.W. Pittman, B. Arunarwati, F. Stolle, M.K. Steininger, M. Carroll, and C. DiMiceli. Humid tropical forest clearing from 2000 to 2005 quantified by using multitemporal and multiresolution remotely sensed data. *Proc. Natl. Acad. Sci.*, 105(27):9439–9444, 2008.
- R. Hein, P.J. Crutzen, and M. Heimann. An inverse modeling approach to investigate the global atmospheric methane cycle. *Global Biogeochem. Cycles*, 11:43–76, 1997.
- R.A. Houghton. The annual net flux of carbon to the atmosphere from changes in land use 1850–1990. *Tellus*, 51(B):298–313, 1999.
- R.A. Houghton. Revised estimates of the annual net flux of carbon to the atmosphere from changes in land use 1850–2000. *Tellus*, 55(B):378–390, 2003.
- R.A. Houghton. *Carbon Flux to the Atmosphere from Land-Use Changes 1850-2005*. Carbon Dioxide Information Analysis Center, 2008.
- R.A. Houghton and J.L. Hackler. Continental scale estimates of the biotic carbon flux from land cover change: 1850–1980. Technical report, Oak Ridge National Laboratory, Oak Ridge, Tennessee, 1995.
- R.A. Houghton, J.E. Hobbie, J.M. Melillo, B. Moore, B.J. Peterson, G.R. Shaver, and G.M. Woodwell. Changes in the carbon content of terrestrial biota and soils between 1860 and 1980: A net release of CO₂ to the atmosphere. *Ecol. Monogr.*, 53(3):235–262, 1983.
- J.I. House, I.C. Prentice, and C. Le Quéré. Maximum impacts of future reforestation or deforestation on atmospheric CO₂. *Global Change Biol.*, 8:1047–1052, 2002.
- G.C. Hurtt, S. Frohking, M.G. Fearon, B. Moore, E. Shevliakova, S. Malyshev, S.W. Pacala, and R.A. Houghton. The underpinning of land-use history: three centuries of global gridded land-use transitions, wood-harvest activity, and resulting secondary lands. *Global Change Biol.*, 12:1208–1229, 2006.

- Intergovernmental Panel on Climate Change (IPCC) National Greenhouse Gas Inventories Programme. Good practice guidance for land use, land-use change and forestry. Institute for Global Environmental Strategies (IGES), Japan, 2003.
- A. Jain and X. Yang. Modeling the effects of two different land cover change data sets on the carbon stocks of plants and soils in concert with CO₂ and climate change. *Global Biogeochem. Cycles*, 19:GB2015, doi:10.1029/2004GB002349, 2005.
- E. Jansen, J. Overpeck, K.R. Briffa, J.-C. Duplessy, F. Joos, V. Masson-Delmotte, D. Olago, B. Otto-Bliesner, W.R. Peltier, S. Rahmstorf, R. Ramesh, D. Raynaud, D. Rind, O. Solomina, R. Villalba, and D. Zhang. Palaeoclimate. In S. Solomon, D. Qin, M. Manning, Z. Chen, M. Marquis, K.B. Averyt, M. Tignor, and H.L. Miller, editors, *Climate Change 2007: The Physical Science Basis. Contribution of Working Group I to the Fourth Assessment Report of the Intergovernmental Panel on Climate Change*, pages 433–497. Cambridge University Press, Cambridge, United Kingdom and New York, NY, USA, 2007.
- M. Jin, R.E. Dickinson, and D.-L. Zhang. The footprint of urban areas on global climate as characterized by MODIS. *J. Clim.*, 18:1551–1565, 2005.
- F. Joos, S. Gerber, I.C. Prentice, B.L. Otto-Bliesner, and P.J. Valdes. Transient simulations of Holocene atmospheric carbon dioxide and terrestrial carbon since the Last Glacial Maximum. *Global Biogeochem. Cycles*, 18:GB2002, 2004.
- J.H. Jungclauss, N. Keenlyside, M. Botzet, H. Haak, J.-J. Luo, M. Latif, J. Marotzke, U. Mikolajewicz, and E. Roeckner. Ocean circulation and tropical variability in the coupled model ECHAM5/MPI-OM. *J. Clim.*, 19:3952–3972, 2006.
- D.M. Kammen and B.D. Marino. On the origin and magnitude of pre-industrial anthropogenic CO₂ and CH₄ emissions. *Chemosphere*, 26(1–4):69–86, 1993.
- C. Kerven, I.I. Alimaev, R. Behnke, G. Davidson, N. Malmakov, A. Smailov, and I. Wright. Fragmenting pastoral mobility: Changing grazing patterns in post-Soviet Kazakhstan. *USDA Forest Service Proceedings*, 39:99–110, 2006.
- A. Kleidon. The climate sensitivity to human appropriation of vegetation productivity and its thermodynamic characterization. *Glob. Planet. Change*, 54:109–127, 2006.
- K. Klein Goldewijk. Estimating global land use change over the past 300 years: The HYDE Database. *Global Biogeochem. Cycles*, 15(2):417–433, 2001.
- K. Klein Goldewijk and N. Ramankutty. Land cover change over the last three centuries due to human activities: The availability of new global data sets. *Geo-Journal*, 61:335–344, 2004.
- H.H. Lamb. The early Medieval warm epoch and its sequel. *Palaeogeography, Palaeoclimatology, Palaeoecology*, 1:13–37, 1965.

- E.F. Lambin, B.L. Turner, H.J. Geist, S.B. Agbola, A. Angelsen, J.W. Bruce, O.T. Coomes, R. Dirzo, G. Fischer, C. Folkei, P.S. George, K. Homewood, J. Imbernon, R. Leemans, X. Li, E.F. Moran, M. Mortimore, P.S. Ramakrishnan, J.F. Richards, H. Skånes, W. Steffen, G.D. Stone, U. Svedin, T.A. Veldkamp, C. Vogel, and J. Xu. The causes of land-use and land-cover change: moving beyond the myths. *Global Environ. Change*, 11:261–269, 2001.
- A. Maddison. *The World Economy: A Millennial Perspective*. Development Centre of the Organisation for Economic Co-Operation and Development, Paris, 2001.
- M.E. Mann and R.S. Bradley. Northern Hemisphere temperatures during the past millennium: inferences, uncertainties, and limitations. *Geophys. Res. Lett.*, 26: 759–762, 1999.
- M.E. Mann, R.S. Bradley, and M.K. Hughes. Global-scale temperature patterns and climate forcing over the past six centuries. *Nature*, 392:779–787, 1998.
- G. Marland, B. Andres, and T. Boden. *Global CO₂ emissions from fossil-fuel burning, cement manufacture, and gas flaring: 1751-2005*. Carbon Dioxide Information Analysis Center, 2008.
- S.J. Marsland, H. Haak, J.H. Jungclaus, M. Latif, and F. Roeske. The Max-Planck-Institute global ocean/sea ice model with orthogonal curvilinear coordinates. *Ocean Modell*, 5:91–127, 2003.
- H.D. Matthews, A.J. Weaver, M. Eby, and K.J. Meissner. Radiative forcing of climate by historical land cover change. *Geophys. Res. Lett.*, 30(2):1055, 2003.
- H.D. Matthews, A.J. Weaver, K.J. Meissner, N.P. Gillett, and M. Eby. Natural and anthropogenic climate change: incorporating historical land cover change, vegetation dynamics and the global carbon cycle. *Clim. Dyn.*, 22:461–479, 2004.
- C. McEvedy and R. Jones. *Atlas of World Population History*. Penguin Books, Harmondsworth, 1978.
- A.D. McGuire, S. Sitch, J.S. Clein, R. Dargaville, G. Esser, J. Foley, M. Heimann, F. Joos, J. Kaplan, D.W. Kicklighter, R.A. Meier, J.M. Melillo, B. Moore II, I.C. Prentice, N. Ramankutty, T. Reichenau, A. Schloss, H. Tian, L.J. Williams, and U. Wittenberg. Carbon balance of the terrestrial biosphere in the twentieth century: Analyses of CO₂, climate and land use effects with four process-based ecosystem models. *Global Biogeochem. Cycles*, 15:183–206, 2001.
- G.A. Meehl, T.F. Stocker, W.D. Collins, P. Friedlingstein, A.T. Gaye, J.M. Gregory, A. Kitoh, R. Knutti, J.M. Murphy, A. Noda, S.C.B. Raper, I.G. Watterson, A.J. Weaver, and Z.-C. Zhao. Global climate projections. In S. Solomon, D. Qin, M. Manning, Z. Chen, M. Marquis, K.B. Averyt, M. Tignor, and H.L. Miller, editors, *Climate Change 2007: The Physical Science Basis. Contribution of Working*

- Group I to the Fourth Assessment Report of the Intergovernmental Panel on Climate Change*, pages 748–845. Cambridge University Press, Cambridge, United Kingdom and New York, NY, USA, 2007.
- Millennium Ecosystem Assessment. *Ecosystems and human well-being: Synthesis*. Island Press, Washington, DC, 2005.
- R. Moss, M. Babiker, S. Brinkman, E. Calvo, T. Carter, J. Edmonds, I. Elgizouli, S. Emori, L. Erda, K. Hibbard, R. Jones, M. Kainuma, J. Kelleher, J.F. Lamarque, M. Manning, B. Matthews, J. Meehl, L. Meyer, J. Mitchell, N. Nakicenovic, B. O'Neill, R. Pichs, K. Riahi, S. Rose, P. Runci, R. Stouffer, D. van Vuuren, J. Weyant, T. Wilbanks, J.P. van Ypersele, and M. Zurek. *Towards New Scenarios for Analysis of Emissions, Climate Change, Impacts, and Response Strategies*. Intergovernmental Panel on Climate Change, Geneva, 2008.
- G. Myhre and A. Myhre. Uncertainties in radiative forcing due to surface albedo changes caused by land-use changes. *J. Climate*, 16:1511–1524, 2003.
- G. Myhre, E.J. Highwood, K.P. Shine, and F. Stordal. New estimates of radiative forcing due to well mixed greenhouse gases. *Geophys. Res. Lett.*, 25(14):2715–2718, 1998.
- G.J. Nabuurs, O. Masera, K. Andrasko, P. Benitez-Ponce, R. Boer, M. Dutschke, E. Elsiddig, J. Ford-Robertson, P. Frumhoff, T. Karjalainen, O. Krankina, W.A. Kurz, M. Matsumoto, W. Oyhantcabal, N.H. Ravindranath, M.J. Sanz Sanchez, and X. Zhang. Forestry. In B. Metz, O.R. Davidson, P.R. Bosch, R. Dave, and L.A. Meyer, editors, *Climate Change 2007: Mitigation. Contribution of Working Group III to the Fourth Assessment Report of the Intergovernmental Panel on Climate Change*, pages 541–584. Cambridge University Press, Cambridge, United Kingdom and New York, NY, USA, 2007.
- N. Nakicenovic, J. Alcamo, G. Davis, B. de Vries, J. Fenhann, S. Gaffin, K. Gregory, A. Grübler, T.Y. Jung, T. Kram, E.L. La Rovere, L. Michaelis, S. Mori, T. Morita, W. Pepper, H. Pitcher, L. Price, K. Riahi, A. Roehrl, H.-H. Rogner, A. Sankovski, M. Schlesinger, P. Shukla, S. Smith, R. Swart, S. van Rooijen, N. Victor, and Z. Dadi. *Special Report on Emissions Scenarios*. page <http://www.ipcc.ch/ipccreports/sres/emission/index.html>. Cambridge Univ. Press, Cambridge, 2000.
- J. Olofsson and T. Hickler. Effects of human land-use on the global carbon cycle during the last 6,000 years. *Vegetation History and Archeobotany*, 17:605–615, 2008.
- United Nations Framework Convention on Climate Change (UNFCCC). *Kyoto Protocol to the United Nations Framework Convention on Climate Change*. 1998.
- T.J. Osborn and K.R. Briffa. The spatial extent of 20th-century warmth in the context of the past 1200 years. *Science*, 311:841–844, 2006.

- R.A. Pielke, Sr., G. Marland, R.A. Betts, T.N. Chase, J.L. Eastman, J.O. Niles, D.D.S. Niyogi, and S.W. Running. The influence of land-use change and landscape dynamics on the climate system: relevance to climate-change policy beyond the radiative effect of greenhouse gases. *Phil. Trans. R. Soc. Lond. A*, 360:1705–1719, 2002.
- A.J. Pitman, H. Dolman, B. Kruijt, R. Valentini, and D. Baldocchi. The climate near the ground. In P. Kabat, M. Claussen, P.A. Dirmeyer, J.H.C. Gasha, L.B. de Guenni, M. Meybeck, R.A. Pielke Sr., C.J. Vörösmarty, R.W.A. Hutjes, and S. Lütkemeier, editors, *Vegetation, Water, Humans and the Climate*, pages 9–19. Springer, Berlin, 2004.
- A.J. Pitman, N. de Noblet-Ducoudré, F.T. Cruz, E.L. Davin, G.B. Bonan, V. Brovkin, M. Claussen, C. Delire, L. Ganzeveld, V. Gayler, B.J.J.M. van den Hurk, P.J. Lawrence, M.K. van der Molen, C. Müller, C.H. Reick, S.I. Seneviratne, B.J. Strengers, and A. Voldoire. Land use and climate via the LUCID intercomparison study: implications for experimental design in AR5. *Geophys. Res. Lett.*, submitted.
- J. Pongratz, C. Reick, T. Raddatz, and M. Claussen. *A Global Land Cover Reconstruction AD 800 to 1992 - Technical Description*, volume 51 of *Reports on Earth System Science*. Max Planck Institute for Meteorology, Hamburg, Germany, 2008a.
- J. Pongratz, C. Reick, T. Raddatz, and M. Claussen. A reconstruction of global agricultural areas and land cover for the last millennium. *Global Biogeochem. Cycles*, 22(GB3018, doi:10.1029/2007GB003153), 2008b.
- J. Pongratz, T. Raddatz, C.H. Reick, M. Esch, and M. Claussen. Radiative forcing from anthropogenic land cover change since A.D. 800. *Geophys. Res. Lett.*, 36 (L02709, doi:10.1029/2008GL036394), 2009.
- J. Pongratz, C.H. Reick, T. Raddatz, and M. Claussen. Effects of anthropogenic land cover change on the carbon cycle of the last millennium. *Global Biogeochem. Cycles*, submitted.
- T.J. Raddatz, C.H. Reick, W. Knorr, J. Kattge, E. Roeckner, R. Schnur, K.-G. Schnitzler, P. Wetzler, and J. Jungclaus. Will the tropical land biosphere dominate the climate-carbon cycle feedback during the twenty-first century? *Clim. Dyn.*, 29:565–574, 2007.
- N. Ramankutty. Croplands in West Africa: a geographically explicit dataset for use in models. *Earth Interactions*, 8(23):1–22, 2004.
- N. Ramankutty and J.A. Foley. Characterizing patterns of global land use: An analysis of global croplands data. *Global Biogeochem. Cycles*, 12(4):667–685, 1998.

- N. Ramankutty and J.A. Foley. Estimating historical changes in global land cover: Croplands from 1700 to 1992. *Global Biogeochem. Cycles*, 13(4):997–1027, 1999.
- N. Ramankutty, L. Graumlich, F. Achard, D. Alves, A. Chhabra, R.S. DeFries, J.A. Foley, H. Geist, R.A. Houghton, K. Klein Goldewijk, E.F. Lambin, A. Millington, K. Rasmussen, R.S. Reid, and B.L. Turner II. Global land-cover change: recent progress, remaining challenges. In E.F. Lambin and H.J. Geist, editors, *Land-Use and Land-Cover Change. Local processes and Global Impacts*, The IGBP Series, pages 9–39, Berlin, 2006. Springer-Verlag.
- D. Rechid, T.J. Raddatz, and D. Jacob. Parameterization of snow-free land surface albedo as a function of vegetation phenology based on MODIS data and applied in climate modelling. *Theor. Appl. Climatol.*, DOI 10.1007/s00704-008-0003-y, 2008.
- D.C. Reicosky, W.A. Dugas, and H.A. Torbert. Tillage-induced soil carbon dioxide loss from different cropping systems. *Soil and Tillage Research*, 41(1–2):105–118, 1997.
- J.F. Richards. Transformations of the global environment: Land transformation. In B.L. Turner, editor, *The earth as transformed by human action: global and regional changes in the biosphere over the past 300 years*, pages 163–178, New York, 1990. Cambridge University Press.
- D.A. Robinson and G. Kukla. Albedo of a dissipating snow cover. *J. Appl. Meteor.*, 23(12):1626–1634, 1984.
- C. Rödenbeck, S. Houweling, M. Gloor, and M. Heimann. CO₂ flux history 1982–2001 inferred from atmospheric data using a global inversion of atmospheric transport. *Atmos. Chem. Phys.*, 3:1919–1964, 2003.
- E. Roeckner, G. Bäuml, L. Bonaventura, R. Brokopf, M. Esch, M. Giorgetta, S. Hagemann, I. Kirchner, L. Kornbluh, E. Manzini, A. Rhodin, U. Schlese, U. Schulzweida, and A. Tompkins. *The atmospheric general circulation model ECHAM5. Part I: Model description*, volume 349. Report, Max Planck Institute for Meteorology, Hamburg, Germany, 2003.
- W. Ruddiman. The anthropogenic greenhouse era began thousands of years ago. *Climatic Change*, 61:261–293, 2003.
- W. Ruddiman. The early anthropogenic hypothesis: Challenges and responses. *Rev. Geophys.*, 45, RG 4001:37 pp., 2007.
- V. Ruttan. Productivity growth in world agriculture: Sources and constraints. *J. Econ. Perspect.*, 16(4):161–184, 2002.
- C.L. Sabine, R.A. Feely, N. Gruber, R.M. Key, K. Lee, J.L. Bullister, R. Wanninkhof, C.S. Wong, D.W.R. Wallace, B. Tilbrook, F.J. Millero, T.-H. Peng, A. Kozyr, T. Ono, and A.F. Rios. The oceanic sink for anthropogenic CO₂. *Science*, 305: 367–371, 2004.

- D. Schimel, J.I. House, K.A. Hibbard, P. Bousquet, P. Ciais, P. Peylin, B.H. Braswell, M.J. Apps, D. Baker, A. Bondeau, J. Canadell, G. Churkina, W. Cramer, A.S. Denning, C.B. Field, P. Friedlingstein, C. Goodale, M. Heimann, R.A. Houghton, J.M. Melillo, B. Moore III, D. Murdiyarso, I. Noble, S.W. Pacala, I.C. Prentice, M.R. Raupach, P.J. Rayner, R.J. Scholes, W.L. Steffen, and C. Wirth. Recent patterns and mechanisms of carbon exchange by terrestrial ecosystems. *Nature*, 414:169–172, 2001.
- T. Searchinger, R. Heimlich, R.A. Houghton, F. Dong, A. Elobeid, J. Fabiosa, S. Tokgoz, D. Hayes, and T.-H. Yu. Use of U.S. croplands for biofuels increases greenhouse gases through emissions from land-use change. *Science*, 319:1238–1240, 2008.
- P.J. Sellers, J.A. Berry, G.J. Collatz, C.B. Field, and F.G. Hall. Canopy reflectance, photosynthesis, and transpiration. III. A reanalysis using improved leaf models and a new canopy integration scheme. *Remote Sens. Environ.*, 42:187–216, 1992.
- R.P. Sieferle. *Rückblick auf die Natur*. Luchterhand, München, 1997.
- S. Sitch, V. Brovkin, W. von Bloh, D. van Vuuren, B. Eickhout, and A. Ganopolski. Impacts of future land cover changes on atmospheric CO₂ and climate. *Global Biogeochem. Cycles*, 19(GB2013, doi:10.1029/2004GB002311), 2005.
- B.H. Slicher van Bath. *Yield Ratios, 810-1820*. Landbouwhogeschool, Afdeling Agarische Geschiedenis, Wageningen, 1963.
- M. Stendel, I.A. Mogensen, and J.H. Christensen. Influence of various forcings on global climate in historical times using a coupled atmosphere-ocean general circulation model. *Clim. Dyn.*, 26:1–15, 2006.
- K.M. Strassmann, F. Joos, and G. Fischer. Simulating effects of land use changes on carbon fluxes: past contributions to atmospheric CO₂ increases and future commitments due to losses of terrestrial sink capacity. *Tellus*, 60B:583–603, 2008.
- S.F.B. Tett, R. Betts, T.J. Crowley, J. Gregory, T.C. Johns, A. Jones, T.J. Osborn, E. Öström, D.L. Roberts, and M.J. Woodage. The impact of natural and anthropogenic forcings on climate and hydrology since 1550. *Clim. Dyn.*, 28:3–34, 2007.
- J. Townshend, C. Justice, W. Li, C. Gurney, and J. McManus. Global land cover classification by remote sensing: present capabilities and future possibilities. *Remote Sens. Environ.*, 35(2–3):243–255, 1991.
- K.E. Trenberth, P.D. Jones, P. Ambenje, R. Bojariu, D. Easterling, A. Klein Tank, D. Parker, F. Rahimzadeh, J.A. Renwick, M. Rusticucci, B. Soden, and P. Zhai. Observations: Surface and atmospheric climate change. In S. Solomon, D. Qin, M. Manning, Z. Chen, M. Marquis, K.B. Averyt, M. Tignor, and H.L. Miller, editors, *Climate Change 2007: The Physical Science Basis. Contribution of Working*

- Group I to the Fourth Assessment Report of the Intergovernmental Panel on Climate Change*, pages 235–336. Cambridge University Press, Cambridge, United Kingdom and New York, NY, USA, 2007.
- B.L. Turner II, D. Skole, S. Sanderson, G. Fischer, L. Fresco, and R. Leemans. Land-use and land-cover change science/research plan. Number 7 in IHDP Report. 1995.
- United Nations Environment Program (UNEP). Global biodiversity assessment. Cambridge University Press, Cambridge, 1995.
- United Nations Framework Convention on Climate Change (UNFCCC). Reducing emissions from deforestation in developing countries: approaches to stimulate action. Report of the Conference of the Parties on its thirteenth session, held in Bali from 3 to 15 December 2007, 2007.
- United Nations Statistics Division. Population density and urbanization. *UN Department of Economic and Social Affairs*, 2006.
- D.E. Vasey. *An ecological history of agriculture: 10,000 B.C. – A.D. 10,000*. Iowa State University Press, Ames, Iowa, 1992.
- P. M. Vitousek, H. A. Mooney, J. Lubchenco, and J. M. Melillo. Human domination of earth’s ecosystems. *Science*, 277(5325):494–499, 1997.
- P. Wetzel, A. Winguth, and E. Maier-Reimer. Sea-to-air CO₂ fluxes from 1948 to 2003. *Global Biogeochem. Cycles*, 19(GB2005):doi:10.1029/2004GB002339, 2005.
- K.W. Wirtz and C. Lemmen. A global dynamic model for the Neolithic transition. *Clim. Change*, 59(3):333–367(35), 2003.
- M. Zhao, A.J. Pitman, and T. Chase. The impact of land cover change on the atmospheric circulation. *Clim. Dyn.*, 17(5,6):467–477, 2001.

List of Publications

The following publications were submitted during the work on this thesis.

Peer-reviewed publications

- **J. Pongratz**, C. Reick, T. Raddatz, and M. Claussen. *A Global Land Cover Reconstruction AD 800 to 1992 - Technical Description*. Reports on Earth System Science, ISSN 1614-1199, vol. 51, 83 pages, 2008.
- **J. Pongratz**, C. Reick, T. Raddatz, and M. Claussen. *A reconstruction of global agricultural areas and land cover for the last millennium*. Global Biogeochem. Cycles, vol. 22, GB3018, doi:10.1029/2007GB003153, 2008.
- **J. Pongratz**, T. Raddatz, C.H. Reick, M. Esch, and M. Claussen. *Radiative forcing from anthropogenic land cover change since A.D. 800*. Geophys. Res. Lett., vol. 36, L02709, doi:10.1029/2008GL036394, 2009.
- **J. Pongratz** and C.H. Reick. *Vorindustrielle Landwirtschaft: Klimawandel ohne Öl und Kohle*. To be published in Jahrbuch der Max-Planck-Gesellschaft 2009.
- **J. Pongratz**, C.H. Reick, T. Raddatz, and M. Claussen. *Effects of anthropogenic land cover change on the carbon cycle of the last millennium*. Submitted to Global Biogeochem. Cycles, 2009.
- K. Hibbard, A. Janetos, D. van Vuuren, **J. Pongratz**, S. Rose, R. Betts, M. Herold, J. Feddema. *Research priorities in land use and land cover change for the Earth System and Integrated Assessment Modelling*. Submitted to International Journal of Climatology, 2009.
- E. Röckner, M. Giorgetta, T. Crüger, M. Esch, **J. Pongratz**. *Emission pathways to climate stabilization simulated in a global climate model*. To be submitted.

Conference contributions

- **J. Pongratz**, C. Reick, T. Raddatz, M. Claussen. *Anthropogenic land cover change in the last millenium — assessing its extent and consequences for climate*. Geophysical Research Abstracts, Vol. 9, 01878, 2007.
- **J. Pongratz**, C. Reick, T. Raddatz, M. Claussen. *A millennium of anthropogenic land cover change and its effects on climate*. Eos Trans. AGU, 88(52), Fall Meet. Suppl., Abstract GC54C-01, 2007.
- **J. Pongratz**, C. Reick, T. Raddatz, M. Claussen. *Biogeophysical effects of anthropogenic land cover change during the last millennium*. Geophysical Research Abstracts, Vol. 10, EGU2008-A-03996, 2008.

This contribution was awarded the **Young Scientists' Outstanding Poster Paper (YSOPP) Award 2008** by the European Geosciences Union.

- C.H. Reick, T. Raddatz, **J. Pongratz**, M. Claussen. *Reconstructed preindustrial landuse change emissions and atmospheric CO₂ from icecores are inconsistent*. Geophysical Research Abstracts, Vol. 10, EGU2008-A-04146, 2008.
- **J. Pongratz**, T. Raddatz, C.H. Reick, M. Claussen. *Effects of pre-industrial agricultural expansion and epidemics on the climate and the carbon cycle*. Eos Trans. AGU, 89(53), Fall Meet. Suppl., Abstract U31A-0007, 2008.
- **J. Pongratz**, C.H. Reick, T. Raddatz, M. Claussen. *Preindustrial agriculture and the carbon cycle - a GCM study on the beginning of the Anthropocene*. Geophysical Research Abstracts, Vol. 11, EGU2009-5697, 2009.

Acknowledgements

I would like to thank the many people who supported the creation of this thesis. First and foremost, I thank Christian Reick for being an excellent supervisor. I am greatly indebted to him for his scientific advice and guidance and the continuous support throughout the last years. I extend sincere thanks to Martin Claussen for the academic supervision of this work, for his time, interest, and fruitful discussions. He initiated the project and gave me the opportunity to work on this interesting topic. I thank Thomas Raddatz for answering all my questions and sharing his visionary ideas. Thanks, Thomas and Christian, for making me understand and like JSBACH, despite my antipathy to Baroque music.

Many other people contributed to making my time at the MPI pleasurable and productive: I am very grateful for the technical support I received from Veronika Gayler and Reiner Schnur: Veronika patiently started me out on the modeling framework, and Reiner performed the millennium simulations presented in this study. These simulations were overseen by the Millennium Group in Hamburg, and many thanks go to the participants, especially Johann Jungclauss. I thank Victor Brovkin for helpful discussions and first-hand insight into the world of EMICs. I further thank Katharina Six, Erich Roeckner, Andreas Chlond, Monika Esch, Dirk Notz, and Michael Böttinger for scientific and technical advice. At all times, I greatly enjoyed the friendly, cooperative, and inspiring atmosphere at the institute.

Great organizational backup was provided by Barbara Zinecker. The library and administration staff as well as the CIS group provided invaluable assistance. I would have returned to pen and paper without CIS.

My PhD work was funded by the International Max Planck Research School on Earth System Modelling. I thank Wolfgang Cramer for being my panel chair. Many thanks go to Antje Weitz and Cornelia Kampmann for their continuous support, both administratively and morally. It has been great to be part of the IMPRS!

The last three years would not have been that much fun without the help and company of my fellow PhD students. Special thanks go to Freja Vamborg and Juliane Otto for being supportive and entertaining office mates/neighbors and for Swedish sweets and home-made cookies. Thanks also to all in atmosphere and ocean to get us Geomatikum people out of our ivory tower for regular coffee breaks. And thanks to the WOODSTOCK Development Team for award-winning climate modeling with hammer and saw.

I thank my family for their material and non-material support, including ap-

proximately 150 highly appreciated letters that kept me in touch with my home. Finally, I want to thank Eberhard for his assistance and patience during the last three years, and for everything beyond this. Without him, neither the titlepage nor my life would be as nice and colorful as they are.

Die gesamten Veröffentlichungen in der Publikationsreihe des MPI-M
„Berichte zur Erdsystemforschung“,
„Reports on Earth System Science“,
ISSN 1614-1199

sind über die Internetseiten des Max-Planck-Instituts für Meteorologie erhältlich:

<http://www.mpimet.mpg.de/wissenschaft/publikationen.html>

